



**HAL**  
open science

## The 2020 edition of the GEISA spectroscopic database

T. Delahaye, Raymond Armante, N.A. Scott, N. Jacquinet-Husson, A. Chédin, L. Crépeau, C. Crevoisier, V. Douet, A. Perrin, A. Barbe, et al.

### ► To cite this version:

T. Delahaye, Raymond Armante, N.A. Scott, N. Jacquinet-Husson, A. Chédin, et al.. The 2020 edition of the GEISA spectroscopic database. *Journal of Molecular Spectroscopy*, 2021, 380, pp.111510. 10.1016/j.jms.2021.111510 . hal-03337047

**HAL Id: hal-03337047**

**<https://hal.science/hal-03337047v1>**

Submitted on 28 Oct 2021

**HAL** is a multi-disciplinary open access archive for the deposit and dissemination of scientific research documents, whether they are published or not. The documents may come from teaching and research institutions in France or abroad, or from public or private research centers.

L'archive ouverte pluridisciplinaire **HAL**, est destinée au dépôt et à la diffusion de documents scientifiques de niveau recherche, publiés ou non, émanant des établissements d'enseignement et de recherche français ou étrangers, des laboratoires publics ou privés.

## The 2020 edition of the GEISA spectroscopic database

T. Delahaye<sup>1</sup>, R. Armante<sup>1</sup>, N.A. Scott<sup>1</sup>, N. Jacquinet-Husson<sup>1</sup>, A. Chédin<sup>1</sup>, L. Crépeau<sup>1</sup>, C. Crevoisier<sup>1</sup>, V. Douet<sup>2</sup>, A. Perrin<sup>1</sup>, A. Barbe<sup>3</sup>, V. Boudon<sup>4</sup>, A. Campargue<sup>5</sup>, L.H. Coudert<sup>6</sup>, V. Ebert<sup>14,15</sup>, J.-M. Flaud<sup>7</sup>, R.R. Gamache<sup>9</sup>, D. Jacquemart<sup>10</sup>, A. Jolly<sup>7</sup>, F. Kwabia Tchana<sup>7</sup>, A. Kyuberis<sup>22</sup>, G. Li<sup>14</sup>, O.M. Lyulin<sup>11</sup>, L. Manceron<sup>10,16</sup>, S. Mikhailenko<sup>11</sup>, N. Moazzen-Ahmadi<sup>23</sup>, H.S.P. Müller<sup>12</sup>, O.V. Naumenko<sup>11</sup>, A. Nikitin<sup>11</sup>, V.I. Perevalov<sup>11</sup>, C. Richard<sup>4</sup>, E. Starikova<sup>11</sup>, S.A. Tashkun<sup>11</sup>, V.I.G. Tyuterev<sup>3,17</sup>, J. Vander Auwera<sup>13</sup>, B. Vispoel<sup>9,18,19</sup>, A. Yachmenev<sup>20,21</sup>, S. Yurchenko<sup>8</sup>.

<sup>1</sup>Laboratoire de Météorologie Dynamique/IPSL, CNRS, Ecole Polytechnique, Université Paris-Saclay, 91128, Palaiseau, France

<sup>2</sup>Institut Pierre Simon Laplace, Université Pierre et Marie Curie, 75252 Paris, France

<sup>3</sup>Université de Reims-Champagne-Ardenne, Groupe de Spectrométrie Moléculaire et Atmosphérique, 51062 Reims, France

<sup>4</sup>Laboratoire Interdisciplinaire Carnot de Bourgogne, UMR 6303 CNRS-Univ. Bourgogne Franche-Comté, 9 Avenue Alain Savary, BP 47 870, F-21078 DIJON Cedex, France

<sup>5</sup>Univ. Grenoble Alpes, CNRS, LIPhy, 38000 Grenoble, France

<sup>6</sup>Université Paris-Saclay, CNRS, Institut des Sciences Moléculaires d'Orsay, 91405 Orsay, France

<sup>7</sup>Laboratoire Interuniversitaire des Systèmes Atmosphériques (LISA), UMR CNRS 7583, Université de Paris, Université Paris-Est Créteil, Institut Pierre-Simon Laplace, 61 avenue du Général de Gaulle, 94010 Créteil Cedex, France

<sup>8</sup>Department of Physics and Astronomy, University College London, London WC1E 6BT, United Kingdom

<sup>9</sup>University of Massachusetts Lowell, Department of Environmental Earth and Atmospheric Sciences, Lowell, MA 01854, USA

<sup>10</sup>Sorbonne Université, CNRS, De la MOlécule aux NANO-objets : Réactivité, Interactions et Spectroscopies, MONARIS, 75005 Paris, France

<sup>11</sup>V.E. Zuev Institute of Atmospheric Optics, SB, Russian Academy of Sciences, 1, Academician Zuev square, 634055, Tomsk, Russia

<sup>12</sup>I. Physikalisches Institut, Universität zu Köln, 50937 Köln, Germany

<sup>13</sup>Spectroscopy, Quantum Chemistry and Atmospheric Remote Sensing (SQUARES), C.P. 160/09, Université Libre de Bruxelles, 50 avenue F.D. Roosevelt, B-1050 Brussels, Belgium.

<sup>14</sup>Physikalisch-Technische Bundesanstalt, Bundesallee 100, 38116 Braunschweig, Germany

<sup>15</sup>Reactive Flows and Diagnostics, Technische Universität Darmstadt, Otto-Berndt-Str. 3 64287 Darmstadt, Germany

<sup>16</sup>Synchrotron Soleil Ligne AILES, BP 48, 91192 Cedex Gif-sur-Yvette, France

<sup>17</sup>QUAMER laboratory, Tomsk State University, 36 Lenin Ave., Tomsk, Russia 634050

<sup>18</sup>Research Unit Lasers and Spectroscopies (LLS), Institute of Life, Earth and Environment (ILEE), University of Namur (UNamur), 61 rue de Bruxelles, B-5000, Namur, Belgium

<sup>19</sup>Royal Belgian Institute for Space Aeronomy (BIRA-IASB), 3 Avenue Circulaire, 1180, Brussels, Belgium

<sup>20</sup>Center for Free-Electron Laser Science, Deutsches Elektronen-Synchrotron DESY, Notkestraße 85, 22607 Hamburg, Germany

<sup>21</sup> Center for Ultrafast Imaging, Universität Hamburg, Luruper Chaussee 149, 22761  
Hamburg, Germany

<sup>22</sup> Van Swinderen Institute for Particle Physics and Gravity, University of Groningen,  
Nijenborgh 4, 9747 Groningen, The Netherlands

<sup>23</sup> Department of Physics and Astronomy, University of Calgary, 2500 University Drive North  
West, Calgary, Alberta T2N 1N4, Canada

### Highlights

- GEISA-2020 database release: 6,746,987 entries in the line parameters database
- 23 molecules updated and 6 new molecules added (HONO, COFCl, CH<sub>3</sub>F, CH<sub>3</sub>I, RuO<sub>4</sub>, H<sub>2</sub>C<sub>3</sub>H<sub>2</sub> (isomer of C<sub>3</sub>H<sub>4</sub>))
- Evaluation of the spectroscopic parameters through radiative transfer simulations compared to atmospheric spectra (SPARTE chain)

### Corresponding author

Dr. Raymond Armante

Phone: +33169335111

E-mail: [raymond.armante@lmd.ipsl.fr](mailto:raymond.armante@lmd.ipsl.fr)

## ABSTRACT

This paper describes the 2020 release of the GEISA database (Gestion et Etude des Informations Spectroscopiques Atmosphériques: Management and Study of Atmospheric Spectroscopic Information), developed and maintained at LMD since 1974. GEISA is the reference database for several current or planned Thermal and Short-Wave InfraRed (TIR and SWIR) space missions IASI (Infrared Atmospheric Sounding Interferometer), IASI-NG (IASI New Generation), MicroCarb (Carbon Dioxide Monitoring Mission), Merlin (MEthane Remote sensing LIdar mission). It is actually a compilation of three databases: the “line parameters database”, the “cross-section sub-database” and the “microphysical and optical properties of atmospheric aerosols sub-database”. The new edition concerns only the line parameters dataset, with significant updates and additions implemented using the best available spectroscopic data.

The GEISA-2020 line parameters database involves 58 molecules (145 isotopic species) and contains 6,746,987 entries, in the spectral range from  $10^{-6}$  to  $35877\text{ cm}^{-1}$ . In this version, 23 molecules have been updated (with 10 new isotopic species) and 6 new molecules have been added (HONO, COFCl, CH<sub>3</sub>F, CH<sub>3</sub>I, RuO<sub>4</sub>, H<sub>2</sub>C<sub>3</sub>H<sub>2</sub> (isomer of C<sub>3</sub>H<sub>4</sub>)) corresponding to 15 isotopic species. The compilation can be accessed through the AERIS data and services center for the atmosphere website (<https://geisa.aeris-data.fr/>), with the development of a powerful graphical tool and convenient searching, filtering, and plotting of data using modern technologies (PostgreSQL database, REST API, VueJS, Plotly).

Based on four examples (H<sub>2</sub>O, O<sub>3</sub>, O<sub>2</sub> and SF<sub>6</sub>), this paper also shows how the LMD in house validation algorithm SPARTE (Spectroscopic Parameters And Radiative Transfer Evaluation) helps to evaluate, correct, reject or defer the input of new spectroscopic data into GEISA and this, thanks to iterations with researchers from different communities (spectroscopy, radiative transfer).

**Key words:** molecular spectroscopic database ; line parameters ; earth and planetary radiative transfer ; atmospheric absorption ; spectroscopic parameters evaluation

## 1 Introduction<sup>1</sup>:

From the mid 1960's, various scientific communities (Remote Sensing, Astrophysics, Atmospheric Physics, Metrology, Climate and Chemistry) have required access to databases detailing the spectral characteristics of atmospheric molecular absorption and atmospheric particle scattering. The purpose of spectroscopic databases like GEISA [1] and HITRAN [2] is to give, to each community, access to the best information at a given time.

In France, archiving spectroscopic data in conjunction with remote sensing applications was first initiated in the 70's. The first release of the GEISA database [3] included major absorbers ( $\text{N}_2$ ,  $\text{O}_2$ ,  $\text{H}_2\text{O}$ ,  $\text{CO}_2$ ,  $\text{O}_3$ ,  $\text{N}_2\text{O}$ ,  $\text{CO}$ ,  $\text{CH}_4$ ) of the earth atmosphere as well as complementary species (e.g.  $\text{NH}_3$ ,  $\text{HNO}_3$ ,  $\text{PH}_3$ ,  $\text{C}_2\text{H}_4$ ,  $\text{C}_2\text{H}_2$ ,  $\text{HC}_3\text{N}$ ,  $\text{HCOOH}$ ,  $\text{NO}$ ,  $\text{SO}_2$ ,  $\text{NO}_2$ ). Some molecules, mainly related to planetary atmospheres (e.g. within the frame of the Voyager experiment and observations of the giant planets) like  $\text{GeH}_4$ ,  $\text{C}_3\text{H}_8$ ,  $\text{C}_2\text{N}_2$ ,  $\text{C}_3\text{H}_4$ ,  $\text{HNC}$ ,  $\text{C}_6\text{H}_6$ , and  $\text{C}_2\text{HD}$  were also included. Since its first publication, (Chédin *et al.* (1982) [3]), including spectroscopic data and management softwares, GEISA has undergone numerous updates (Husson *et al.* (1992) [4], Jacquinet-Husson *et al.* (1999, 2008, 2009, 2016) [1,5–7]).

One of the differences of GEISA, in comparison with other databases such as HITRAN, is that we treat isotopologues with a symmetry property as separate molecules, when necessary. For example, the molecule index for  $\text{CH}_4$  is 6, while that of  $\text{CH}_3\text{D}$  is 23. See Table 2 for further examples. This was initiated in the mid 70's with  $\text{CH}_3\text{D}$  and  $\text{CH}_4$  within the frame of the Voyager experiment and later on with  $\text{HDO}$  and  $\text{H}_2\text{O}$ ,  $\text{C}_2\text{HD}$  and  $\text{C}_2\text{H}_2$ . Another difference is that some species are specifically considered by only one database (for example  $\text{O}$  and  $\text{H}_2$  for HITRAN,  $\text{C}_3\text{H}_8$  and  $\text{C}_3\text{H}_4$  for GEISA).

Among the important number of information updated, a large part has been done with the valuable and sustained support of the international spatial agencies. Especially, since the launch of [Metop-A](#) (24 October 2006), GEISA became the official reference spectroscopic database used by the international working group (ISSWG) in charge of the [IASI](#) instrument. GEISA is also now involved in the definition of three future space missions: [IASI-NG](#), [Merlin](#) and [MicroCarb](#).

---

<sup>1</sup> Acronyms used in the text are documented in Appendix A

GEISA and its associated management software facilities are implemented and distributed (in the same way as GEISA-2011) via the atmospheric pole AERIS. It is used on-line by more than 350 laboratories working in various fields including atmospheric physics, planetary science, astronomy, astrophysics.

As in previous editions of GEISA, new data have been provided by different groups. They are listed in Column 3 of Table 1 together with their contribution.

Since the beginning of the 2000's, a specific effort has been made in GEISA and HITRAN to undertake a more systematic evaluation of spectroscopic parameters when selecting, introducing or replacing data. This has been enabled by the evolving capacity of several space-borne, ground-based or laboratory observations that have reached a level of precision sufficient to evaluate a large range of spectroscopic parameters produced by laboratory measurements or theory. Concerning GEISA, use is made of the now well-established evaluation method (called SPARTE, Spectroscopic Parameters And Radiative Transfer Evaluation) [8] that was developed and first used during the former GEISA release (called GEISA-2015 in the following). Using high resolution and high signal-to-noise ratio space-borne or ground-based measurements (like the one provided in the Near and Short-Wave Infrared by ground-based spectrometers of the Total Carbon Column Observing Network (TCCON) [9] and in the Thermal Infrared by the Infrared Atmospheric Sounding Interferometer (IASI) SPARTE enables to identify spectroscopic issues by investigating the differences between observations and simulations performed using the 4A/OP radiative transfer code [10].

This paper provides, in section 2, a detailed description of the data newly implemented or corrected in the latest 2020 GEISA release, for the line parameters sub-database only (the corresponding cross-section and aerosol will be updated and documented in a forthcoming paper). In this GEISA-2020 edition, the format is unchanged from the previous one. The inclusion of additional spectroscopic parameters describing refined collisional effects such as the speed dependence and Dicke narrowing effects is planned for a forthcoming version.

Examples of spectroscopic evaluations performed using, among others, the SPARTE algorithm are presented in Section 3. Focusing on H<sub>2</sub>O, O<sub>2</sub>, O<sub>3</sub> and SF<sub>6</sub> molecules, we illustrate how the evaluation guided our selection of sources of line parameters.

## **2 GEISA-2020 Line parameters database description**

### *General Overview*

The GEISA-2020 edition is based on the release of spectroscopic data for 23 molecules in the range of  $10^{-6}$  to  $35,877\text{ cm}^{-1}$ , and on the addition of 6 molecules in the range 296 to  $1913\text{ cm}^{-1}$  (i.e. 'HONO, COFCl, CH<sub>3</sub>I, CH<sub>3</sub>F, RuO<sub>4</sub> and H<sub>2</sub>C<sub>3</sub>H<sub>2</sub> (allene, isomer of C<sub>3</sub>H<sub>4</sub>)), whose

molecule code number (parameter I) has been fixed to 53 to 58, respectively. The molecules which were updated are listed in Table 1, together with their molecule code in the GEISA notation and indication about the involved research groups. Note that the choice has been made in GEISA not to provide partition sums calculations. We have always relied on the use of TIPS code by Gamache *et al.* [11]. As TIPS is based on HITRAN molecule list, and as differences subsist with the two databases in the molecular content, we suggested several times in the past that TIPS add extra molecules as for GeH<sub>4</sub>, C<sub>3</sub>H<sub>8</sub>, HNC or C<sub>2</sub>H<sub>6</sub>. The new version of TIPS is based on HITRAN2020 and doesn't include HONO for example, as in GEISA-2020. We plan to suggest to R. Gamache to include data for missing molecules in TIPS, if possible.

Molecule ID.	Code	Contributors	GEISA code
H <sub>2</sub> O	1	A. Campargue, S. Mikhailenko, Y. Yurchenko, B. Gamache	CA6, CA9, K19, Y20
CO <sub>2</sub>	2	V. Perevalov, S. Tashkun	P19
O <sub>3</sub>	3	A.Barbe, S.Mikhailenko, E.Starikova, V. Tyuterev	T19, M19
N <sub>2</sub> O	4	V. Ebert, G. Li	L19
CO	5	G. Li, I. Gordon	L19
CH <sub>4</sub>	6	A. Nikitin, V.Tyuterev, E.Starikova	N19, S19
SO <sub>2</sub>	9	O. Naumenko	1N9, 2N9, 3N9, 4N9, 5N9
NO <sub>2</sub>	10	A. Perrin, L. Manceron	P19
NH <sub>3</sub>	11	N. Maaroufi, F. Kwabia	M19
PH <sub>3</sub>	12	A. Nikitin	N19
HNO <sub>3</sub>	13	A. Perrin	P19
HF, HBr, HI	15,17,18	G. Li, I. Gordon	L19
HCl	16	G. Li, V. Ebert	L19
OCS	20	S. Galalou, F. Kwabia	A16, G19
C <sub>2</sub> H <sub>6</sub>	22	N. Moazzen-Ahmadi	M19
C <sub>2</sub> H <sub>2</sub>	24	D. Jacquemart, A. Campargue, V. Perevalov, O. Lyulin	J19, J20, L19, C19
C <sub>2</sub> H <sub>4</sub>	25	J. Vander Auwera	A19
GeH <sub>4</sub>	26	V. Boudon	B19
NO <sup>+</sup>	45	H.S.P. Müller	M18
CF <sub>4</sub>	49	V. Boudon	B19
HDO	51	L. Coudert, A. Kyuberis	CO9, K19
<b>New molecules</b>			
HONO	53	A. Perrin	P18
COFCl	54	A. Perrin	P19
CH <sub>3</sub> I	55	F. Kwabia, A. Perrin	P19
CH <sub>3</sub> F	56	D. Jacquemart	J19
RuO <sub>4</sub>	57	V. Boudon	B19
H <sub>2</sub> C <sub>3</sub> H <sub>2</sub> , Allene (C <sub>3</sub> H <sub>4</sub> isomer)	58	A. Jolly	J19

**Table 1:** Updated molecular species in the GEISA-2020 edition. The internal GEISA code for the identification of the source of the data is indicated within parentheses (parameter G).

To have a more precise idea of the update, Table 2 gives the main differences between GEISA-2015 and GEISA-2020 (in term of spectral range, number of lines and integrated intensity range).

		GEISA-2015				GEISA-2020			
Mol.	ID	Spectral range (cm <sup>-1</sup> )	# lines	Exponent of the intensity (cm molecule <sup>-1</sup> ) at 296 K.		Spectral range (cm <sup>-1</sup> )	# lines	Exponent of the intensity (cm molecule <sup>-1</sup> ) at 296 K.	
				Max.	Min.			Max.	Min.
H <sub>2</sub> O	1	0.052 - 25336.949	191846	-18	-36	0.053 - 25336.949	362222	-18	-36
CO <sub>2</sub>	2	5.890 - 14075.298	534227	-18	-30	345.936 - 14075.301	532533	-18	-30
O <sub>3</sub>	3	0.026 - 6996.681	405919	-20	-31	0.026 - 6996.681	464288	-20	-31
N <sub>2</sub> O	4	0.838 - 7796.633	50633	-17	-25	0.838 - 7796.633	50633	-18	-26
CO	5	3.414 - 8464.882	13515	-18	-77	3.402 - 14477.377	14985	-19	-78
CH <sub>4</sub>	6	0.001 - 11501.877	421811	-19	-39	0.001 - 11501.877	447004	-19	-39
O <sub>2</sub>	7	10-6 - 15927.804	16197	-24	-54	0.000 - 15927.804	16197	-24	-54
NO *	8	10-6 - 9273.214	105079	-19	-94	0.000 - 9273.214	105079	-20	-95
SO <sub>2</sub>	9	0.017 - 4092.948	83668	-20	-30	0.017 - 4159.945	561008	-20	-30
NO <sub>2</sub>	10	0.498 - 3074.152	104223	-18	-27	0.498 - 4775.314	185965	-19	-28
NH <sub>3</sub>	11	0.058 - 6999.429	46414	-19	-39	0.058 - 6999.429	46414	-19	-39
PH <sub>3</sub>	12	17.805 - 3601.652	20364	-18	-27	8.904 - 3659.266	34542	-19	-28
HNO <sub>3</sub>	13	0.012 - 1769.982	691161	-20	-28	0.012 - 1769.982	738171	-20	-28
OH *	14	0.005 - 35877.031	42866	-16	-84	0.005 - 35877.031	42866	-17	-85
HF	15	41.111 - 11535.570	107	-16	-25	13.620 - 32351.592	20010	-17	-99
HCl	16	20.240 - 13457.841	533	-18	-25	5.342 - 20231.245	53436	-19	-99
HBr	17	16.231 - 9758.564	1293	-18	-32	7.656 - 16033.492	8980	-19	-71
HI	18	12.509 - 8487.305	806	-19	-29	5.888 - 13907.689	4751	-20	-64
ClO *	19	0.015 - 1207.639	7230	-20	-29	0.015 - 1207.639	7230	-21	-30
OCS	20	0.381 - 4199.671	33809	-17	-27	0.381 - 7821.109	37479	-18	-28
H <sub>2</sub> CO *	21	0.000 - 3099.958	44611	-20	-39	0.000 - 3099.958	44611	-20	-39
C <sub>2</sub> H <sub>6</sub>	22	706.601 - 3070.971	53803	-20	-29	225.045 - 3070.971	65741	-20	-38
CH <sub>3</sub> D *	23	7.760 - 6510.324	58763	-23	-30	7.760 - 6510.324	58763	-23	-30
C <sub>2</sub> H <sub>2</sub>	24	604.774 - 9889.038	12969	-18	-28	13.624 - 9889.038	70107	-18	-31
C <sub>2</sub> H <sub>4</sub>	25	614.740 - 3242.172	53227	-20	-37	614.740 - 3242.172	100100	-20	-37
GeH <sub>4</sub>	26	1937.371 - 224.570	824	-18	-21	1928.902 - 2265.678	32372	-19	-23
HCN *	27	0.018 - 17581.009	138103	-19	-32	0.019 - 17581.009	138103	-19	-32
C <sub>3</sub> H <sub>8</sub> *	28	700.015 - 799.930	8983	-21	-23	700.015 - 799.930	8983	-22	-24
C <sub>2</sub> N <sub>2</sub> *	29	200.817 - 2181.690	71954	-20	-24	200.818 - 2181.690	71954	-20	-24
C <sub>4</sub> H <sub>2</sub> *	30	189.422 - 1302.217	417540	-19	-24	189.423 - 1302.217	417540	-19	-24
HC <sub>3</sub> N *	31	463.604 - 759.989	179347	-19	-23	463.604 - 759.989	179347	-20	-24
HOCl *	32	0.0236 - 3799.682	17862	-19	-27	0.024 - 3799.682	17862	-20	-28
N <sub>2</sub> *	33	1992.63 - 2625.497	120	-27	-33	1992.628 - 2625.497	120	-28	-34
CH <sub>3</sub> Cl *	34	0.872 - 3197.961	83043	-21	-32	0.873 - 3197.961	83043	-21	-32
H <sub>2</sub> O <sub>2</sub> *	35	0.043 - 1730.371	126983	-19	-28	0.043 - 1730.371	126983	-20	-29
H <sub>2</sub> S *	36	1.030 - 1329.780	58650	-19	-30	1.031 - 11329.780	58650	-19	-30
HCOOH *	37	10.018 - 1889.334	62684	-19	-25	10.018 - 1889.334	62684	-20	-26
COF <sub>2</sub> *	38	725.005 - 2001.348	70904	-19	-23	725.005 - 2001.348	70904	-20	-24
SF <sub>6</sub> *	39	588.488 - 975.787	92398	-19	-23	588.488 - 975.787	92398	-20	-24
C <sub>3</sub> H <sub>4</sub> *	40	288.913 - 673.479	19001	-19	-23	288.913 - 673.479	19001	-20	-24
HO <sub>2</sub> *	41	0.173 - 3675.819	38804	-19	-25	0.173 - 3675.819	38804	-20	-26



		GEISA-2015				GEISA-2020			
Mol.	ID	Spectral range (cm <sup>-1</sup> )	# lines	Exponent of the intensity (cm molecule <sup>-1</sup> ) at 296 K.		Spectral range (cm <sup>-1</sup> )	# lines	Exponent of the intensity (cm molecule <sup>-1</sup> ) at 296 K.	
				Max.	Min.			Max.	Min.
				ClONO <sub>2</sub> *	42			0.636 - 797.741	356899
CH <sub>3</sub> Br *	43	794.403 - 1705.612	36911	-21	-27	794.403 - 1705.612	36911	-21	-27
CH <sub>3</sub> OH *	44	0.019 - 1407.206	19897	-19	-34	0.019 - 1407.206	19897	-20	-35
NO <sup>+</sup>	45	1634.83 - 2530.462	1206	-18	-80	3.938 - 4742.008	1333	-19	-81
HNC *	46	0.145 - 4692.098	75554	-18	-30	0.146 - 4692.098	75554	-18	-30
C <sub>6</sub> H <sub>6</sub> *	47	642.427 - 705.262	9797	-20	-23	642.427 - 705.262	9797	-21	-24
C <sub>2</sub> HD *	48	416.785 - 3421.864	15512	-22	-28	416.785 - 3421.864	15512	-23	-29
CF <sub>4</sub>	49	594.581 - 1312.647	60033	-19	-23	1.173 - 1329.697	258208	-20	-30
CH <sub>3</sub> CN *	50	890.052 - 1650.000	17172	-19	-37	890.052 - 1650.000	17172	-20	-38
HDO	51	0.007 - 17080.098	63641	-22	-33	0.000 - 19935.167	77599	-22	-39
SO <sub>3</sub> *	52	0.477 - 2824.347	10881	-19	-31	0.478 - 2824.347	10881	-19	-31
HONO	53					722.534 - 996.281	26041	-20	-25
COFCL	54					734.997 - 1912.632	215639	-20	-24
CH <sub>3</sub> I	55					693.022 - 1125.255	70291	-21	-31
CH <sub>3</sub> F	56					1067.375 - 1290.255	1499	-21	-24
RUO <sub>4</sub>	57					889.987 - 948.138	30205	-20	-23
H <sub>2</sub> C <sub>3</sub> H <sub>2</sub>	58					296.316 - 1192.446	31686	-20	-27
<b>Total # lines</b>			5,067,351			6,746,987			

\*: Molecule which has not been updated in the GEISA-2020

**Table 2.** Contents of the GEISA-2020 line parameters database. Details per molecule of the evolution of GEISA contents since its 2015 edition. Reference temperature is 296 K.

### *Description of updates per individual molecular species*

This description is given in sub-sections 2.2.1 to 2.2.25, for each molecular species identified by its formula associated with its GEISA identification code.

#### **2.1.1 H<sub>2</sub>O and HDO**

##### **2.1.1.1 H<sub>2</sub>O (molecule 1)**

New H<sub>2</sub>O data implemented in GEISA-2020 consist in three main parts which are: (i) an updated line list for the main H<sub>2</sub><sup>16</sup>O isotopologue between 5850 and 8340 cm<sup>-1</sup>, (ii) the addition of electric-quadrupole transitions up to 10000 cm<sup>-1</sup>, and (iii) a major update of doubly deuterated D<sub>2</sub>O isotopologues up to 18,000 cm<sup>-1</sup>.

GEISA-2020 was updated using line intensities, air-broadening and -shifting coefficients provided from Mikhailenko *et al.* [12], whereas the line positions were refined using the most recent version of their line list [13]. Note that local discrepancies due to erroneous broadening values of some H<sub>2</sub>O lines were found in these line lists and in GEISA-2015 (see for example residuals of the H<sub>2</sub>O line at 7804.6092 cm<sup>-1</sup> in section 3.1.1), these lines were corrected in GEISA-2020 with calculated air-broadening parameters from Vispoel *et al.* [14,15] were used

to correct the incriminated lines (see details below). As a result, 40,980 lines were updated in GEISA-2020 (from which 7572 are new lines not referenced in GEISA-2015). Note that we present in section 3.1.1 a quantitative evaluation of these H<sub>2</sub>O data.

The internal GEISA code presented in Table 1 for the data identification has been set to **CA6** and **CA9**.

Up to now, similarly to all other databases, the GEISA H<sub>2</sub>O database was limited to ro-vibrational electric-dipole transitions. Electric-quadrupole transitions do also exist, but they are typically a million times weaker than electric-dipole transitions, making their observation extremely challenging. The recent detection of weak quadrupole transitions in the spectrum of water vapor [16,17] has shown that in their present status the spectroscopic databases are not complete for polyatomic molecules. Actually, databases provide lists of electric-dipole transitions above an intensity cut-off (*e.g.* 10<sup>-36</sup> cm/molecule for water in the GEISA database) largely below intensity values of the strongest electric-quadrupole lines (*e.g.* up to 10<sup>-26</sup> cm/molecule for water vapor [17]). The laboratory measurements of Refs [16,17] (in total, about twenty quadrupole lines near 5.4, 2.5 and 1.3 μm) have validated the *ab initio* intensities computed in Ref. [16] within the experimental error bars. Consequently, in the present release, the *ab initio* quadrupole line list of Ref. [16] up to 10,000 cm<sup>-1</sup> (6429 lines in total above a 10<sup>-30</sup> cm/molecule intensity cut-off) has been incorporated in the water vapor line list for the main isotopologue H<sub>2</sub><sup>16</sup>O. Figure 1 shows an overview of the electric-dipole and electric-quadrupole transitions listed in GEISA 2020, up to 9500 cm<sup>-1</sup>. In the calculations of Ref. [16], the variational values of the lower and upper energy levels of H<sub>2</sub><sup>16</sup>O were replaced by the corresponding empirical values from IUPAC [18]. The resulting line position accuracy is thus expected to be of the order of 10<sup>-3</sup> cm<sup>-1</sup> for most of the quadrupole lines.

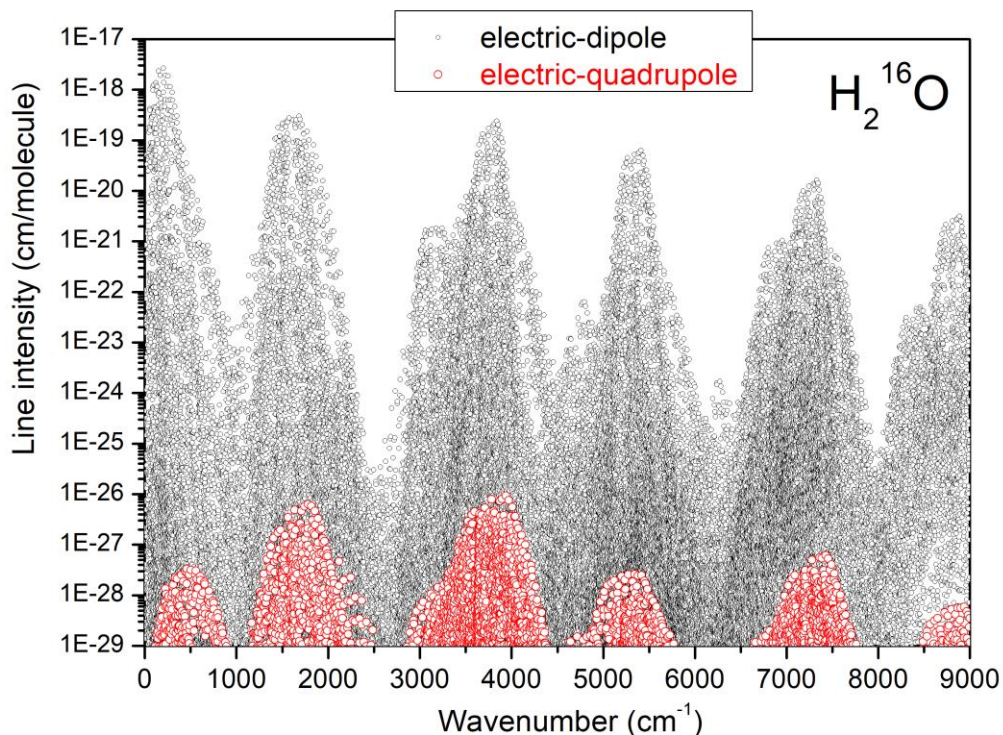


**Figure 1:** Overview of the  $\text{H}_2^{16}\text{O}$  absorption line list in GEISA-2020 up to  $9000\text{ cm}^{-1}$ . The electric-quadrupole transitions (red dots) are superimposed to the electric-dipole transitions (black dots).

The internal GEISA code for the data identification has been set to [Y20](#).

As line shape parameters are critical for atmospheric applications, an updated calculation for  $\text{H}_2\text{O}-\text{H}_2\text{O}$ ,  $\text{H}_2\text{O}-\text{N}_2$  and  $\text{H}_2\text{O}-\text{O}_2$  broadenings and shifts, along with the temperature dependence of these parameters was provided by Gamache and Vispoel (unpublished data, 2020). These parameters were calculated for  $\text{H}_2^{16}\text{O}$ ,  $\text{H}_2^{18}\text{O}$ ,  $\text{H}_2^{17}\text{O}$  (but also  $\text{HD}^{17}\text{O}$ ,  $\text{HD}^{18}\text{O}$ ,  $\text{D}_2^{16}\text{O}$ ,  $\text{D}_2^{18}\text{O}$ , and  $\text{D}_2^{17}\text{O}$  species), and include the  $\text{H}_2^{16}\text{O}$  quadrupole transitions. From values calculated using the Modified Complex Robert Bonamy (MCRB) model by Vispoel *et al.* [14] for  $\text{H}_2\text{O}-\text{N}_2$  and  $\text{H}_2\text{O}-\text{O}_2$  (Vispoel and Gamache, unpublished data, 2020), the pressure broadening information for  $\text{H}_2\text{O}-\text{air}$  was produced considering  $\gamma(\text{air}) = 0.79\gamma(\text{N}_2) + 0.21\gamma(\text{O}_2)$ , with a similar formula for the line shift. Note that the calculations were performed for 13 temperatures from 200 K to 3000 K, considering 10,782 rotational transitions in the rotational band and for 1 to 4 vibrational quanta changes in the  $\nu_1$ ,  $\nu_2$ , and  $\nu_3$  bands, giving updated profile parameters for about 140,000 transitions.

Pressure-broadening and -shifting parameters of more than 300,000 dipole transitions needed to be carefully selected, evaluated and systematically compared to previous data of the database.

This specific process being a task of major importance, it will be part of a future dedicated publication on H<sub>2</sub>O. As a result, only line-shape parameters for quadrupole transitions were considered for this update of GEISA, except for some problematic electric-dipole isolated lines known to be problematic in GEISA-2015 (cf. section 3.1.1 for a detailed example of H<sub>2</sub>O data validation). For GEISA-2020, line-shape parameters of 6475 lines were updated in this way.

Besides the main isotopologue H<sub>2</sub><sup>16</sup>O, another update was made in GEISA-2020 for the doubly deuterated D<sub>2</sub>O isotopologues of water vapor, based on the recent work of Kyuberis *et al.* [19]. A total of 156,375 new lines were added and 5860 lines updated with respect to the previous version of the database. In particular, data for the isotopologue D<sub>2</sub><sup>17</sup>O, which were missing in all previous versions of GEISA, were implemented. These *ab initio* calculations were obtained using the base PES (Potential Energy Surface) of Shirin *et al.* [20] which was explicitly developed for D<sub>2</sub>O. More details can be found in Ref. [19]. Half-width and pressure-shift data were taken from the measurement database of Gamache and Hartmann [21] for 228, 227, 133 (119, 119, 88 for line shifts) transitions of D<sub>2</sub><sup>16</sup>O, D<sub>2</sub><sup>18</sup>O, and D<sub>2</sub><sup>17</sup>O, respectively. For the remaining transitions, data from Ref. [19] were retained.

The internal GEISA code for the data identification has been set to [K19](#).

#### 2.1.1.2 HDO (molecule 51)

Following the data update made for H<sub>2</sub>O (cf. previous section), the HDO linelist was also updated using line intensities and air-broadening and -shifting coefficients provided by Mikhailenko *et al.* [12], and line positions which were refined using the most recent version of their line list [13]. As a result, 17,015 lines were updated in GEISA-2020 (from which 4468 are new lines not referenced in GEISA-2015).

The internal GEISA code for the data identification has been set to [CA6](#) and [CA9](#).

Moreover, recent data from Coudert [22], based on the line positions and line strengths analyses spanning the 0 to 2000 cm<sup>-1</sup> spectral range, were added in the new version of GEISA. The line list contains rovibrational transitions between the ground and (010) states as well as transitions belonging to the  $\nu_2$  band. The maximum value of the rotational quantum number  $J$  was set to 22 and an intensity cut-off of 10<sup>-28</sup> cm<sup>-1</sup> / (molecule cm<sup>-2</sup>) was used for a temperature of 296 K and an isotopic abundance [23] of 3.107×10<sup>-4</sup>. In total 5813 lines were updated, including 260 lines for the first time in GEISA-2020.

The internal GEISA code for the data identification has been set to [CO9](#).

Finally, *ab initio* predictions from Kyuberis *et al.* [19] were also considered. The most abundant deuterated water species HD<sup>16</sup>O required the most extensive variational calculations. The base potential was the fitted HDO07 PES due to Yurchenko *et al.* [24]. Calculations were performed for  $J$  up to 23 but intensities were limited to transitions below 20 000 cm<sup>-1</sup>. Concerning HD<sup>17</sup>O and HD<sup>18</sup>O, isotopic abundance factors imply that only strong lines are important for atmospheric studies, which raises fewer issues with unstable intensities. For these species line lists generated by Down [25] were used (see Ref. [19] for more information). In total 67,928 lines were updated, from which 9230 lines were not referenced in GEISA-2015.

The internal GEISA code for the data identification has been set to **K19**.

### 2.1.2 CO<sub>2</sub> (molecule 2)

The GEISA-2020 carbon dioxide line list has been updated between 345.935625 and 14075.301276 cm<sup>-1</sup> based on the updated version of the CDS-296 databank [26]. Compared to the previous version of the CDS-296 [27] on which GEISA-2015 was based [1], in the new version, the  $\Delta P=9$  region for all isotopologues was updated [ $P=2V_1+V_2+3V_3$  is the polyad number ( $V_i$  being the vibrational quantum numbers)]. Moreover, in the previous version of the CDS-296, the line intensities of some asymmetric isotopologues were incorrectly recalculated from the effective dipole moment parameters of more abundant ones, and were corrected in this new version GEISA-2020. After the publication of the updated version of the CDS-296 [26], some updates were made [28] and also included in GEISA-2020. First, the line intensities for the  $\Delta P=6$  series of transitions in the <sup>16</sup>O<sup>12</sup>C<sup>18</sup>O isotopologue were recalculated using the new set of the effective dipole moment parameters. Secondly, 226 lines with  $\Delta \ell_2=4$  for the <sup>12</sup>C<sup>16</sup>O<sub>2</sub>, <sup>13</sup>C<sup>16</sup>O<sub>2</sub> and <sup>16</sup>O<sup>12</sup>C<sup>18</sup>O isotopologues were newly added, which were not available in the CDS-296 because of the used  $\Delta \ell_2 < 4$  cut-off.

The 01111-00001 band and the respective hot bands of the <sup>16</sup>O<sup>12</sup>C<sup>18</sup>O isotopologue were excluded from the last version of the CDS-296 because their effective dipole moment parameters responsible for the line intensities of these bands were fitted to the line intensities deduced from the Venus spectra obtained by the Venus Express satellite [29]. These line intensities have been considered as not sufficiently precise. Considering its importance for the astronomer's community [30], only this specific 01111-00001 band has been added to the GEISA-2020 release: the corresponding values are from the GEISA-2011 version.

All these updates are now included in GEISA-2020 and have been referenced with the identifier **P19** (J internal code parameter).

### 2.1.3 $O_3$ (molecule 3)

Due to the importance of the ozone molecule for atmospheric applications, measurements and calculations of ozone spectra undergo continuous extension and improvement [31–34] (and references therein). The current GEISA-2020 update corresponds essentially to the S&MPO-2020 version of the “Spectroscopy and Molecular Properties of Ozone” information system [35] jointly developed by Reims and Tomsk groups. The linelists were produced using effective Hamiltonian and effective transition dipole moment models derived from analyses of experimental Fourier Transform spectra in the infrared as described in [35,36].

#### (i) Main ozone isotopologue $^{16}O_3$

Eighteen bands of the main ozone isotopologue  $^{16}O_3$  were newly included in GEISA-2020. In the range between 4384 and 4826  $\text{cm}^{-1}$  the hot bands corresponding to the upper tetrad of strongly coupled vibrational states (213)/(080)/(114)/(321) were included. Cold bands of the (023)/(122)/(400) triad of interacting states (4268 – 4455  $\text{cm}^{-1}$ ) were calculated using unpublished<sup>2</sup> parameters of Barbe and Mikhailenko [37,38] available at the S&MPO web site (<https://smpo.iao.ru/transitions/params>). The resonance coupling parameters were given in the representation of ladder angular momentum components as defined in [35]. The transition moment parameters for the line intensities of the hot bands between 3564 and 3752  $\text{cm}^{-1}$  are those of Ref. [32]. The hot bands  $5\nu_3-\nu_2$ ,  $3\nu_1+\nu_2+\nu_3-\nu_2$  and  $\nu_1+4\nu_3-\nu_2$  (in the region 4128 – 4229  $\text{cm}^{-1}$ ) were calculated using Effective Hamiltonian (EH) parameters [39] and unpublished transition moment parameters obtained by Barbe [37,38]. In addition, five previously missing hot bands between 598 and 1542  $\text{cm}^{-1}$  belonging to the tetrad of interacting (002)/(101)/(030)/(200) vibrational states were added. Unpublished EH parameters of the upper states [37,38] as well as published parameters of the lower states [40–42] were used for line position calculations. Line intensity calculations used unpublished parameters for the  $2\nu_1-\nu_2$  band [37,38] and parameters of Refs. [43,44] for the  $3\nu_2-2\nu_2$ ,  $\nu_1+\nu_3-2\nu_2$ ,  $3\nu_2-\nu_1$ , and  $3\nu_2-\nu_3$  bands.

Twenty-four bands previously included in the GEISA line list between 281 and 4122  $\text{cm}^{-1}$  were updated:

– The  $\nu_3-\nu_2$  and  $\nu_1-\nu_2$  hot bands (281 – 446  $\text{cm}^{-1}$ ) were calculated using EH parameters of Flaud *et al.* [40] and dipole moment transition parameters of Birk *et al.* [45].

---

<sup>2</sup> Note: described data are mostly coming from currently unpublished work, planned to be presented in Ref. [37]. These data are also available at the S&MPO web site (<https://smpo.iao.ru>).

- Three hot bands (002)/(101)/(030) – (010) in the 1302 – 1476 cm<sup>-1</sup> range were calculated using unpublished upper state EH parameters by Barbe and Tyuterev [37,38] and the dipole moment transition parameters of S&MPO-2015. The lower state parameters were taken from [41].
- The same upper state EH parameters were used for six hot bands (002)/(101)/(200) – (001)/(100) (899 – 1235 cm<sup>-1</sup>) with the dipole moment transition parameters of [44]. The lower state parameters were taken from [40].
- Two cold bands 2ν<sub>2</sub>+ν<sub>3</sub> and ν<sub>1</sub>+2ν<sub>2</sub> (2336 – 2617 cm<sup>-1</sup>) were calculated using parameters by Barbe, Sulakshina *et al.* [46].
- The line positions of the hot (ν<sub>2</sub>+3ν<sub>3</sub>-ν<sub>2</sub> and ν<sub>1</sub>+ν<sub>2</sub>+2ν<sub>3</sub>-ν<sub>2</sub> (2899 – 3122 cm<sup>-1</sup>)) and cold (ν<sub>2</sub>+3ν<sub>3</sub> and ν<sub>1</sub>+ν<sub>2</sub>+2ν<sub>3</sub> (3584 – 3831 cm<sup>-1</sup>)) bands were calculated using EH parameters from [40,41,47]. The dipole moment parameters of [47] were used for the calculations of the line intensities of the cold bands. The intensities of the hot bands were calculated using unpublished parameters by Mikhailenko and Barbe.
- The results of a re-investigation of the spectral range from 3600 to 4300 cm<sup>-1</sup> led to a large improvement of the analysis for the strongest ν<sub>1</sub>+3ν<sub>3</sub> band in this range [32]. A recent observation of the hot band 4ν<sub>3</sub>-ν<sub>3</sub> [32] enabled to identify the strong anharmonic resonance with the “dark” 3ν<sub>1</sub>+ν<sub>2</sub> band. As the upper (310) state is also in interaction with the (211) state, it was necessary to include seven vibration states to correctly reproduce 3389 transitions with the root mean square deviation of 3.54×10<sup>-3</sup> cm<sup>-1</sup> for line positions and 1295 intensities within 8.6%. Seven calculated bands in this range were included in the compilation, for a total number of 13536 updated transitions (from which 7447 are new lines in GEISA) between 2816 and 4122 cm<sup>-1</sup>. Newly included bands are summarized in the Table 3. Figure 2 gives an overview of the added lines in the considered spectral range.

The internal GEISA code for the data described above was set to *M19*.

Band	#lines	Spectral range (cm <sup>-1</sup> )	S <sub>tot</sub> * (cm/molecule)
030 – 020	2558	598.26 – 804.86	1.928E-21
101 – 020	6	656.12 – 725.68	4.902E-25
030 – 100	20	956.13 – 1170.40	1.902E-23
030 – 001	15	957.33 – 1201.66	2.238E-24
200 – 010	102	1366.62 – 1541.76	5.267E-24
023 – 010	1355	3564.72 – 3657.05	3.650E-22
122 – 010	620	3584.75 – 3751.75	3.505E-23
400 – 010	4	3623.87 – 3653.87	6.695E-25
005 – 010	848	4128.33 – 4228.24	2.354E-23
311 – 010	1018	4129.14 – 4228.62	3.420E-23



104 – 010	66	4146.09 – 4228.28	6.265E-25
023 – 000	1192	4268.37 – 4357.21	1.914E-22
122 – 000	724	4284.15 – 4454.93	4.328E-23
400 – 000	8	4325.56 – 4398.58	5.854E-25
213 – 100	63	4384.72 – 4423.50	1.407E-24
321 – 100	126	4429.78 – 4466.82	5.709E-24
114 – 001	306	4452.15 – 4508.72	1.304E-23
213 – 010	503	4757.08 – 4825.80	2.329E-23
<b>Total</b>	<b>9534</b>	<b>598.26 – 4825.80</b>	<b>2.6928E-21</b>

\*: Line intensities are given for 99.29%  $^{16}\text{O}_3$  abundance.

**Table 3.** The list of new  $^{16}\text{O}_3$  ozone bands in the GEISA-2020 release. #lines: Number of transitions,  $S_{\text{tot}}$  is the sum of the line intensities.

Recent *ab initio* calculations by Tyuterev *et al.* [31], using the dipole moment functions of [48], have suggested that absolute intensities of the strongest bands in most of spectroscopic databases [1,2,35] should be corrected to achieve the consistency between microwave and infrared 5  $\mu\text{m}$  and 10  $\mu\text{m}$  spectral ranges. The recommended intensity scaling corrections with respect to the HITRAN2016 data were +3%, +3% and +3.5% for the dominant rotational,  $\nu_3$  and  $\nu_1+\nu_3$  bands. These corrections have been found in agreement [31] with accurate Stark-effect measurements and the JPL catalogue based on these measurements in the microwave, as well with the most recent infrared FTS measurements by Barbe *et al.* [31], and by Jacquemart *et al.* (unpublished data) for 5  $\mu\text{m}$  and 10  $\mu\text{m}$ . This was also consistent with DRL FTS measurements in the 10  $\mu\text{m}$  range reported by Wagner *et al.* (unpublished data) within less than 1% for strong lines. The GEISA-2015 data being somewhat different from HITRAN2016, particularly in the 5  $\mu\text{m}$  range, the *ab initio* scaling factors of [31] with respect to GEISA-2015 were thus adapted to the three corresponding strongest bands as given in #: internal data identification set to [T19](#)

**Table 4.**

Spectral Region	Band	Intensity scaling factor with respect to GEISA- 2015	Nb. affected lines <sup>#</sup>
Microwave	000-000	1.030	5493
10 $\mu\text{m}$	001-000	1.027	7498
5 $\mu\text{m}$	101-000	1.015	6878

<sup>#</sup>: internal data identification set to [T19](#)

**Table 4.** Scaling factors applied to  $^{16}\text{O}_3$  intensities and number of affected lines in GEISA-2020 for the three spectral regions considered.



In total, 81773 (sum of **M19** and **T19**) transitions of  $^{16}\text{O}_3$  were inserted in GEISA-2020 that correspond to the integrated absorption (sum of line intensities)  $S_{\text{tot}} = 1.5983\text{E-}17$  cm/molecule at 296 K.

(ii) *Ozone isotopic species*

A significant update was also carried out for the ozone isotopologues  $^{16}\text{O}^{16}\text{O}^{18}\text{O}$ ,  $^{16}\text{O}^{16}\text{O}^{17}\text{O}$ , and  $^{16}\text{O}^{17}\text{O}^{16}\text{O}$ , using linelists obtained from the analyses of Reims FTS spectra [49,50] with the internal data identification set to **T19**.

For the asymmetric  $^{18}\text{O}$  enriched isotopologues  $^{16}\text{O}^{16}\text{O}^{18}\text{O}$  the 49148 lines of thirteen bands in the spectral range  $961 - 3164 \text{ cm}^{-1}$  are concerned by these changes with the integrated band intensity (sum of all lines)  $S_{\text{tot}} = 6.101 \times 10^{-20}$  cm/molecule at 296 K for the natural isotopic abundance [35]. Six bands are new with respect to GEISA-2015: these are  $2\nu_2$  and the second dyad bands  $\nu_2 + \nu_3 / \nu_1 + \nu_2$  in the range  $1342 - 1894 \text{ cm}^{-1}$ , as well as  $3\nu_3 / \nu_1 + 2\nu_3 / 2\nu_1 + \nu_3$  in the range  $2930 - 3164 \text{ cm}^{-1}$ . The contributions for new bands of 668 are collected in Table 5.

Band	#lines	Spectral range ( $\text{cm}^{-1}$ )	$S_{\text{tot}}^*$ (cm/molecule)
020 – 000	505	1342.895 – 1398.807	7.706E-25
011 – 000	2474	1644.367 – 1720.541	2.033E-22
110 – 000	4188	1663.383 – 1894.671	6.376E-23
003 – 000	1562	2930.525 – 3011.532	4.316E-22
102 – 000	3241	2965.774 – 3123.188	1.221E-22
201 – 000	1940	3103.035 – 3164.883	3.782E-23

\* Line intensities are given for the natural abundance of 0.00398194.

**Table 5.** New bands of ozone  $^{16}\text{O}^{16}\text{O}^{18}\text{O}$  species [50] in GEISA-2020. #lines: Number of transitions,  $S_{\text{tot}}$  is the sum of the line intensities.

Another seven bands of  $^{16}\text{O}^{16}\text{O}^{18}\text{O}$  were updated with respect to the previous GEISA release. This includes the first dyad  $\nu_1/\nu_3$  ( $961 - 1187 \text{ cm}^{-1}$ ) and the first triad bands  $2\nu_3/\nu_1 + \nu_3/2\nu_1$  ( $1897 - 2274 \text{ cm}^{-1}$ ), where the resonance interaction parameters have been predicted by contact transformation method using MOL\_CT code [51] from the potential energy surface in order to separate resonance contributions in the A-type and B-type sub-bands [50]. The line position and intensity values were updated for 4076 transitions of cold  $\nu_1 + \nu_2 + \nu_3$  ( $2701 - 2767 \text{ cm}^{-1}$ ) and of hot  $\nu_1 + \nu_2 + \nu_3 - \nu_2$  ( $2015 - 2084 \text{ cm}^{-1}$ ) bands.

Four bands of  $^{17}\text{O}$  enriched species were updated according new analyses of Ref. [49]. For the asymmetric  $^{16}\text{O}^{16}\text{O}^{17}\text{O}$  isotopologue 2135 transitions of the  $\nu_1 + \nu_3$  ( $2045 - 2121 \text{ cm}^{-1}$ ) were updated, whereas for the symmetric  $^{16}\text{O}^{17}\text{O}^{16}\text{O}$  species 2148 transitions of two

fundamentals  $\nu_1/\nu_3$  ( $968 - 1054 \text{ cm}^{-1}$ ) and the strongest combination band  $\nu_1+\nu_3$  ( $2029 - 2101 \text{ cm}^{-1}$ ) were updated. The integrated absorption of these inserted lines of  $^{17}\text{O}$  enriched species corresponds to  $S_{\text{tot}} = 5.768\text{E-}21 \text{ cm/molecule}$  at 296 K for a sample in the natural isotopic abundance.

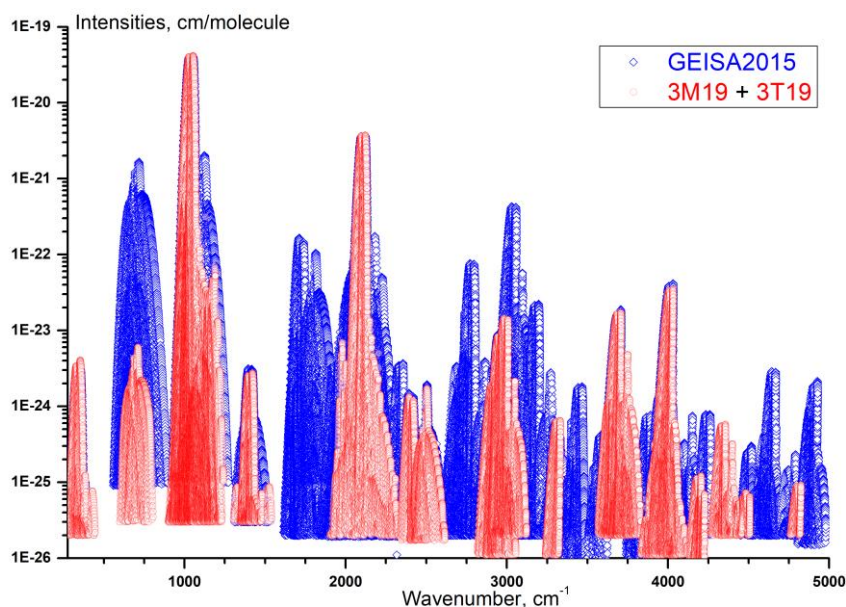


**Figure 2:** Overview of the updated  $^{16}\text{O}_3$  lines added to GEISA 2020 (red circles), compared to the previous  $\text{O}_3$  linelist of GEISA2015 (blue diamonds).

#### 2.1.4 $\text{N}_2\text{O}$ (molecule 4)

Since GEISA-2011 (no update in the GEISA-2015 version), two contributions have been studied. The first one comes from the work of Tashkun *et al* [52,53]. This update concerns lines with intensities at least 3 orders of magnitude lower than those in the former database. With such low values of the intensities, it is difficult to make an evaluation of the line list with the SPARTE chain. Combined to the fact, as mentioned in HITRAN 2016, that “*For the line intensities from these line lists, the uncertainty code 3 (> 20%) is adopted.* », we have decided not to retain these data for GEISA-2020 and to wait for eventual new data in 2021.

Finally, only a small update has been performed: line intensities, Einstein-A coefficients, self- and air-induced broadening parameters of the R-branch lines of the  $00^0_2-00^0_0$  band of  $^{14}\text{N}^{14}\text{N}^{16}\text{O}$  have been updated using the values in references [54], [55] and [56]. This represents 41 lines between  $4418.201960$  and  $4439.791160 \text{ cm}^{-1}$ . For all these lines, the pressure shift parameters were kept unchanged from the former version of GEISA.

The corresponding internal code J has been set to [L19](#).

### 2.1.5 CO (molecule 5)

The new CO line list originates from the work of Li *et al.* [57]. In this paper, a small incompatibility issue between the definition of potential curve parameters in the LEVEL 8.0 program [58] and in the work of Coxon *et al.* [59] causes drifts in line positions of up to 0.03 cm<sup>-1</sup> for high  $J$  lines of the high overtone and hot bands. As discussed by Medvedev *et al.* [60][61], using CO as an example, the intensities of Li *et al.* initially dropped with the wavenumber exponentially as they should. However, after that plateau-like structures in dipole moment curve, their intensity calculations started to generate very small intensities ( $<10^{-40}$  cm. molecule<sup>-1</sup>), which suggested artefacts in their dipole at very high vibrational excitations. Therefore, applying an intensity cutoff was necessary. This issue has been fixed, and the calculated line positions now agree very well with the experimental values. A few other minor changes to the original Li *et al.* line list [57] have been discussed and described in HITRAN2016 paper [2] and are also adopted here, resulting in an identical CO line list between HITRAN2016 and GEISA-2020. It corresponds to a total of 5381 lines updated between 3.401910 and 14477.377142 cm<sup>-1</sup>, of which 1470 are new lines.

The internal GEISA code for the data identification has been set to [L19](#).

### 2.1.6 CH<sub>4</sub> (molecule 6)

The new list of CH<sub>4</sub> lines in the 5300-5850 cm<sup>-1</sup> range of the tetradecad, based on the work of Nikitin *et al.* [62]-[63], contains more than 15000 transitions, a significant part of which includes quantum identifications. Line positions and intensities have been retrieved by non-linear least square curve-fitting procedures from observed spectra recorded for different temperatures and pressures. The spectra in the 5695-5859 cm<sup>-1</sup> range [62] were recorded in Grenoble (France) at room temperature and 80K, by differential absorption spectroscopy (DAS) with a noise equivalent absorption of about  $\alpha_{\min} \approx 1.5 \times 10^{-7}$  cm<sup>-1</sup> (except the 5718.8-5724.25 and 5792.36-5814.29 cm<sup>-1</sup> intervals). In the 5300- 5695 cm<sup>-1</sup> range [64] [63], long path (202, 602, 1604 and 1804 m) room temperature spectra of natural methane samples at different pressures were recorded with a Fourier transform spectrometer in Reims (France). One cold spectrum of enriched <sup>12</sup>CH<sub>4</sub> at 80 K has been recorded in Jet Propulsion Laboratory (JPL, Pasadena, USA). This spectrum was useful for low- $J$  line positions. Another cold spectrum at 80 K of enriched <sup>13</sup>CH<sub>4</sub> from JPL was used to identify the isotopic species lines. Quantum assignments were made using the effective Hamiltonian based on high order contact transformation [65] and the effective dipole moment expressed in terms of irreducible tensor operators adapted to spherical top molecules. Self-broadening and air-broadening coefficient from [66,67] were added to the

final line list. In total, 8192 lines have been updated between 5300.147847 and 5849.825960  $\text{cm}^{-1}$ .

The corresponding internal code J has been set to [N19](#).

New data for  $^{13}\text{CH}_4$  in the  $2\nu_3$  band were also implemented, based on the work of Starikova *et al.* [68]. This line list was generated using the line list retrieved from DAS spectra recorded at 80 K and room temperature. Assignments were transferred from the cold spectrum analysis of Ref. [68]. The broadening coefficients were calculated according to the methodology used for the GOSAT project [66,67]. When no quantitative information was determined, a default value of the lower energy level of  $-0.9999 \text{ cm}^{-1}$  is given (cf. Appendix B) while corresponding default values for the air- and self- broadening coefficients are  $0.08100 \text{ cm}^{-1}\text{atm}^{-1}$  and  $0.06030 \text{ cm}^{-1}\text{atm}^{-1}$ , respectively, and an air-shifting coefficient of  $-0.012 \text{ cm}^{-1}\text{atm}^{-1}$  is adopted. 7195 lines have thus been updated between 5853.282300 and 6200.882900  $\text{cm}^{-1}$ .

The corresponding internal code J has been set to [S19](#).

### 2.1.7 $\text{O}_2$ (molecule 7)

No major update was made for the  $\text{O}_2$  molecule, the main reason being that recent studies mainly considered non-Voigt profiles for the line-shape determination. However, the work from Tran *et al.* [69] in the  $a^1\Delta_g - X^3\Sigma_g^- (0 - 0)$  band of  $\text{O}_2$  centered at  $1.27 \mu\text{m}$ , and tested by comparison with high-resolution ground-based atmospheric TCCON measurements, highlighted systematic errors using air-broadened line-shift parameters from the GEISA-2015 or HITRAN 2016 databases. Therefore, we decided to partially update the GEISA-2020 database, considering only the new line intensities, line positions and air-broadened line-shift parameters determined in the work of Tran *et al.* [70] (cf. section 3.1.2 for an illustrative validation of these  $\text{O}_2$  data using TCCON measurements). Parameters for 223 air-broadened transitions, from  $7784.797157$  to  $7915.856072 \text{ cm}^{-1}$ , were retrieved from spectra measured by a cavity ring down spectrometer referenced to a frequency comb, for a large range of pressure values, from 6.7 to 94 kPa (50 to 700 Torr). The data published in the work of Tran *et al.* were originally determined using the quadratic speed dependent Nelkin-Ghatak (qsdNG) profile, but for the GEISA-2020 update (which is currently limited to Voigt profile parameters) the authors also refitted these lines using Voigt profiles from which the new air-broadened line-shift parameters are derived (unpublished data).

The corresponding internal code J has been set to [T19](#).

### 2.1.8 $SO_2$ (molecule 9)

The  $^{32}S^{16}O_2$  empirical list is mainly based on the experimental energy levels recently derived in [71] and variational intensities presented in [72]. In addition to experimental energy levels derived in [71], the new experimental energy levels obtained from the analysis of Fourier transform spectra of  $SO_2$  by ExoMol [73] were also used. In parallel with pure experimental energy levels, the predicted energy levels obtained from the effective Hamiltonian calculations performed in [71] were used for evaluation of the line positions.

Most part of the line positions (63%) have an estimated accuracy between 0.0001 and 0.001  $cm^{-1}$  in accordance with the uncertainties of the corresponding experimental energy levels reported in [71]. For 185,637 transitions (34%) derived from the calculated energy levels the positions accuracy corresponds to the 0.001 - 0.01  $cm^{-1}$  error range. In case of the (110)-(000), (011)-(000), (101)-(000), (111)-(010) bands the calculated intensities [72] are substituted by the recent experimental data [74],[75] when available. We estimate the quality of variational intensities as 5-10% on average.

The resulting empirical list of  $^{32}S^{16}O_2$  transitions was compared both with the HITRAN 2016 database and a recent study [76] performed by the AMES group at NASA where the similar empirical lists for  $SO_2$  isotopologues have been reported based on the experimental energy levels [71] and new variational calculations. Disagreements between GEISA and HITRAN's line positions amount up to 0.01 - 0.16  $cm^{-1}$  for 3308 lines. The calculated intensities [72] adopted in our empirical list also may differ from the HITRAN data by up to 40% for relatively strong lines and disagree by up to 60 -100% for weakest lines. A comparison of our list with HITRAN and AMES data [76] is shown in Figure 3 (note that HITRAN2016 and GEISA-2015 line lists are comparable, so only HITRAN2016 is plotted, as in the original publication). It is obvious from the figure that the presently generated empirical list for  $^{32}S^{16}O_2$  molecule includes a considerably large number of lines, including very strong ones (up to  $5E^{-20}$   $cm/molecule$ ). Air-broadening coefficients were set to a default value of 0.11  $cm^{-1}/atm$ , as in previous versions of GEISA. In total 549,200 lines have been added or updated between 0.035669 and 4159.945167  $cm^{-1}$

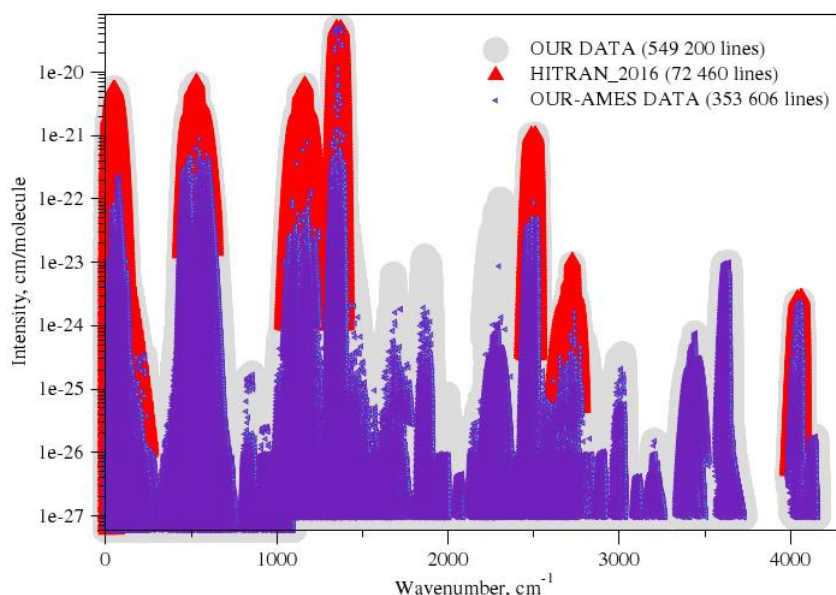


**Figure 3:** Comparison of the new empirical list for  $^{32}\text{S}^{16}\text{O}_2$  molecule with the HITRAN 2016 (comparable to GEISA-2015 line list) and Ames [76] data.

The internal GEISA codes for the data identification have been set to:

- **1N9**: positions are determined from the upper and lower experimental energy levels, intensities are calculated (variational) from [72].
- **2N9**: positions are determined from the upper and lower experimental energy levels, intensities are experimental from [74].
- **3N9**: positions are determined from the upper and lower experimental energy levels, intensities are experimental from [75].
- **4N9**: one of the two energy levels (or both) used for position determination is predicted by the effective Hamiltonian calculation, intensities are calculated (variational) from [72].
- **5N9**: pure experimental value is taken for most accurate position.

### 2.1.9 $\text{NO}_2$ (molecule 10)

For nitrogen dioxide the previous GEISA compilation included over 100,000  $^{14}\text{N}^{16}\text{O}_2$  lines covering 0–3074  $\text{cm}^{-1}$ . The new list includes 185,965 lines and covers the 0-4776  $\text{cm}^{-1}$  spectral range. This new list includes lines from both the  $^{14}\text{N}^{16}\text{O}_2$  and  $^{15}\text{N}^{16}\text{O}_2$  isotopic species.

In two recent studies [77], [78], a list of line positions, line intensities and line shape parameters of  $\text{NO}_2$  covering the 0 to 4776  $\text{cm}^{-1}$  spectral range was generated. Except for the far infrared and the 13.3  $\mu\text{m}$  regions, all bands in all spectral regions are significantly affected by this update. For the 6.2  $\mu\text{m}$  and 3.4  $\mu\text{m}$  spectral regions, the new list involves the main cold bands ( $\nu_1$ ,  $2\nu_2$  and  $\nu_3$  and  $\nu_1 + \nu_3$ , respectively) together with their associated first hot bands (originating from the (0,1,0) first vibrational state), and, whenever possible, hot bands



(involving the (1,0,0), (0,2,0) and (0,0,1), (1,1,0), (2,0,0) or (0,0,2) states as lower states). Also several weak cold bands ( $\nu_1 + \nu_2$ ,  $\nu_2 + \nu_3$ ,  $2\nu_1$ ,  $2\nu_2 + \nu_3$ ,  $2\nu_3$ ,  $2\nu_2 + \nu_3$ ,  $\nu_1 + \nu_2 + \nu_3$ ,  $2\nu_1 + \nu_3$ , and  $3\nu_3$ ) were added for the first time in the GEISA database. Finally we included the  $\nu_3$  [79] and  $\nu_1 + \nu_3$  [80] bands for  $^{15}\text{N}^{16}\text{O}_2$  which is the second most abundant isotopologue of  $\text{NO}_2$  [23]. These new lists were generated using existing literature line positions or intensity parameters. When necessary, these parameters were updated using experimental data issued from high resolution Fourier transform spectra recorded at SOLEIL at 296K for this purpose [77], [78]. Also, the line broadening parameters were computed using the line shape parameters achieved for the  $\nu_3$  band by Benner *et al.* [81].

Figure 4 gives an overview of cross sections calculated from the list of  $\text{NO}_2$  line parameters in GEISA-2020 for the 1000-4780  $\text{cm}^{-1}$  spectral range and compares it to the status of HITEMP-2019 [82] and of HITRAN-2016 or GEISA-2015 (old GEISA).

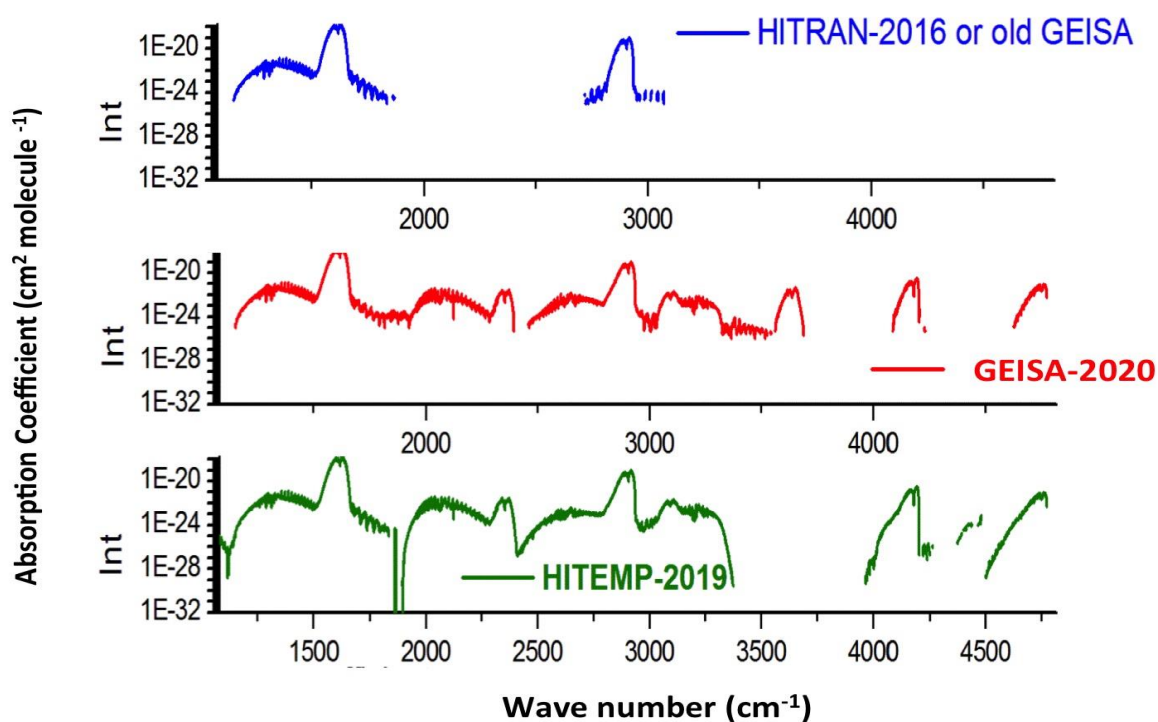


**Figure 4:** Calculated absorption cross sections of  $\text{NO}_2$  at 296 K using line lists from HITRAN-2016/GEISA-2015 (old GEISA), HITEMP-2019 and GEISA-2020.

The validation of this new update, which concerns the 1153- 4776  $\text{cm}^{-1}$  region, was performed through a careful comparison between computed and observed spectra using laboratory spectra recorded either during recent investigations [78], [77] or during previous analyses of the literature (see Refs. [78], [77] for detailed references). In parallel, similar inter comparisons at  $T=296\text{K}$  were also performed using the most recent versions (HITRAN-2020 and HITEMP-2019) of the HITRAN and HITEMP databases [82]. The results of these investigations prove

that, for each vibrational bands, the individual lines in GEISA-2020 are more precise than those included in HITRAN-2020 or HITEMP-2019 (or those of previous versions). Concerning the number of vibrational bands, the GEISA linelist is also more extended than HITRAN-2020, but less than HITEMP-2019 which is generated for hot temperature conditions and includes lines involving very high rotational quantum numbers (up to  $N=100$ ) and a significant number of additional hot bands when compared to GEISA-2020. In total 185965 lines were added or updated in the  $0.497999 - 4775.314437 \text{ cm}^{-1}$  spectral range.

The internal GEISA code for the data identification has been set to **P19**.

#### **2.1.10 $\text{NH}_3$ (molecule 11)**

GEISA-2020 includes, for the first time, a line list at  $3.0 \mu\text{m}$  for the first-most abundant isotopologue of ammonia,  $^{14}\text{NH}_3$ . The  $2\nu_4$  vibrational band for this isotopologue was added using a high resolution Fourier transform investigation performed at  $3.0 \mu\text{m}$  by Maaroufi *et al.* [83]. Absolute line intensities and self-broadening and shift coefficients were measured at room temperature, for rovibrational lines ranging from  $1 \leq J \leq 11$  and  $0 \leq K \leq 11$ , and located in the spectral range  $3078.80407 - 3532.50519 \text{ cm}^{-1}$ . This represents a total of 298 entries. The lines were fitted with a single spectrum non-linear least squares fitting procedure with a Voigt profile suited to fit the experimental line shapes without the need of considering line mixing effects, in the pressure range used. Mean accuracies of the measurements are estimated to  $\pm 4\%$  for line intensities and self-broadening coefficients and to  $\pm 13\%$  for self-shift coefficients.

The  $J$  and  $K$  dependences of the self-broadening coefficients ( $\gamma_0$ ) were observed and modeled using an empirical polynomial expression suggested by Nemtchinov *et al.* [84]:

$$\gamma_0(m, K) = \beta_0 + \beta_1 m + \beta_2 K + \beta_3 m^2 + \beta_4 K^2 + \beta_5 mK$$

where  $m = | -J, J, J+1 |$  for  $P, Q$  and  $R$  branches, and  $\beta_i$  are the polynomial coefficients. The polynomial expression reproduced the observed self-broadening coefficients within an average accuracy of 9.6% for the  $2\nu_4$  band of  $^{14}\text{NH}_3$  [83]. In total, 298 lines were added or updated between  $3078.804070$  and  $3532.505190 \text{ cm}^{-1}$ .

The internal GEISA code for the data identification has been set to **M19**.

#### **2.1.11 $\text{PH}_3$ (molecule 12)**

The  $\text{PH}_3$  line list in the  $2733\text{-}3660 \text{ cm}^{-1}$  range is based on an improved analysis of positions and intensities of phosphine spectral lines from Nikitin *et al.* [85]. Some 5768 positions and 1752



intensities have been modeled with RMS deviations of  $0.00185 \text{ cm}^{-1}$  and 10.9%, respectively. Based on an *ab initio* potential energy surface, the full Hamiltonian of phosphine nuclear motion was reduced to an effective Hamiltonian using a high-order Contact Transformations method adapted to polyads of symmetric top  $AB_3$ -type molecules with a subsequent empirical optimization of parameters. The line list also contains more than 2000 new ro-vibrational assignments for all 13 vibrational octad sublevels. A comparison of this line list with experimental spectra of PNNL [86] showed that the new set of line parameters from this work permits better simulations of observed cross-sections than GEISA-2015 or HITRAN 2016 linelists. Vibrational assignments were also added to current the GEISA line list. In total 18283 lines were added or updated between  $2733.587100$  and  $3659.265700 \text{ cm}^{-1}$ .

The internal GEISA code for the data identification has been set to [N19](#).

### 2.1.12 $HNO_3$ (molecule 13)

A new investigation of laboratory spectra of nitric acid in the  $7.6 \mu\text{m}$  region was performed using a suitable theoretical model which involves six interacting states, instead of two in the previous computation [87]. In this way, an improved set of line positions and intensities have been generated for the  $7.6 \mu\text{m}$  spectral region. This new list, which includes also the  $\nu_3+\nu_9-\nu_9$  for the first time was validated using atmospheric spectra recorded by the Michelson Interferometer for Passive Atmospheric Sounding (MIPAS) limb emission radiances in the 11 and  $7.6 \mu\text{m}$  domains [88]. Table 6 describes the new list for  $HNO_3$  and compares with the list included in GEISA-2015. In total 87906 lines have been added or updated between  $1233.107220$  and  $1395.679470 \text{ cm}^{-1}$ . Note that the GEISA-2015 line list was largely extrapolated to high- $J$  value lines, characterized by significant uncertainties; we chose to limit the extrapolation for the GEISA-2020 list, explaining the reduction of the number of lines in the  $\nu_3$  and  $\nu_4$  bands.

**Table 6:**  $HNO_3$  line parameters in the  $7.6 \mu\text{m}$  region [#lines is the number of lines,  $\sigma_{\min}$  and  $\sigma_{\max}$  ( $\text{cm}^{-1}$ ) are the lower and upper limits,  $S_{\min}$  and  $S_{\max}$  are the smallest and largest line intensity ( $\text{cm}^{-1}/\{\text{molecule cm}^2\}$  at 296 K) and  $S_{\text{tot}}$  is the sum of the line intensities]

Band	#lines	$S_{\text{tot}}$ ( $10^{-18}$ )	$\sigma_{\min}$	$\sigma_{\max}$	$S_{\min}$ ( $10^{-25}$ )	$S_{\max}$ ( $10^{-21}$ )
<b><i>GEISA-2020 database</i></b>						
$\nu_3$	16408	24.94	1252.010	1387.081	4.910	32.0

$\nu_4$	18105	9.834	1238.929	1387.561	4.020	21.4
$2\nu_6$	2451	0.1194	1243.465	1348.275	4.624	3.660
$\nu_5+\nu_9$	13817	0.7163	1246.929	1390.071	2.081	3.543
$\nu_7+\nu_8$	11125	0.7615	1246.422	1395.679	2.314	5.017
$3\nu_9$	13894	1.177	1233.107	1388.497	4.582	2.378
Sum		37.55				
$\nu_3+\nu_9-\nu_9$	12106	1.408	1271.050	1394.899	5.285	1.798
<b><i>GEISA-2015 database</i></b>						
$\nu_3$	21308	25.37	1098.376	1387.849	1.037	31.33
$\nu_4$	19584	12.78	1229.867	1387.561	1.037	18.67
Sum		38.15				

The Internal GEISA code for these data identification has been set to [P19](#).

### **2.1.13 Hydrogen Halides HF, HCl, HBr, HI (resp. molecule 15, 16, 17 and 18)**

The new hydrogen halides line lists originate from refs. [89] and [90], with higher overtone bands removed due to abnormalities when intensities were extrapolated outside of experimental temperature and pressure ranges – the latter being particularly important for HCl which is known to have intensity depletion effects at higher pressures due to collisions induced effects. For the first time in GEISA, deuterated isotopologues of hydrogen halides  $D^{19}F$ ,  $D^{35}Cl$ ,  $D^{37}Cl$ ,  $D^{79}Br$ ,  $D^{81}Br$ , and  $D^{127}I$  have been implemented. Except for the 2-0 band of HCl, the HX line lists are identical to those in HITRAN2016. For P10 to R10 lines of the HCl 2-0 band, line intensities, Einstein A-coefficients and self-induced broadenings have been updated with reference [91], whilst air-induced broadenings and shifts have been updated with reference [92]. The following spectral ranges were updated in GEISA-2020 for the four species: 13.620106 - 32351.592077  $cm^{-1}$  for HF (20010 lines), 5.341824 - 20231.245131  $cm^{-1}$  for HCl (53252 lines), 7.656152 - 16033.492029  $cm^{-1}$  for HBr (8980 lines) and 5.887799 - 13907.688695  $cm^{-1}$  for HI (4751 lines).

The Internal GEISA code for these data identification has been set to [L19](#).

### **2.1.14 OCS (molecule 20)**

The 5 $\mu m$  spectral region is used to monitor OCS [93], which is the most abundant sulfur reservoir species in the Earth atmosphere. In the last years, Cavity Ring Down Spectroscopy

made the near infrared spectral range more and more attractive, especially for the in situ detection of trace gases [94].

Firstly, the line list used in the HITRAN2016 database [2] has been adopted in the new GEISA-2020 release. This line list was derived from Fourier transform spectra of OCS recorded in the 6170 – 6680  $\text{cm}^{-1}$  (dominated by the  $3\nu_1+2\nu_3$  band) and 7700 – 8160  $\text{cm}^{-1}$  (dominated by the  $2\nu_1+3\nu_3$  band) spectral ranges using a femto/OPO laser absorption source and cavity enhanced spectroscopy [95]. It contains 3670 lines in the ranges 6484 – 6660  $\text{cm}^{-1}$  and 7728 – 7821  $\text{cm}^{-1}$ . The accuracies of the line positions and intensities (parameters A' and B', see Appendix B) have been estimated to be at best 0.001  $\text{cm}^{-1}$  and 10 to 20%, respectively. In total 3670 lines were added or updated in the 6484.533500 - 7821.108700  $\text{cm}^{-1}$  spectral range.

The Internal GEISA code for these data identification has been set to [A16](#).

Secondly, 104 new spectroscopic line parameters for the main isotopologue  $^{16}\text{O}^{12}\text{C}^{32}\text{S}$  have been included in GEISA-2020. The update focuses on the broadening and shift coefficients in the  $4\nu_2$  band of OCS perturbed by  $\text{N}_2$ ,  $\text{O}_2$  and Air, measured and calculated at room temperature, in the spectral region 2087.4280 - 2130.7584  $\text{cm}^{-1}$ . These data, which were derived from high resolution Fourier transform spectra, are rather accurate: the uncertainties can be estimated to be ~ 3% for the broadening coefficients and ~ 10% for the shift coefficients [96]. In addition, theoretical calculations of broadening and line shift coefficients were performed, using the semi classical Robert and Bonamy formalism that reproduces fairly well the experimental quantum number dependence,  $m$ , for the  $\text{N}_2$  and  $\text{O}_2$  broadening coefficients.

The Internal GEISA code for these data identification has been set to [G19](#).

#### **2.1.15 $\text{C}_2\text{H}_6$ (molecule 22)**

As forecasted in GEISA-2015, the data from Moazzen-Ahmadi *et al.* [97] have been incorporated in GEISA-2020, with no further update since the data set listed in HITRAN 2016 [2]. To sum up, 11938 lines were added or updated between 225.044600 and 320.966100  $\text{cm}^{-1}$ .

The internal GEISA code for these data identification has been set to [M19](#).

#### **2.1.16 $\text{C}_2\text{H}_2$ (molecule 24)**

The GEISA-2020 list of acetylene has been significantly extended compared to the GEISA-2015 version [1] (see Figure 5). The changes concern four spectral regions. Three line lists in

the far-infrared and infrared domains ( $\Delta P = 0$  between 13 and 248  $\text{cm}^{-1}$ ,  $\Delta P = 1$  between 389 and 893  $\text{cm}^{-1}$  and  $\Delta P = 6$  between 3738 and 3993  $\text{cm}^{-1}$ ) were generated based on the global model developed by Lyulin and Perevalov [98][99]. Here  $P$  is a polyad number defined as  $P = 5V_1 + 3V_2 + 5V_3 + V_4 + V_5$  where  $V_i = 1-5$  are the main quantum numbers of the  $\text{C}_2\text{H}_2$  harmonic oscillator. The prediction capability of the model in the  $\Delta P = 0,1$  regions was investigated experimentally in [100,101] leading to line lists of calculated positions and intensities for the  $\Delta P = 0$  region (5479 transitions) and for the  $\Delta P = 1$  region (41021 transitions). A complete description of the line lists in  $\Delta P = 0$  and 1 regions can be found in [100,101]. For the  $\Delta P = 6$  region around 3900  $\text{cm}^{-1}$ , the strong Q branch around 3882  $\text{cm}^{-1}$  as well as other weaker structures were missing in GEISA-2015. The two strong cold bands already present in GEISA have been updated and eight bands have been added based on the global model [98][99] for line positions and intensities. A summary of updated/included bands is given in Table 7. Note that the vibrational assignment from the global model [98][99] (linear combination of vibrational basis functions) has been reformulated in order to have a unique vibrational assignment for a series of rotational transitions.

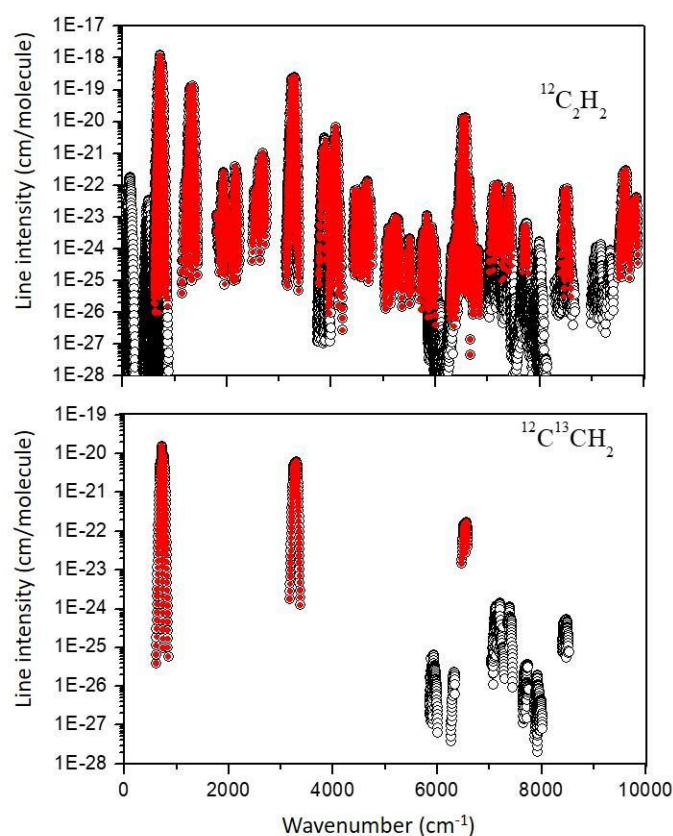


**Figure 5:** Overview of the GEISA-2015 (solid red circles) and GEISA-2020 (open black circles) databases for acetylene  $^{12}\text{C}_2\text{H}_2$  and  $^{12}\text{C}^{13}\text{CH}_2$  isotopologues.

The fourth line list is the empirical database (EDB17, hereafter) elaborated by Lyulin and Campargue [102] for the wide 5850-9415  $\text{cm}^{-1}$  near-infrared region. The EDB17 covers the

range of the  $\Delta P = 9$ -14 series excluding the 6341-7000  $\text{cm}^{-1}$  interval roughly corresponding to the  $\Delta P = 10$  series. The EDB17 was constructed by gathering results of three studies by Fourier transform spectroscopy [103–105] and three studies by cavity ring down spectroscopy (CRDS) [106–108]. In the regions of low absorption, the sensitivity of the CRDS technique enabled the detection of weak lines with intensities on the order of  $10^{-29}$   $\text{cm}/\text{molecule}$ . The assignment of the experimental spectra relies in great part on the predicted data of the Acetylene Spectroscopic Databank (ASD) [99]. For each branch of a given band, the line positions and line intensities were calculated for all the transitions up to a maximum  $J$  value exceeding by 1 the largest  $J$  value of the observations in the considered branch. Such an approach enabled smoothing the measurement errors, completing the experimental line list by interpolation and extending slightly beyond the observations. Compared to the HITRAN2016 [2] and GEISA-2015 [1] lists in the region, the number of bands and lines was increased by more than a factor of ten (see Figure 5). As a result, the EDB includes a total of 10973 lines belonging to 146 bands of  $^{12}\text{C}_2\text{H}_2$  and 29 bands of  $^{12}\text{C}^{13}\text{CH}_2$ . For comparison the GEISA-2015 database in the same region includes 869 lines of 14 bands, all belonging to  $^{12}\text{C}_2\text{H}_2$ .

For all  $^{12}\text{C}_2\text{H}_2$  and  $^{12}\text{C}^{13}\text{CH}_2$  isotopologues, the vibrational assignment has been changed to V1 V2 V3 V4 V5  $\ell_4$   $\ell_5$  from V1 V2 V3 V4 V5  $\ell$ , where  $\ell$  is the sum of  $\ell_4$  and  $\ell_5$ . Indeed, the  $\ell_4$  and  $\ell_5$  quantum numbers are necessary to assign the various bands that include strong resonance interactions between ro-vibrational states [100–108] used to update the GEISA-2020 database. Based on the new vibrational assignment and the symmetry E/F of the rotational levels, the symmetries +/- have been generated for all transitions of both isotopologues, and symmetry u/g have been generated only for symmetric  $^{12}\text{C}_2\text{H}_2$  isotopologue. For all transitions, Einstein-A coefficients have been calculated from line intensities at 296 K using Eq. 20 of [109], state-independent weight  $g_i = 1$  and 8 respectively for  $^{12}\text{C}_2\text{H}_2$  and  $^{12}\text{C}^{13}\text{CH}_2$  isotopologues, and state-dependent weight  $g_s = 1$  or 3 for  $^{12}\text{C}_2\text{H}_2$  (depending on symmetries) and  $g_s = 1$  for  $^{12}\text{C}^{13}\text{CH}_2$ . Total internal partition functions [110] equal to 412.45 and 1656.2 at 296 K have been used for the  $^{12}\text{C}_2\text{H}_2$  and  $^{12}\text{C}^{13}\text{CH}_2$  isotopologues respectively. Smoothed values of air-broadening coefficients (Table 5 of [111]) already in previous GEISA editions have been used for new entries since no vibrational dependence of the widths is observed.

Vibrational Assignment		#lines	$\sigma_{min}$	$\sigma_{max}$	$S_{tot}$	$S_{min}$	$S_{max}$	$J_{min}$	$J_{max}$	
Upper	Lower									
00110 1 0	00000 0 0	155	3738.098	3995.170	5.96E-20	1.3E-27	3.0E-21	0	53	GEISA-2015
01031 3-1	00010 1 0	263	3744.789	3968.111	5.80E-21	1.0E-27	1.4E-22	1	49	
01022 2-2	00001 0 1	251	3749.044	3958.870	1.18E-21	1.2E-27	3.6E-23	1	45	
01021 2-1	00000 0 0	153	3752.906	3980.295	5.54E-20	1.2E-27	2.7E-21	0	53	GEISA-2015
01022 2 0	00001 0 1	220	3756.621	3962.215	1.31E-21	1.2E-27	3.7E-23	1	45	
00120 2 0	00010 1 0	250	3770.399	3983.995	5.76E-21	1.2E-27	1.5E-22	1	48	
00111 1 1	00001 0 1	240	3772.294	3979.654	2.03E-21	1.3E-27	5.6E-23	1	45	
00111 1-1	00001 0 1	233	3780.389	3974.747	1.63E-21	1.2E-27	3.8E-23	1	46	
01031 1-1	00010 1 0	205	3794.438	3976.946	3.58E-21	1.4E-27	2.4E-22	1	40	

**Table 7:** Summary of bands updated or included in GEISA-2020 in the  $\Delta P = 6$  region. The first column corresponds to the vibrational labeling used for series of transitions (bands). #lines is the total number of transitions belonging to a given band. Minimum and maximum wavenumbers of calculated transitions belonging to the band are given in  $\text{cm}^{-1}$ ,  $S_{\text{tot}}$  is the sum of calculated line intensities (see text) in  $\text{cm}^{-1}/(\text{molecule}\cdot\text{cm}^{-2})$  at 296K for  $\text{C}_2\text{H}_2$  in natural abundances.  $S_{\text{min}}$  and  $S_{\text{max}}$  are respectively the minimum and maximum calculated line intensities in the band. Minimum and maximum values of  $J$  in the band are given.<sup>3</sup>

For self-broadening coefficients, an improved set of parameters (given in Table 8) based on the work performed in [111] has been used for all  $\text{C}_2\text{H}_2$  transitions in GEISA-2020. For  $J$  values greater than 36 self-broadening coefficients have been fixed to  $0.078 \text{ cm}^{-1}/\text{atm}$ . Default values have been used for the temperature dependence of air-broadening coefficients (equal to 0.75) and for air-shifting coefficients (equal to  $-0.001 \text{ cm}^{-1}/\text{atm}$ ).

In total, 59747 lines were added or updated in the  $13.624350 - 9415.084280 \text{ cm}^{-1}$  spectral range.

$m$	$\gamma_{\text{self}}(296\text{K})$	$m$	$\gamma_{\text{self}}(296\text{K})$	$m$	$\gamma_{\text{self}}(296\text{K})$
1	0.2055	13	0.1438	25	0.1088
2	0.1925	14	0.1407	26	0.1059
3	0.1823	15	0.1376	27	0.1030
4	0.1744	16	0.1347	28	0.0999
5	0.1683	17	0.1319	29	0.0967
6	0.1635	18	0.1291	30	0.0934
7	0.1598	19	0.1264	31	0.0898
8	0.1568	20	0.1225	32	0.0861
9	0.1543	21	0.1198	33	0.0831
10	0.1520	22	0.1171	34	0.0812
11	0.1499	23	0.1143	35	0.0800
12	0.1471	24	0.1117	36	0.0780

**Table 8:** Self-broadening coefficients used in GEISA-2020 as a function of  $m = |-J, J, J+1|$  for  $P$ ,  $Q$  and  $R$  branches.

The internal GEISA code for the data identification has been set to **C19**, **L19**, **J19** and **J20**.

<sup>3</sup> Note: The vibrational labeling for upper and lower state corresponds to  $V_1 V_2 V_3 V_4 V_5 \ell_4 \ell_5$ . GEISA-2015 refers to the two strongest bands already present in GEISA-2015 but updated in GEISA-2020.

### 2.1.17 C<sub>2</sub>H<sub>4</sub> (molecule 25)

The <sup>12</sup>C<sub>2</sub>H<sub>4</sub> update in GEISA-2020 was generated using data for the  $\nu_{10}$ ,  $\nu_7$  and  $\nu_4$  bands from the corrected line list of Ref. [112], however ignoring weak lines whose intensities are lower than  $10^{-30}$  cm<sup>-1</sup>/(molecule cm<sup>-2</sup>) at 296 K. Note that errors in the degeneracies provided for the rotational levels in the 10<sup>1</sup> and 7<sup>1</sup> vibrational levels in the linelists of Refs. [112] and [113] were corrected (I. Gordon is acknowledged for bringing them to our attention). The positions and intensities of the  $\nu_{12}$  band lines were taken from GEISA-2015, excluding 187 lines having an intensity smaller than  $10^{-30}$  cm<sup>-1</sup>/(molecule cm<sup>-2</sup>) at 296 K to be consistent with the information provided for the  $\nu_{10}$ ,  $\nu_7$  and  $\nu_4$  bands. For all the lines, the self-broadening coefficients were calculated using the empirical expressions reported in Ref. [114], the air-broadening coefficients were generated as described in [115], and the temperature dependence exponent  $n$  was set to 0.76, following the suggestion from Ref. [113]. In total, 52655 lines have been added or updated between 620.057948 and 1524.702536 cm<sup>-1</sup>.

The internal GEISA code for the data identification has been set to [A19](#).

### 2.1.18 GeH<sub>4</sub> (molecule 26)

Germane (GeH<sub>4</sub>) is a molecule that has been detected in giant gas planets like Jupiter and Saturn [116], [117]. The current [Juno](#) mission has renewed its spectroscopy interest especially in the 4.5 – 5.0  $\mu$ m window where an accurate model is needed for radiative transfer computations. The former version of GEISA only contained lines for <sup>74</sup>GeH<sub>4</sub>. A first complete analysis of the  $\nu_1/\nu_3$  stretching dyad region for all natural five isotopologues (<sup>70</sup>GeH<sub>4</sub>, <sup>72</sup>GeH<sub>4</sub>, <sup>73</sup>GeH<sub>4</sub>, <sup>74</sup>GeH<sub>4</sub> and <sup>76</sup>GeH<sub>4</sub>) was recently performed by Boudon *et al.* [118] for line positions and absolute line intensities. This study led to a set of 32,378 calculated lines, covering the range 1929 cm<sup>-1</sup> to 2266 cm<sup>-1</sup>, that have been introduced in the new GeCaSDa [119][120] database in Dijon and in the present version of GEISA.

In total, 32372 lines have been added or updated between 1928.902023 and 2265.677939 cm<sup>-1</sup>.

The Internal GEISA code for the data identification has been set to [B19](#).

### 2.1.19 NO<sup>+</sup> (molecule 45)

Nitrosylium, NO<sup>+</sup>, was detected in the Earth's ionosphere as an important trace species [121] and tentatively in the interstellar medium [122]. The rovibrational transitions have been introduced into GEISA-2020, based on version 2 of the CDMS [123] entry (tag 030512). Rotational transition frequencies [122],[124] were fitted together with rovibrational data

[121],[125]. The dipole moments are 0.368 D and 0.380 D in  $v = 0$  and 1, respectively [126]. In total, 247 lines have been added or updated between 3.938076 and 4742.008075  $\text{cm}^{-1}$ .

The Internal GEISA code for the data identification has been set to **M18**.

#### **2.1.20 $\text{CF}_4$ (molecule 49)**

Carbon tetrafluoride ( $\text{CF}_4$ ) is a strong greenhouse gas of both natural and anthropogenic origin whose concentration is monitored using, among other techniques, solar occultation measurements from space [127]. It has been shown that, up to now, the line-by-line databases were quite incomplete because of missing hot bands lines expected for polyatomic species [128]. Recently, a systematic study of many low-lying energy levels was undertaken by the SOLEIL/AILES and Dijon groups to deal with this problem, resulting in a global analysis that enabled to simulate the major hot bands in the strongly absorbing  $\nu_3$  C-F stretching region [129]. Moreover, line positions and intensities for purely rotational transitions in the  $\nu_3 = 1$  state were recorded and fitted in the far infrared (THz) region, thanks to synchrotron radiation [130]. These last two studies are used for the present update of  $^{12}\text{CF}_4$  lines in GEISA. We also adapted the line intensity thresholds in each spectral region to avoid unwanted inaccurate extrapolated lines of very low intensity (in  $\text{cm}^{-1}/\text{molecule}\cdot\text{cm}^{-2}$ :  $1\text{E}^{-30}$  in the 0-100  $\text{cm}^{-1}$  region,  $1\text{E}^{-24}$  in the 500-700  $\text{cm}^{-1}$  region and  $1\text{E}^{-22}$  above 12000  $\text{cm}^{-1}$ ). These line lists contain 258,208 lines and are included in the new TFMCaSDa [120,131] Dijon's database, as well as in the present version of GEISA. In total, 258208 lines have been added or updated between 1.173350 and 1329.697261  $\text{cm}^{-1}$ .

The Internal GEISA code for the data identification has been set to **B19**.

#### **2.1.21 HONO (new molecule 53)**

Using spectroscopic data collected in the literature, a linelist of positions and intensities has been generated for the 11  $\mu\text{m}$  region of HONO [132] which correspond to the  $\nu_6$  bands located at 790.117 and 851.943  $\text{cm}^{-1}$  for the Cis- and Trans- isomers, respectively.

For the computation of line positions, the vibrational energies and rotational constants quoted in Refs. [133] and [134] were used for the upper and lower state energies. On the other hand the line intensities were calibrated relatively to band intensities measured by Kagann and Maki [135]. The problem of the uncertainties associated to these intensities was discussed in details in Ref. [132]. Indeed, in usual laboratory conditions nitrous acid exists only in the form of an equilibrium mixture with other species like NO,  $\text{NO}_2$  and  $\text{H}_2\text{O}$ , together with smaller quantities



of N<sub>2</sub>O<sub>3</sub>, N<sub>2</sub>O<sub>5</sub>, and HNO<sub>3</sub> [135]. Due to these difficulties, one may estimate an overall uncertainty on the absolute intensities between 20% to 30%, while, on the relative scale, one may expect the intensities of the Trans- and Cis species at 296K to be rather consistent, with an uncertainty of 5% on average, and of 10% for the weaker lines.

To our knowledge, line shape parameters are absent in the literature for HONO. As the permanent dipole moment of Trans-HONO and Cis-HONO have values similar to those of water, HONO line shape parameters adopted “a priori” values similar to those of water. More explicitly,

$$\gamma_{\text{Air}}=0.1 \text{ cm}^{-1}/\text{Atm}, \gamma_{\text{Self}}=0.4 \text{ cm}^{-1}/\text{Atm}, \text{ and } n_{\text{Air}}=0.7$$

were implemented for the air-broadened half width, self-broadened half-width and for the n-temperature dependent coefficient, respectively.

Species	#lines	$\sigma_{\min}$	$\sigma_{\max}$	$S_{\max}^{\#}$ $\times 10^{-17}$	Total_A <sup>#</sup> $\times 10^{-17}$	Total_B <sup>#</sup> $\times 10^{-17}$	$S_{\text{tot}}^{\#}$ $\times 10^{-17}$
Trans- HONO	7621	724.39	838.57	0.166	1.218	0.0	1.218
Cis-HONO	18420	722.53	996.28	0.148	1.115	0.1338	1.249
All	26041						2.467

<sup>#</sup> All intensities in  $\text{cm}^{-1}/(\text{molecule}\cdot\text{cm}^{-2})$  at 296K.

**Table 9:** The HONO linelist in GEISA. The following abbreviations are used: #lines: number of lines;  $\sigma_{\min} / \sigma_{\max}$ ; minimum and maximum sigma values (in  $\text{cm}^{-1}$ );  $S_{\max}$ : Maximum intensity; Total-A/Total\_B: sum of the intensities for A- type and B- type transitions, respectively;  $S_{\text{tot}}$ : sum of the individual intensity for the Trans and Cis species,  $\text{TransInt}(v_4, T=296\text{K})$  and  $\text{CisInt}(v_4, T=296\text{K})$ , respectively.

The minimum of intensity retained is  $0.5 \cdot 10^{-24} \text{ cm}^{-1}/(\text{molecule}\cdot\text{cm}^{-2})$ . In total, 26041 lines have been added between 722.533940 and 996.280840  $\text{cm}^{-1}$ . Note that

The internal GEISA code for the data identification has been set to [P18](#).

### 2.1.22 COFCl (new molecule 54)

Carbonylchlorofluoride (COFCl) is a new molecule identified as molecule 54 in the GEISA notation. A list of line positions and of line intensities was implemented for the  $\nu_1$ ,  $\nu_2$ , and  $\nu_3$  fundamental bands of the  $^{12}\text{C}^{16}\text{O}^{35}\text{Cl}$  and  $^{12}\text{C}^{16}\text{O}^{37}\text{Cl}$  isotopologues of carbonylchlorofluoride, located at 5.3, 9.1, and 13.1  $\mu\text{m}$ , respectively [136]. In addition, for the

most abundant isotopologue  $^{12}\text{C}^{16}\text{O}^{35}\text{Cl}$ , this line list includes also the contributions from the first two associated hot bands. The parameters included in this database were generated by combining the results of previous experimental analyses [137] and *ab initio* calculations [138]. To our knowledge, no line broadening or shifting parameters data exists in the literature for COFCl. Therefore, default values for the self and air-broadening coefficients of  $0.1 \text{ cm}^{-1} \text{ atm}^{-1}$  and temperature dependence of  $n=0.75$  are given in the present database. This COFCl linelist was generated in order to improve the quality of remote sensing of the atmosphere in the mid-IR. Analyses of atmospheric solar occultation spectra measured by the JPL MkIV interferometer [136] show that the new line list not only improves the quality of retrievals of COFCl, but also of several other overlapping gases. In total, 215639 lines have been added between  $734.996930$  and  $1912.632380 \text{ cm}^{-1}$ .

The internal code for the data identification has been set to *P19*.

### 2.1.23 $\text{CH}_3\text{I}$ (new molecule 55)

Methyl iodide ( $\text{CH}_3\text{I}$ ) is a new molecule identified as molecule 55 in the GEISA notation. The line list in GEISA involves the  $\nu_6$  and  $2\nu_3$  interacting bands at  $11 \mu\text{m}$ . For the computation of the line positions and intensities, the hyperfine structure due to the iodine nuclear quadrupole moment was accounted for explicitly, together with the vibration-rotation resonances. Analyses of line positions and line intensities, based on effective models adjustment, is described in Refs. [139] and [140], respectively. In addition, detailed self-  $\text{N}_2$  [141] and  $\text{O}_2$  [142] line shape parameters were measured. In total, 70291 lines have been added between  $693.022430$  and  $1125.254590 \text{ cm}^{-1}$ .

Band	#lines	$S_{\text{tot}}$	$S_{\text{max}}$	$\sigma_{\text{min}}$	$\sigma_{\text{max}}$	$J_{\text{max}}$	$K_{\text{max}}$
		$\times 10^{-19}$	$\times 10^{-23}$				
$\nu_6$	49603	12.3	220	693.02	1125.25	88	24
$2\nu_3$	20688	0.181	3.3	985.67	1076.68	88	21
Total	70291	12.5					

**Table 10:** Linelist for Methyl iodide ( $^{12}\text{CH}_3\text{I}$ ) in the  $11 \mu\text{m}$  region for GEISA-2020. #lines is the number of lines.  $S_{\text{tot}}$  and  $S_{\text{max}}$  (maximum value of the computed line intensities) are in  $\text{cm}^{-1}/(\text{molecule cm}^{-2})$ .  $\sigma_{\text{min}}$  and  $\sigma_{\text{max}}$  are the minimum and maximum values of the computed line positions (in  $\text{cm}^{-1}$ ), respectively.

The Internal GEISA code for the data identification has been set to *P19*.

### 2.1.24 CH<sub>3</sub>F (new molecule 56)

Methyl fluoride (CH<sub>3</sub>F) is present as traces in the Earth atmosphere. A line list for the  $\nu_6$  band around 1200 cm<sup>-1</sup> is now included for the first time in GEISA, based on the work of Papoušek *et al.* [143] for line positions, on the work of Jacquemart and Guinet [144] for line intensities and self-broadening coefficients, and on the work of Ramchani *et al.* [145] for N<sub>2</sub>-broadening coefficients. In total, 1499 lines have been added between 1067.375090 and 1290.254930 cm<sup>-1</sup>.

The internal GEISA code for data identification has been set to **J19**.

### 2.1.25 RuO<sub>4</sub> (new molecule 57)

Ruthenium tetroxide is a molecule of importance for nuclear power plant security and other industrial applications (see [146], [147], [148] and references therein). In natural abundance, it possesses seven isotopologues, due to the different ruthenium isotopes (we do not consider here oxygen isotopes): <sup>97</sup>RuO<sub>4</sub>, <sup>98</sup>RuO<sub>4</sub>, <sup>99</sup>RuO<sub>4</sub>, <sup>100</sup>RuO<sub>4</sub>, <sup>101</sup>RuO<sub>4</sub>, <sup>102</sup>RuO<sub>4</sub> (the main one) and <sup>104</sup>RuO<sub>4</sub>. There are also two radioactive, short-lived, isotopologues, <sup>103</sup>RuO<sub>4</sub> and <sup>106</sup>RuO<sub>4</sub>. In Ref. [146], the  $\nu_3$  band for all observable isotopologues was analyzed, and the parameters for the radioactive ones were extrapolated. Absolute line intensities were also analyzed in Ref. [148] for <sup>102</sup>RuO<sub>4</sub>. In this work we assumed that the dipole moment derivative parameters do not change significantly for the different isotopologues, so that the dipole moment parameters determined for <sup>102</sup>RuO<sub>4</sub> were used to calculate the line lists for the other eight isotopologues. These line lists contain 30,205 lines and are included in the new RuCaSDa [120,149] Dijon's database, as well as in the present version of GEISA.

When the broadening parameters are unknown, in general, a default value is given (as 0.1 cm<sup>-1</sup>/atm for the air). Please note that in this update, and to specifically indicate that these values are unknown, the air and self-broadening have been set to -.9999 and -9.9999, respectively. In total, 30250 lines have been added between 889.986739 and 948.138145 cm<sup>-1</sup>.

The Internal GEISA code for the data identification has been set to **B19**.

### 2.1.26 H<sub>2</sub>C<sub>3</sub>H<sub>2</sub> (new molecule 58, Allene, isomer of C<sub>3</sub>H<sub>4</sub>)

H<sub>2</sub>C<sub>3</sub>H<sub>2</sub> (Allene, isomer of C<sub>3</sub>H<sub>4</sub>) is the last new molecule added to GEISA-2020, and identified as molecule 58 in the GEISA notation. This linelist includes the  $\nu_{11}$  far infrared band near 352 cm<sup>-1</sup> as well as the  $\nu_{10}/\nu_9$  region peaking at 845 cm<sup>-1</sup>. It is a result of the search for allene (also called propadiene) in Titan's atmosphere using the CIRS (Composite InfraRed Spectrometer) instrument on board the Cassini-mission [150] that was positively concluded by a clear detection using high resolution observations from the ground [151]. No allene linelist was

available neither in HITRAN nor in GEISA but the linelist of propyne ( $C_3H_4$ ) which is an isomer of allene has been provided by GEISA for a long time [1].

Coustenis *et al.* [152] started to investigate the detectability of allene in Titan's atmosphere using spectroscopic parameters by Chazelas *et al.* [153] for the  $\nu_{10}$  band and from Pliva and Kauppinen for  $\nu_{11}$  [154]. Line intensities could be obtained from band intensity measurements by Koga *et al.* [155]. Later Jolly *et al.* [156] used the same spectroscopic study but also added spectroscopic parameters obtained by high resolution studies by Nissen *et al.* [157] and Hegelund *et al.* [158] which also include spectroscopic parameters for the hot bands. The hot band contribution is particularly important at room temperature and needs to be included in order to compare the calculated line lists with room temperature spectra. No new high-resolution measurements were needed to establish this new linelist. It is essentially based on the sub-band analysis from previously mentioned authors but has also been validated against new measurements.

As described in Lombardo *et al.* [150], calculated band profiles have been compared to room and high temperature cross section measurements recorded at  $0.08\text{ cm}^{-1}$  resolution in the  $\nu_{10}/\nu_9$  wavenumber range [159]. All sub-band intensities could be fitted using those intensity calibrated measurements. Concerning the far infrared region where the  $\nu_{11}$  band of allene can be observed, room temperature spectra were recorded at the resolution of  $0.1\text{ cm}^{-1}$  at the SOLEIL-AILES synchrotron beamline as described in Jolly *et al.* [156]. Band intensities were found to be in agreement with Koga *et al.* [156]

This linelist that we have adopted is the same that was used for the search and detection of allene on Titan. It provides for each line the position, the intensity and the lower energy but does not provide any quantum assignment. Pressure shift is fixed to the undefined value  $0.0\text{ cm}^{-1}/\text{atm}$  and self-broadening to a constant value 0.71 using the same values as for allene's isomere  $C_3H_4$  (propyne). In total, 31686 lines have been added between 296.315900 and 1192.445800  $\text{cm}^{-1}$ .

The internal GEISA code for the data identification has been set to [J19](#).

### 3 Quality assessment of the spectroscopic parameters

The process of updating or expanding spectroscopic databases in order to provide the users with a database that insures an optimal characterization of spectral properties of molecular

absorption is challenging. To help making the most relevant choices and updates, the Spectroscopic Parameters And Radiative Transfer Evaluation (SPARTE) chain [8] was developed at LMD and applied for the first time to the GEISA-2015 release. Figure 6 presents the general principles of the SPARTE chain.

SPARTE relies on the comparison between forward radiative transfer simulations made by the 4A radiative transfer code [10,160], using a given spectroscopic database as input, and various remote sensing observations for several thousands of well-characterized atmospheric situations. Assuming that observed spectra come from instruments characterized by high radiometric and spectral stabilities, each individual residual can be the sum of a random errors coming from the imperfect description of the atmospheric state or from the radiometric noise of the instruments, with systematic errors linked in general to the spectra calculation (spectroscopic parameters, line shape, line mixing, continua, etc.). Averaging the resulting ‘calculated-observed’ spectral residuals thus minimizes the random errors and enables the detection of error features that may come from an imperfect knowledge of lines parameters (see Figure 7 of Ref. [8] for the typical shapes of the ‘calculated-observed’ residuals originating from an error in a given line parameter).

In the following, ‘clear-sky’ observations from two well established instruments have been used: the space-borne IASI instrument (15 to 3.7  $\mu\text{m}$ ) and ground-based Fourier Transform Spectrometers (FTS) instruments at the Park Falls Total Carbon Column Observing Network [9] (TCCON, 2.5 to 0.7  $\mu\text{m}$ ). For IASI, more than 15 000 numbers of observations, spanning the period 2019/01-2019/12, have been used. Atmospheric state determinations that are collocated with IASI observations are from Analyzed RadioSoundings Archive (ARSA) developed and maintained at LMD (<https://ara.lmd.polytechnique.fr/index.php?page=arsa>). Clear sky observations – *i.e.* « free from clouds and aerosols » – are selected through a sophisticated procedure combining microwave and infrared radiances measured by AMSU-A and IASI, both on Metop satellites, respectively. For TCCON, clear-sky observations have been selected to each PI’s station. Here, a set of more than 300 spectra from Park Falls facility, selected based on a good representation of the airmass (*i.e.* solar zenith angle) as well as period of the year, are used. Atmospheric states that are collocated with TCCON observations are coming from the TCCON procedure and delivered together with the spectra.

When possible (*i.e.* for matching spectral coverage and a significant spectral signature of the spectroscopic change), the SPARTE chain was used for the update of GEISA-2020 in a 3-step procedure: (i) to identify improperly described lines (position, intensity, width, pressure shift,

etc.); (ii) to provide feedback and suggest revised values to the contributing spectroscopy research teams; and (iii) to finalize the validation of the updated parameters.

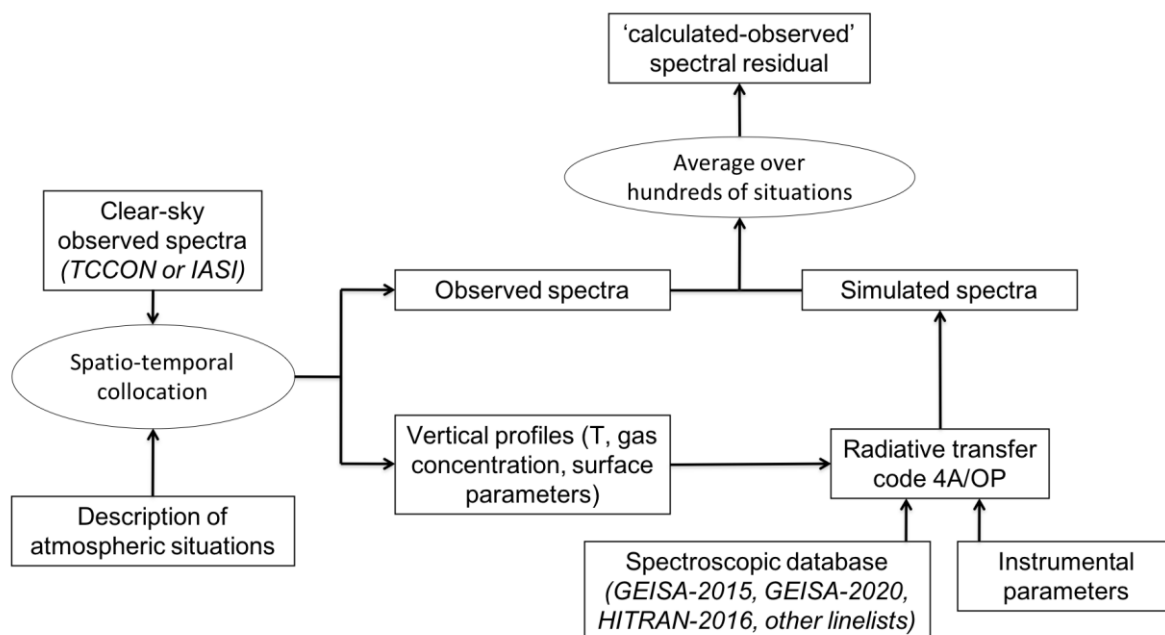


**Figure 6.** The general principle of the SPARTE chain.

### *Four applications and impact on the GEISA-2020 version*

#### **3.1.1 $H_2O$ evaluation in the $6600\text{--}6616\text{ cm}^{-1}$ and $7550\text{--}7575\text{ cm}^{-1}$ spectral region**

As stated in section 2.1.1.1, the major update on  $H_2^{16}O$  was based on the work of Mikhailenko *et al.* [12] (referenced as Mikhailenko 2016 in the following), who published a linelist of  $H_2O$  parameters between  $5830$  and  $8340\text{ cm}^{-1}$  based on a collection of several data. More recently they published refined line positions and shifts with respect to their former linelist [13] (included in GEISA-2020 update). Although much of these new data helped to improve line parameters in the GEISA database, the validation process using SPARTE based on TCCON observations highlighted a few remaining issues or artefacts in the SWIR domain. In the following, we present a selection of three representative cases that illustrate the benefit of a careful further evaluation of the spectroscopic parameters as nominally delivered by the spectroscopist research team.

The first case is the most straightforward as it concerns ‘wide-range’ issues, i.e. systematic errors on one or several line parameters that affect wide ranges of the TCCON spectrum. Figure 7 summarizes the comparisons of the ‘calculated-observed’ residuals between TCCON and 4A/OP [10] when three different spectroscopic databases are used: GEISA-2015 (red), Mikhailenko 2016 (blue) and GEISA-2020 (green). The upper panel shows the spectrum of atmospheric transmission measured by TCCON in the regions  $6600\text{--}6616\text{ cm}^{-1}$  and  $7550\text{--}7575$

cm<sup>-1</sup>. The corresponding residuals (differences of transmissions averaged on the 325 TCCON spectra) are shown in the lower panels. In the left figure, the calculations using the line list from Mikhailenko 2016 results in unexpectedly bad ‘calculated-observed’ values: negative (left panel) or positive (right panel). This wide range behavior, affecting several lines over tens of cm<sup>-1</sup>, combined with the typical ‘line intensity’ residual shape, suggests systematic line-intensity issues in the data reported in the Mikhailenko 2016 list. This is also supported by the fact that the GEISA-2015 residuals - which did not include Mikhailenko 2016 results – not only were smaller but also did not exhibit similar behavior. An analysis of the affected lines showed that they were all coming from Regalia *et al.* [161] work. Removing all the occurrence of this work in the Mikhailenko 2016 linelist enabled to solve these issues. A work is in progress to assess the origin of these systematic intensity-like issues in Regalia *et al.* data.

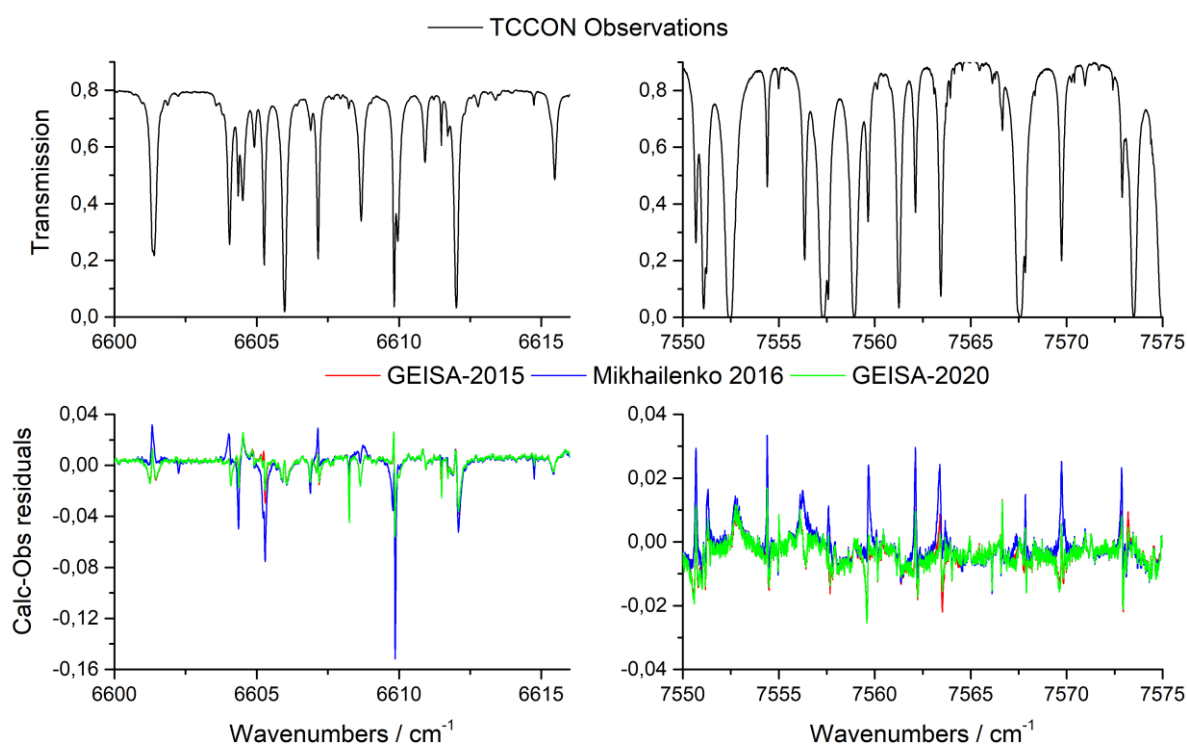


**Figure 7:** Comparison between GEISA-2015, Mikhailenko 2016 [12] and GEISA-2020. Upper panel: Transmission spectrum observed at Park Falls TCCON site (average over 325 spectra). Lower panel: ‘Calculated-observed’ residuals generated by the SPARTE chain for GEISA-2015 (red), Mikhailenko 2016 (blue) and GEISA-2020 (green). Left: 6600–6616 cm<sup>-1</sup>. Right: 7550-7575 cm<sup>-1</sup>.

Figure 8 illustrates a similar case. It shows comparisons of the ‘calculated-observed’ residuals obtained from simulations using the three different spectroscopic line lists in the 6615-6616 cm<sup>-1</sup>, 6669-6672 cm<sup>-1</sup> and 6710-6712 cm<sup>-1</sup> regions, and the corresponding TCCON observations. Significant deviations are observed on the residuals when using Mikhailenko

2016 linelist on some isolated lines of the spectrum, with a deterioration of the situation with regard to GEISA-2015. Careful study of the line parameters gathered in

Position cm <sup>-1</sup>	Intensity cm/atm			Air-broadening cm/cm <sup>-1</sup>		
	GEISA-2015	Ref. [12]	GEISA-2020	GEISA-2015	Ref. [12]	GEISA-2020
6615.451320	<b>1.76E-25</b>	<b>2.49E-25</b>	<b>1.76E-25</b>	0.0729	0.0729	0.0729
6670.485430	<b>5.04E-24</b>	<b>2.52E-23</b>	<b>5.04E-24</b>	0.0360	0.0360	0.0360
6711.331920	<b>1.04E24</b>	<b>1.32E-24</b>	<b>1.04E-24</b>	0.0330	0.0330	0.0330
6031.899200	7.13E-26	7.13E-26	7.13E-26	<b>0.0380</b>	<b>0.0078</b>	<b>0.0300</b>
7804.608830	6.60E-26	6.87E-26	6.87E-26	<b>0.0092</b>	<b>0.0092</b>	<b>0.0478</b>
7851.277170	3.90E-26	4.13E-26	4.13E-26	<b>0.0089</b>	<b>0.0089</b>	<b>0.0300</b>

Table 11 shows that the main differences come from line intensities of some strong lines. For these lines, the data from Macko *et al.* [162] were considered in Mikhailenko 2016. However, the CRDS setup used in [162], being very efficient for the measurement of weak lines but less suitable for the measurement of strong lines, leads to significant uncertainties on these line intensities. As a consequence, the choice has been made in GEISA-2015 and GEISA-2020 to use the line intensities determined by Toth *et al.* [163] using a Fourier Transform spectrometer. Other parameters were updated using the data from references [12] and [13].



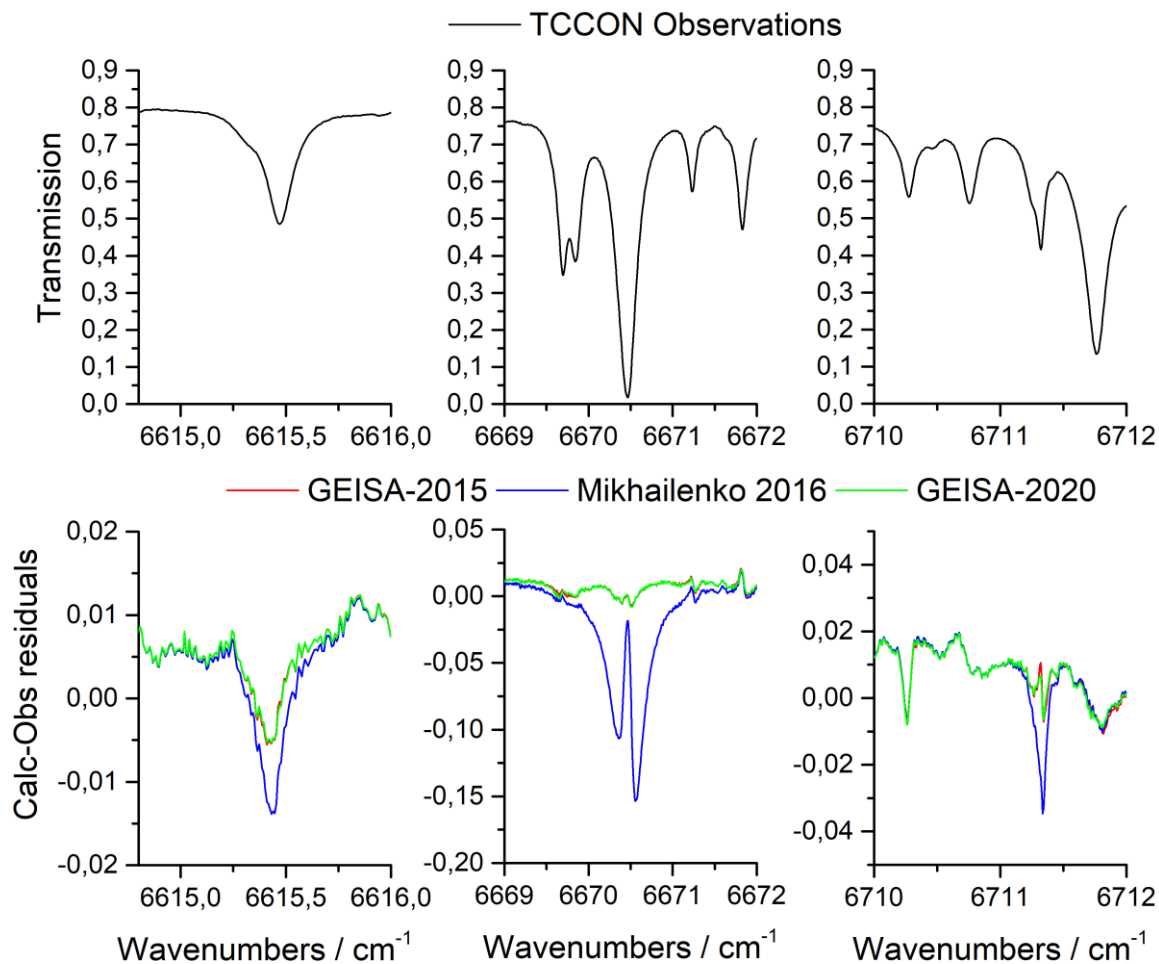


**Figure 8:** Comparison between GEISA-2015, Mikhailenko 2016 [12] and GEISA-2020. Upper panel: Transmission spectrum observed by TCCON, as input (average over 325 spectra). Lower panel: ‘Calculated-observed’ residuals generated by the SPARTE chain for GEISA-2015 (red), Mikhailenko 2016 (blue) and GEISA-2020 (green).

Finally, Figure 9 presents comparisons of the ‘calc-obs’ residuals obtained from the three different spectroscopic line lists in the 6631.5-6632.5  $\text{cm}^{-1}$ , 7804-7805  $\text{cm}^{-1}$  and 7850.5-7851.5  $\text{cm}^{-1}$  regions, and the corresponding TCCON observations. Again, significant deviations are observed on the residuals when using Mikhailenko 2016 linelist on some isolated lines of the spectrum, but also using GEISA-2015, a notable exception being the line in 6032.9  $\text{cm}^{-1}$  for which GEISA-2015 is far better. This time, the residual shapes indicates a significant difference between the air-broadening coefficients of the three line lists, as illustrated in

Position $\text{cm}^{-1}$	Intensity $\text{cm}/\text{atm}$			Air-broadening $\text{cm}/\text{cm}^{-1}$		
	GEISA-2015	Ref. [12]	GEISA-2020	GEISA-2015	Ref. [12]	GEISA-2020
6615.451320	<i>1.76E-25</i>	<i>2.49E-25</i>	<i>1.76E-25</i>	0.0729	0.0729	0.0729
6670.485430	<i>5.04E-24</i>	<i>2.52E-23</i>	<i>5.04E-24</i>	0.0360	0.0360	0.0360
6711.331920	<i>1.04E24</i>	<i>1.32E-24</i>	<i>1.04E-24</i>	0.0330	0.0330	0.0330
6031.899200	7.13E-26	7.13E-26	7.13E-26	<b>0.0380</b>	<b>0.0078</b>	<b>0.0300</b>

7804.608830	6.60E-26	6.87E-26	6.87E-26	<b>0.0092</b>	<b>0.0092</b>	<b>0.0478</b>
7851.277170	3.90E-26	4.13E-26	4.13E-26	<b>0.0089</b>	<b>0.0089</b>	<b>0.0300</b>

Table 11 (a slight difference on line intensities is also seen for the two lines at 7804.61 and 7851.28  $\text{cm}^{-1}$ , but cannot explain the large deviations seen in Figure 9). The values of these parameters reported in GEISA-2015 and Mikhailenko 2016, and determined in a former work of Gamache *et al.* (updated version of Refs. [164,165]), turned out to be too weak, leading to large errors in the ‘calc-obs’ residuals. In this particular case, we gave a feedback to Gamache and coworkers so that they can rework on a revised set of data. The new line parameters were used to correct the problematic lines in GEISA-2020, as stated in section 2.1.1.1. Thus, Figure 9 shows that the residuals obtained using the GEISA-2020 release give much better results than the two other line lists. Also note that SPARTE was able to detect inconsistencies on parameters of very weak lines (e.g. the line centered at 7804.5  $\text{cm}^{-1}$ ).

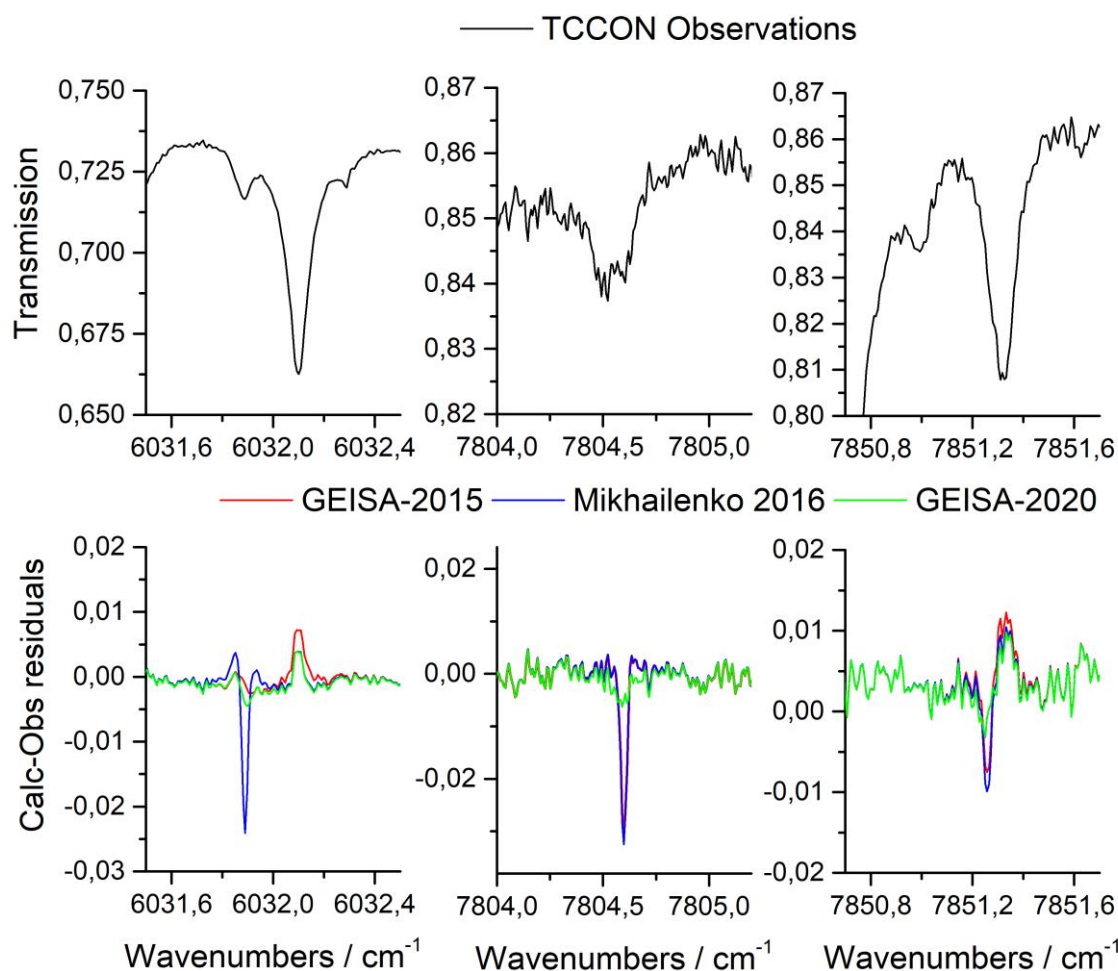


**Figure 9:** Comparison between GEISA-2015, Mikhailenko 2016 [12] and GEISA-2020. Upper panel: Transmission spectrum observed by TCCON, as input (average over 325 spectra). Lower

panel: ‘Calculated-observed’ residuals generated by the SPARTE chain for GEISA-2015 (red), Mikhailenko 2016 (blue) and GEISA-2020 (green).

Position cm <sup>-1</sup>	Intensity cm/atm			Air-broadening cm/cm <sup>-1</sup>		
	GEISA-2015	Ref. [12]	GEISA-2020	GEISA-2015	Ref. [12]	GEISA-2020
6615.451320	<i><b>1.76E-25</b></i>	<i><b>2.49E-25</b></i>	<i><b>1.76E-25</b></i>	0.0729	0.0729	0.0729
6670.485430	<i><b>5.04E-24</b></i>	<i><b>2.52E-23</b></i>	<i><b>5.04E-24</b></i>	0.0360	0.0360	0.0360
6711.331920	<i><b>1.04E24</b></i>	<i><b>1.32E-24</b></i>	<i><b>1.04E-24</b></i>	0.0330	0.0330	0.0330
6031.899200	7.13E-26	7.13E-26	7.13E-26	<i><b>0.0380</b></i>	<i><b>0.0078</b></i>	<i><b>0.0300</b></i>
7804.608830	6.60E-26	6.87E-26	6.87E-26	<i><b>0.0092</b></i>	<i><b>0.0092</b></i>	<i><b>0.0478</b></i>
7851.277170	3.90E-26	4.13E-26	4.13E-26	<i><b>0.0089</b></i>	<i><b>0.0089</b></i>	<i><b>0.0300</b></i>

**Table 11:** Line parameters contained in the 3 spectroscopic databases GEISA-2015, Mikhailenko 2016 and GEISA-2020 for several absorption lines located in the spectral range considered in Figure 8 and Figure 9. Parameters written in italic-bold are those identified as responsible for strong departures in the ‘calculated-observed’ residuals (see text for details).

### 3.1.2 O<sub>2</sub> evaluation

As stated in section 2.2.7, no major update of the O<sub>2</sub> database was made in GEISA-2020. However, a recent work from Tran *et al.* [70] highlighted several errors in the 1.27μm band using <sup>16</sup>O<sub>2</sub> air-broadened line-shift parameters from GEISA-2015 or HITRAN2016 databases. To illustrate these errors, Figure 10 summarizes the comparisons of the ‘calculated-observed’ residuals between the 325 TCCON spectra recorded at Park Falls and 4A/OP when three different spectroscopic databases are used: GEISA-2015 taking into account the Pressure Shift (red, marked GEISA-2015 WPS), GEISA-2015 with <sup>16</sup>O<sub>2</sub> pressure shifts set to zero (blue, marked GEISA-2015 WOPS) and GEISA-2020 (green). Figure 10a shows the atmospheric transmission spectrum measured by TCCON in the region 7785–7915 cm<sup>-1</sup>. The corresponding ‘calc-obs’ residuals are shown in Figure 10b, c, d, for GEISA-2015 WPS, GEISA-2015 WOPS and GEISA-2020, respectively. Comparisons of the residuals between GEISA-2015 WPS and GEISA-2015 WOPS shows that systematic deviations seen in GEISA-2015 are due to erroneous values of the <sup>16</sup>O<sub>2</sub> pressure shifts, as they are mainly addressed when setting these parameters to zero. Figure 10d shows that the new data from Tran *et al.* [70] included in GEISA-2020 (see section 2.1.7) greatly improves these ‘calculated-observed’ deviations. However, several features remain in the residuals, mainly due to the fact that currently GEISA is only referencing Voigt profile parameters. The work of Tran *et al.* [70] using quadratic Speed-dependent Voigt profile along with first order line-mixing parameters greatly improves the

residuals in this region. The future releases of GEISA will be designed to gather such high-level information.

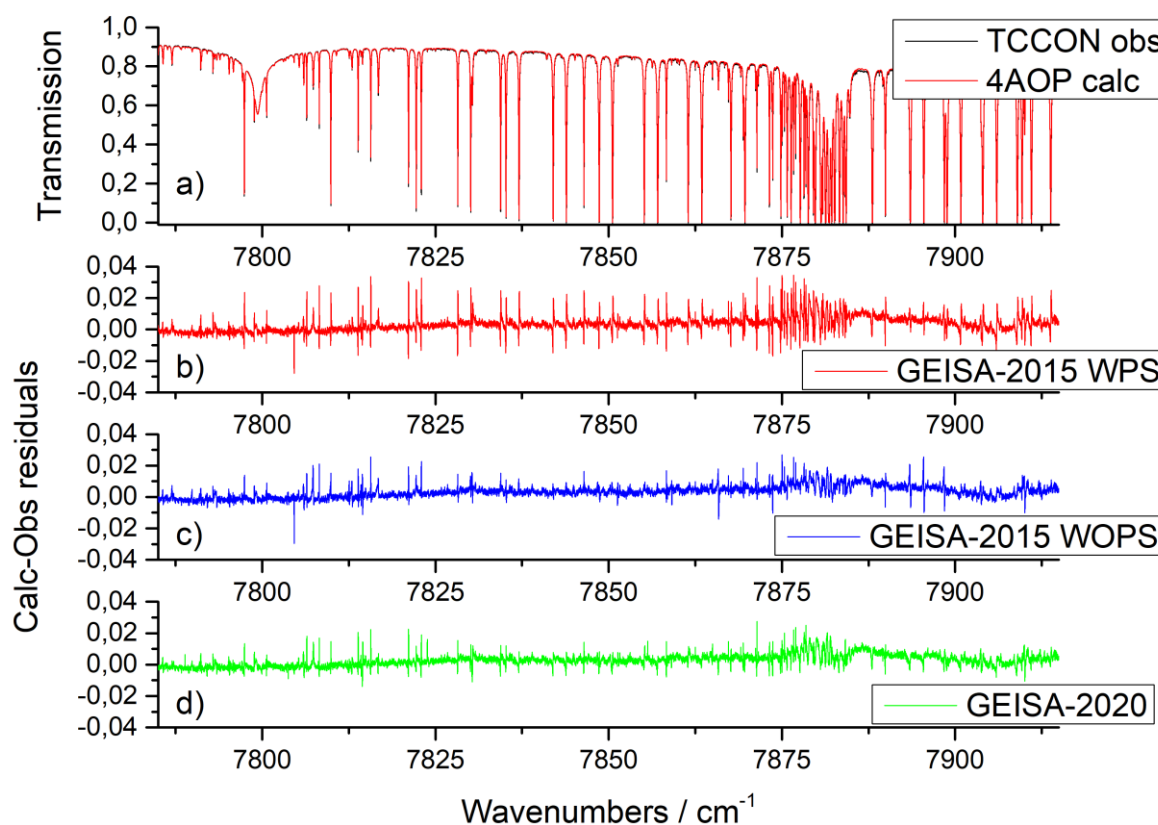


**Figure 10:** Comparison between GEISA-2015 (WPS), GEISA-2015 with <sup>16</sup>O<sub>2</sub> pressure shifts set to zero (GEISA-2015 WOPS) and GEISA-2020. (a) Transmission spectrum observed by TCCON, as input. (b) ‘Calculated-observed’ residuals generated by the SPARTE chain for GEISA-2015 WPS (red), (c) GEISA-2015 WOPS (blue) and GEISA-2020 (green). Please note that this band has been investigated and improved by Tran *et al.* [64] using non-Voigt profiles (not included in GEISA at this time).

### 3.1.3 O<sub>3</sub> evaluation

As described in section 2.1.3, a significant update has been made for the 2020 version of GEISA, notably by the application of intensity scaling factors in three vibrational bands, namely the 000-000, 001-000 and 101-000 bands, respectively in the microwave, 10μm and 5μm spectral regions. Impact of such scaling factors may be evaluated by comparison of simulated spectra generated by the SPARTE chain with observed IASI spectra.

The impact of the release has been studied on the whole IASI spectral range, but a significant impact has been only observed for the 9.6 μm band only. Figure 11 shows the comparisons of ‘calculated-observed’ residuals obtained with the SPARTE chain applied on IASI spectra using the two databases GEISA-2015 (in blue) and GEISA-2020 (in red), in this corresponding

spectral range 975-1075  $\text{cm}^{-1}$ , for the ‘Tropical’ atmospheres collocated with IASI. Figure 11 shows significantly worse results with GEISA-2020 than those obtained with GEISA-2015. When solicited, the spectroscopists have largely documented and justified (by private communications) the changes made in this spectral region, so the reason for such a behavior displayed in Figure 11 can only come from SPARTE. Since the same fixed version of 4A/OP has been used for the results displayed in Figure 11, the reason of this deterioration of the residuals using GEISA-2020 can only come from the ozone profiles. So far, as described in [8],  $\text{O}_3$  atmospheric profiles originate from the ERA Interim reanalysis [166] that are space and time collocated with each individual quality controlled radiosonde profile retained in the ARSA database. As a consequence, we decided to study the impact of a different set of ozone profiles, especially the new ECMWF reanalysis product, ERA5 [167], which is an improvement of the former ERA Interim product. Because the ERA5 database is large (0.25 x 0.25 degrees, every hour), as a first step, we estimated the differences between ERA Interim and ERA 5 by comparing the bias for the whole 2019 period, and for the ‘tropical’ atmospheres only, as shown in Figure 11. The most significant change between the two ERA products being a bias of 8% between 2 and 25 mbars, we evaluated the impact on SPARTE by shifting the ERA Interim profiles by 8% in the pressure range considered in SPARTE. The corresponding residuals are also shown on the Figure 11 in green.

As can be easily seen, the previous bias obtained using ERA Interim profiles along with GEISA-2020 has been largely removed. The remaining spectral residuals can be explained by the fact that the best approach is to collocate each ARSA radiosounding with the corresponding ERA5 ozone profile, an adaptation of SPARTE that will be done in the coming weeks. But, from this evaluation, we estimated that the demonstration of the good quality of the new ozone line list is made here, and thus we decided to keep this new version of ozone spectroscopic parameters in GEISA-2020.

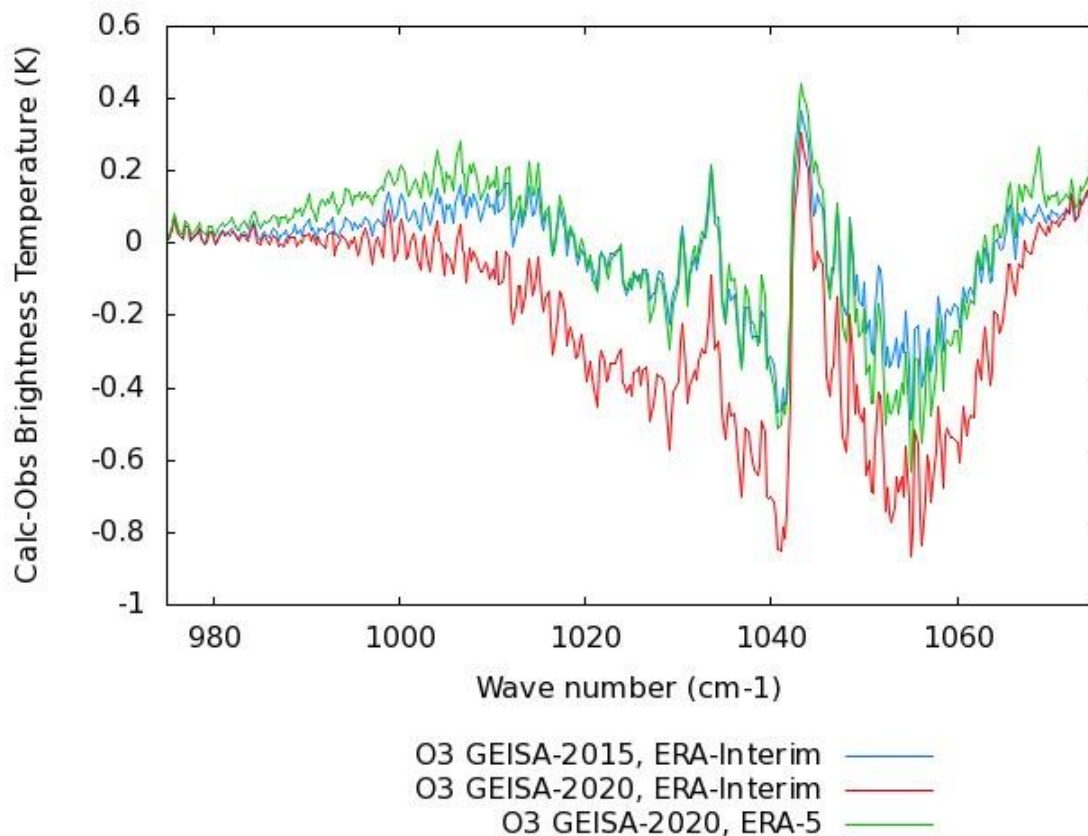


**Figure 11:** Comparison of ‘calculated-observed’ IASI residuals in the 975-1075 cm-1 spectral range and for tropical atmospheres, obtained using GEISA-2015 and GEISA-2020 O<sub>3</sub> line parameters and with different sources of ozone profiles used in the SPARTE chain: GEISA-2015 and ERA in blue, GEISA-2020 and ERA Interim in red and GEISA-2020 and ERA-5 in green).

### 3.1.4 Discussion on SF<sub>6</sub>

.Contrary to the species describe in the section 2, SF<sub>6</sub> has not been updated in the current version of GEISA, although new data were provided by Ke *et al.* from the Dijon’s database SheCaSDa [168]. Indeed, recent data from Nikitin *et al.* [169] consisting of a complete line list based of extensive *ab initio* calculations (from TheoReTS database [170]) leads to significantly different results. The direct comparison of the different available databases with experimental absorption from GEISA-2015 cross-sections database [1] justify why we made the choice not to update the GEISA-2020 database with new data from Dijon.

Figure 12 shows a comparison of SF<sub>6</sub> cross sections at room temperature (296K). The data from the GEISA-2015 cross-sections database are plotted along with simulated spectra derived from GEISA-2015 [1], HITRAN2016 [2], Dijon SheCaSDa [120] and TheoReTS [169] line list databases. Note that we also compared with the widely used PNNL spectra [83], which are similar than to GEISA-2015 cross-sections from Varanasi of *et al.* (Ref. [170] and private

communication), but the latter contains data at higher resolution (0.03 vs. 0.112  $\text{cm}^{-1}$ ) and was retained in the Figure 12. As mentioned by Nikitin *et al.* [169] it appears that *ab initio* cross sections agree much better with the observations than the simulations using SF<sub>6</sub> line lists constructed from effective models as available in HITRAN2016, SheCaSDa and GEISA-2015 line parameters databases. The main reason relies on the fact that effective models, generally derived from cold spectra over a limited set of ground vibrational states, fail to extrapolate data at room temperature which requires an account of more significant contributions of hot bands involving higher vibrational states. On the other hand, *ab initio* calculations succeed in giving a qualitative agreement with experimental data (Nikitin *et al.* mentioned that their calculation should be extended [169]). For this reason, we plan to generalize in future GEISA releases the use of *ab initio* data both as a point of comparison with experimentally derived effective models but also to improve or complete existing data.

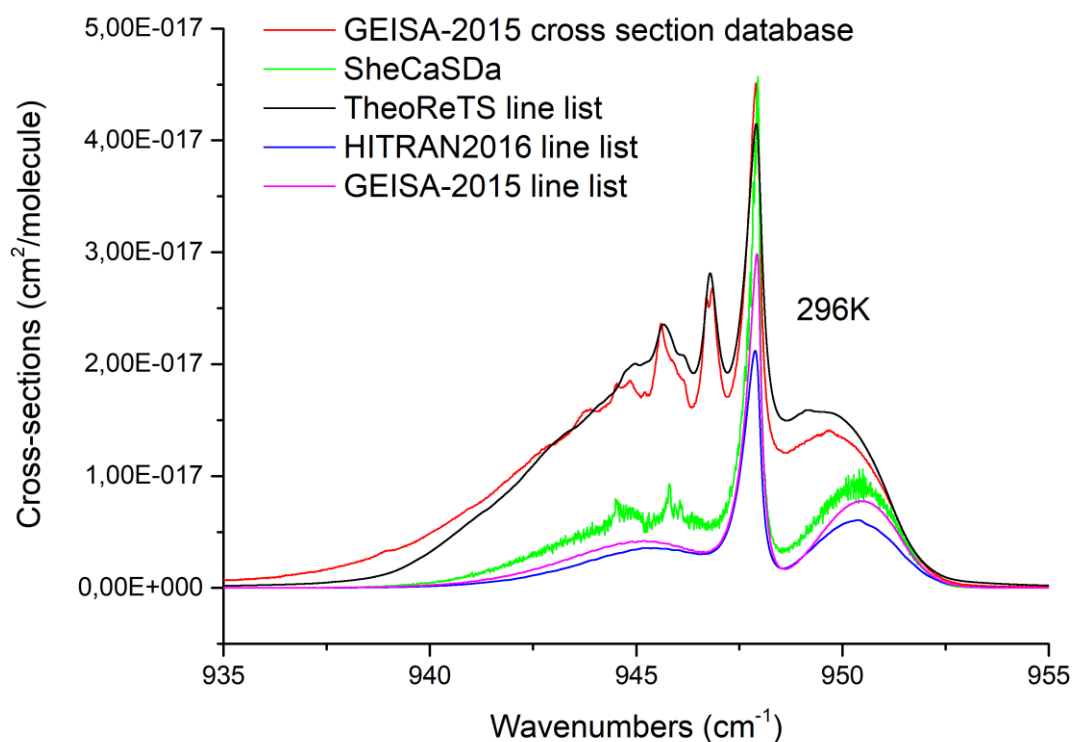


**Figure 12:** Comparison of SF<sub>6</sub> cross-sections at 296 K from the GEISA-2015 cross-sections database [1] (red), the line list of TheoReTS [169] (black), the theoretical calculation of Dijon SheCaSDa [168] (green), and simulations from the line lists of GEISA-2015 [1] (magenta), and HITRAN2016 databases [2] (blue). The GEISA-2015 cross-sections based on the work Varanasi *et al.* (Ref. [171] and private communication) are comparable to the widely used PNNL cross-sections [86], but contains data at higher resolution (0.03 vs. 0.112  $\text{cm}^{-1}$ ).



## 4 Conclusion and perspectives

Since its creation in the mid-1970s, and in order to meet the needs of researchers and international space agencies, GEISA has undergone 6 updates. This was done by collecting, archiving, and distributing the most up to date as well as accurate spectroscopic information and by concomitantly evolving the associated management softwares and quality control tools. Accordingly, the GEISA-2020 edition reported in this paper contains important updates and additions to the line parameters sub-database. With the addition of 6 new molecules (HONO, COFCl, CH<sub>3</sub>F, CH<sub>3</sub>I, RuO<sub>4</sub>, H<sub>2</sub>C<sub>3</sub>H<sub>2</sub>), it now involves 58 molecular species - 145 isotopologues (which 27 are new entries) – representing 6,746,987 entries in the database, which span the spectral range from 10<sup>-6</sup> to 35877 cm<sup>-1</sup>. In close relation with space missions (IASI, IASI-NG, Merlin, MicroCarb) and taking advantage of ground-based observations (here TCCON FTS), noticeable efforts have been made to improve the validation of the updates for species relevant for the Earth's atmosphere, such as H<sub>2</sub>O, O<sub>2</sub>, O<sub>3</sub>, CO<sub>2</sub> and CH<sub>4</sub>. Part of this work was enabled by the systematic use of the validation chain SPARTE to evaluate individual line parameters, detect problematic line parameters and consolidate the choices made by the GEISA team.

While the update presented in this paper highly upgrades the previous GEISA2015 release, there is still significant room for improvement. One of the most important aspects of our work is to make available the results of the quality controls we made during the phase of acquisition and delivery processes of new or updated spectroscopic data. The SPARTE chain proves to be a powerful tool to validate and select data for major species of the Earth's atmosphere, but it is still limited for evaluating more exotic species or species having too small spectral signatures. The improvement of some parts of the SPARTE chain through improvement of underlying models (4A/OP), reference spaceborne observations (ACE-FTS limb measurements) or databases (ARSA, ECMWF Reanalyses...) is under progress. General and systematic cross-comparisons with other databases will also be done in future versions of GEISA. In parallel, we plan to generalize, when possible, the use of *ab initio* data, in collaboration with other teams, both as a point of comparison with experimentally derived effective models traditionally used in spectroscopic databases, but also to improve or complete existing data.

Considering the line parameter database, a crucial path of improvement is the consideration of non-Voigt line-shape parameters. Even though the amount of measurements and calculations involving the recommended Hartmann-Tran profile [172] remains limited so far, the level of precision achieved by the sophisticated non-Voigt profiles is ever increasingly demanded by ground-based or spaceborne instruments. The future releases of GEISA will be designed to gather such high-level information.



The current GEISA-2020 as well as the GEISA-2015 compilations can be accessed through <https://geisa.aeris-data.fr/>. Thanks to an updated user-friendly interface, the operations of selection, extraction, sorting, filtering, graphical representation, statistical analysis of the most characteristic spectroscopic parameters are more attractive than in the previous web version.

## 5 Acknowledgements.

IASI has been developed and built under the responsibility of CNES. It is flown onboard the Metop satellites as part of the EUMETSAT Polar System. The IASI L1 data are received through the EUMETCast near real time data distribution service. We particularly wish to thank the Mésocentre ESPRI services for their help in getting IASI data. TCCON data were obtained from the TCCON Data Archive, hosted by the Carbon Dioxide Information Analysis Center (CDIAC) - [tcon.onrl.gov](http://tcon.onrl.gov). Calculations were performed using the resources of IDRIS, the computing centre of CNRS and of the IPSL data and computing centre Mésocentre ESPRI. This work has been funded by CNES. The authors thank the CNES MicroCarb team for support and fruitful discussions. The authors are thankful to ECMWF for making the ERA-I and ERA5 outputs available through the ECMWF Data Server.

We also thank the AERIS/IPSL/CNES atmospheric data and computing centre for ensuring a friendly access to the GEISA international community and for managing the website.

Pr. R.R. Gamache is pleased to acknowledge support of this research by the National Science Foundation through Grant No. AGS-1156862.

The researches from V.E. Zuev Institute of Atmospheric Optics of Siberian Branch of Russian Academy of Sciences were supported by the Ministry of Science and Higher Education of the Russian Federation.

The financial support of the Natural Sciences and Engineering Research Council of Canada is gratefully acknowledged by Pr. N. Moazzen-Ahmadi.

The work of Tomsk group on ozone spectroscopy was supported by the Russian Science Foundation RNF grant no. 19-12-00171. GSMA Reims and LiPhy Grenoble acknowledge a support from the French-Russian collaboration program LIA CNRS "SAMIA". V. Ebert and G. Li acknowledge support of the work by the EUMETRISPEC project ([www.eumetrispec.org](http://www.eumetrispec.org)) within the European Metrology Research Program (EMRP).

Last but not least, our warmest thanks go to Nicole Jacquinet who has recently retired. Nicole has devoted more than 40 years of her life to the promotion of GEISA around the world and, more generally, of the need for up-to-date spectroscopy in order to benefit from innovative remote sensing observations.

This work could not stop after that.

## 6 Appendix A. List of acronyms

4A	Atlas Automatisé des Absorptions Atmosphériques ; Automatized Atmospheric Absorption Atlas
4A/OP	4A/OPerational release
AERIS	Atmosphere and service data pole (CNES, CNRS, IPSL), France
AFGL	Air Force Geophysics Laboratory
ARA/ABC(t)	Atmospheric Radiation Analysis/Atmosphère-Biosphère-Climat (télédétection)
ASD	Acetylene Spectroscopic Databank
CAL/VAL	Calibration/Validation
CDMS	Cologne Database for Molecular Spectroscopy
CDS	Carbon Dioxide Spectroscopic Databank
CIRS	Composite InfraRed Spectrometer
CNRS	Centre National de la Recherche Scientifique (France)
CNES	Centre National d'Etudes Spatiales (France)
CRB	Complex Robert-Bonamy
CRDS	Cavity ring-down spectroscopy
CVRQD	name of the adiabatic semiglobal PESs of water isotopologues
DAS	Differential laser Absorption Spectroscopy
DMS	Dipole Moment Surface-3D
DVR-3D	Discrete Variable Representation
FT-CEAS	Continuous Wave-Cavity Absorption Spectroscopy
EH	Effective Hamiltonian
ENVISAT	ENVIronmental SATellite
EUMETSAT	European Organisation for the Exploitation of Meteorological Satellites
FTIR	Fourier Transformed InfraRed spectroscopy
FTS	Fourier Transform Spectrometer
GEISA	Gestion et Etude des Informations Spectroscopiques Atmosphériques; Management and study of Atmospheric Spectroscopic Information
GOSAT	Greenhouse Observing SATellite project
GS	Ground State
GSMA	Groupe de Spectroscopie Moléculaire et Atmosphérique (France)
HITRAN	HIGH-resolution TRANsmission molecular absorption database
HWHM	Half Width at Half Maximum
IAO	Institute of Atmospheric Optics (Russia)
IASI	Infrared Atmospheric Sounder Interferometer
IASI/NG	Infrared Atmospheric Sounder Interferometer/New Generation
ICB	Institut Carnot de Bourgogne
ID	Identification code
IDRIS	Institut du développement et des ressources en informatique scientifique
INSU	Institut National des Sciences de l'Univers (France)
IPSL	Institut Pierre Simon Laplace
IR	InfraRed
ISSWG	IASI Sounding Science Working Group
JPL	Jet Propulsion Laboratory (USA)
KIT	Institute for Meteorology and Climate Research Centre Karlsruhe, (Germany)
LIPhy	Laboratoire Interdisciplinaire de Physique (France)

LISA	Laboratoire Inter-Universitaire des Systèmes Atmosphériques (France)
LMD	Laboratoire de Météorologie Dynamique (France)
MCRB	Modified Complex Robert-Bonamy
MERLIN	Methane Remote Sensing Lidar Mission
MICROCARB	MICROsatellite mission to monitor the fluxes of CARBOn dioxide
MIPAS	Michelson Interferometer for Passive Atmospheric Sounding
Metop	Meteorological operational satellite
NASA	National Aeronautics and Space Administration (USA)
NCAR	National Center for Atmospheric research (USA)
NIR	Near-InfraRed
PES	Potential Energy Surface
SPARTE	Spectroscopic Parameters And Radiative Transfer Evaluation
S&MPO	Spectroscopy & molecular properties of Ozone
SWIR	ShortWave Infrared
TIR	Thermal InfraRed
VAMDC	Virtual Atomic and Molecular Data Centre

## 7 Appendix B. Description of the format used for the line parameters stored in the GEISA-2020 edition:

The format of each entry is described in the following Table 12.

Each entry is a 252-character record to describe the 31 spectroscopic line parameters.

First line of Table 12: the 31 Spectroscopic line parameters are listed in the 31 columns and their description is given below.

Line 2 and line 3 display the field length and the FORTRAN format descriptor, respectively.

Line 4 displays the standard\_default values associated to each parameter.

Line 5 displays a cumulative index indicating the position of the last character of the record associated to each of the 31 spectroscopic line parameters.

The standard default values for fields «O'», « T » and « T' », have been changed and set to “zero”. This modification was made to avoid potential misunderstanding and thus improper use of these parameters in some applications especially related to forward radiative transfer. Value in field “M” is documented in GEISA only if it is directly provided by the author of the spectroscopic line entry.

Table 12: Format of each entry in GEISA-2015

Parameter	A	B	C	D	E1	E2	E3	E4	F	G	I	J
Field length	12	11	6	10	25	25	15	15	4	3	3	3
Fortran descriptor	F12.6	1PD11.4	0PF6.4	F10.4	A25	A25	A15	A15	F4.2	I3	I3	A3
Undefined values	NR	-9.9999D-01	-.9999	-0.9999	*	*	*	*	-.99	-99	-99	*
Record counting	12	23	29	39	64	89	104	119	123	126	129	132

K	L	M	N	O	R	A'	B'	C'	F'
2	1	10	7	9	6	10	11	6	4
I2	I1	1PE10.3	0PF7.4	F9.6	F6.4	F10.6	1PD11.4	0PF6.4	F4.2
-9	0	-9.999E-01	-9.9999	0.000000	-.9999	-0.999999	-9.9999D-01	-.9999	-.99
134	135	145	152	161	167	177	188	194	198

O'	R'	N'	S	S'	T	T'	U	U'
9	6	7	4	4	8	8	4	4
F9.6	F6.4	F7.4	F4.2	F4.2	F8.6	F8.6	F4.2	F4.2
0.000000	-.9999	-9.9999	-.99	-.99	0.000000	0.000000	-.99	-.99
207	213	220	224	228	236	244	248	252

A: wave number ( $\text{cm}^{-1}$ ) of the line

B: intensity of the line in ( $\text{cm}^{-1}/(\text{molecule} \cdot \text{cm}^{-2})$ ) at 296K

C: Air broadening pressure halfwidth (HWHM) ( $\text{cm}^{-1}\text{atm}^{-1}$ ) at 296K

D: Energy of the lower transition level ( $\text{cm}^{-1}$ )

E<sub>i</sub> (i=1,2,3,4): Transition quantum identifications for the lower and upper state of the transition

E1: upper state vibrational identification      E2: lower state vibrational identification

E3: upper state rotationnal identification      E4: lower state rotationnal identification

F: temperature dependence coefficient n of the air broadening halfwidth

G: identification code for isotopologue as in GEISA  
 I: identification code for molecule as in GEISA  
 J: Internal GEISA code for the data identification  
 K: Molecule number as in HITRAN  
 L: isotopologue number (1=most abundant, 2= second...etc) as in HITRAN  
 M: Einstein A-coefficient  
 N: self-broadening pressure halfwidth (HWHMself) ( $\text{cm}^{-1}\text{atm}^{-1}$ ) at 296K  
 O: air pressure shift of the line transition ( $\text{cm}^{-1}$ ) at 296K  
 R: temperature dependence coefficient of the air pressure shift  
 A': estimated accuracy ( $\text{cm}^{-1}$ ) on the line position  
 B': estimated accuracy on the intensity of the line in ( $\text{cm}^{-1}/(\text{molecule}\cdot\text{cm}^{-2})$ )  
 C': estimated accuracy on the air collision halfwidth (HWHM) ( $\text{cm}^{-1}\text{atm}^{-1}$ )  
 F': estimated accuracy on the temperature dependence coefficient of the air broadening halfwidth  
 O': estimated accuracy on the air pressure shift of the line transition ( $\text{cm}^{-1}$ ) at 296K  
 R': estimated accuracy on the temperature dependence coefficient of the air pressure shift  
 N': estimated accuracy on the self-broadened (HWHM) ( $\text{cm}^{-1}\text{atm}^{-1}$ ) at 296K  
 S: temperature dependence coefficient of the self-broadening halfwidth  
 S': estimated accuracy on the temperature dependence coefficient of the self-broadening halfwidth  
 T: self pressure shift of the line transition ( $\text{cm}^{-1}$ ) at 296K  
 T': estimated accuracy on the self pressure shift of the line transition ( $\text{cm}^{-1}$ ) at 296K  
 U: temperature dependence coefficient of the self pressure shift  
 U': estimated accuracy on the temperature dependence coefficient of the self pressure shift

As shown in line 4 of Table 12 GEISA undefined values are attributed to the line parameter entries when no value is available from the data provider (missing data).

## 8 Appendix C. Molecules and isotopologues in GEISA-2015

Description of molecule and isotopologue codes in GEISA-2020 are given in Table 13. The molecule names and associated codes are in the two first columns; for each molecule, the isotopologue codes and the corresponding detailed formula are in columns 3 and 4 respectively. The abundance used in GEISA is given in the 5<sup>th</sup> column.

Table 13: Description of the molecule and isotopologue codes in GEISA-2020

Molecule	Molecule Code	I Code	Formula	Abundance
H <sub>2</sub> O	1	161	H <sup>16</sup> OH	0.997317
		181	H <sup>18</sup> OH	0.002000
		171	H <sup>17</sup> OH	$3.718840 \times 10^{-4}$
		262	D <sub>2</sub> <sup>16</sup> O	$2.419700 \times 10^{-8}$

Molecule	Molecule Code	I Code	Formula	Abundance
		282	D <sub>2</sub> <sup>18</sup> O	4.852080 × 10 <sup>-11</sup>
		272	D <sub>2</sub> <sup>17</sup> O	9.022841 × 10 <sup>-12</sup>
CO <sub>2</sub>	2	626	<sup>16</sup> O <sup>12</sup> C <sup>16</sup> O	0.9842
		636	<sup>16</sup> O <sup>13</sup> C <sup>16</sup> O	1.106 x 10 <sup>-2</sup>
		628	<sup>16</sup> O <sup>12</sup> C <sup>18</sup> O	3.947 x 10 <sup>-3</sup>
		627	<sup>16</sup> O <sup>12</sup> C <sup>17</sup> O	7.339 x 10 <sup>-4</sup>
		638	<sup>16</sup> O <sup>13</sup> C <sup>18</sup> O	4.434 x 10 <sup>-5</sup>
		637	<sup>16</sup> O <sup>13</sup> C <sup>17</sup> O	8.246 x 10 <sup>-6</sup>
		828	<sup>18</sup> O <sup>12</sup> C <sup>18</sup> O	3.957 x 10 <sup>-6</sup>
		728	<sup>17</sup> O <sup>12</sup> C <sup>18</sup> O	1.472 x 10 <sup>-6</sup>
		727	<sup>17</sup> O <sup>12</sup> C <sup>17</sup> O	1.430 x 10 <sup>-7</sup>
		838	<sup>18</sup> O <sup>13</sup> C <sup>18</sup> O	4.446 x 10 <sup>-8</sup>
		738	<sup>17</sup> O <sup>13</sup> C <sup>18</sup> O	1.654 x 10 <sup>-8</sup>
737	<sup>17</sup> O <sup>13</sup> C <sup>17</sup> O	1.55 x 10 <sup>-9</sup>		
O <sub>3</sub>	3	666	<sup>16</sup> O <sup>16</sup> O <sup>16</sup> O	0.992901
		668	<sup>16</sup> O <sup>16</sup> O <sup>18</sup> O	0.003982
		686	<sup>16</sup> O <sup>18</sup> O <sup>16</sup> O	0.001991
		667	<sup>16</sup> O <sup>16</sup> O <sup>17</sup> O	7.404750 × 10 <sup>-4</sup>
		676	<sup>16</sup> O <sup>17</sup> O <sup>16</sup> O	3.702370 × 10 <sup>-4</sup>
N <sub>2</sub> O	4	446	<sup>14</sup> N <sup>14</sup> N <sup>16</sup> O	0.990333
		456	<sup>14</sup> N <sup>15</sup> N <sup>16</sup> O	0.003641
		546	<sup>15</sup> N <sup>14</sup> N <sup>16</sup> O	0.003641
		448	<sup>14</sup> N <sup>14</sup> N <sup>18</sup> O	0.001986
		458	<sup>14</sup> N <sup>14</sup> N <sup>18</sup> O	7.300807 × 10 <sup>-4</sup>
		548	<sup>15</sup> N <sup>14</sup> N <sup>18</sup> O	7.300807 × 10 <sup>-4</sup>
		447	<sup>14</sup> N <sup>14</sup> N <sup>17</sup> O	3.692800 × 10 <sup>-4</sup>
		556	<sup>15</sup> N <sup>15</sup> N <sup>16</sup> O	1.338574 × 10 <sup>-5</sup>
CO	5	26	<sup>12</sup> C <sup>16</sup> O	0.986544
		36	<sup>13</sup> C <sup>16</sup> O	0.011084
		28	<sup>12</sup> C <sup>18</sup> O	0.001978
		27	<sup>12</sup> C <sup>17</sup> O	3.678670 × 10 <sup>-4</sup>
		38	<sup>13</sup> C <sup>18</sup> O	2.222500 × 10 <sup>-5</sup>
		37	<sup>13</sup> C <sup>17</sup> O	4.132920 × 10 <sup>-6</sup>
CH <sub>4</sub>	6	211	<sup>12</sup> CH <sub>4</sub>	0.988274
		311	<sup>13</sup> CH <sub>4</sub>	0.011103
O <sub>2</sub>	7	66	<sup>16</sup> O <sup>16</sup> O	0.995262
		68	<sup>16</sup> O <sup>18</sup> O	0.003991
		67	<sup>16</sup> O <sup>17</sup> O	7.422350 × 10 <sup>-4</sup>

Molecule	Molecule Code	I Code	Formula	Abundance
NO	8	46	$^{14}\text{N}^{16}\text{O}$	0.993974
		56	$^{15}\text{N}^{16}\text{O}$	0.003654
		48	$^{14}\text{N}^{18}\text{O}$	0.001993
SO <sub>2</sub>	9	626	$^{32}\text{S}^{16}\text{O}_2$	0.945678
		646	$^{34}\text{S}^{16}\text{O}_2$	0.041950
NO <sub>2</sub>	10	646	$^{14}\text{N}^{16}\text{O}_2$	0.991616
		656	$^{15}\text{N}^{16}\text{O}_2$	0.003646
NH <sub>3</sub>	11	411	$^{14}\text{NH}_3$	0.995872
		511	$^{15}\text{NH}_3$	0.003661
PH <sub>3</sub>	12	131	$^{31}\text{PH}_3$	0.999533
HNO <sub>3</sub>	13	146	$\text{H}^{14}\text{N}^{16}\text{O}$	0.989110
		156	$\text{H}^{15}\text{N}^{16}\text{O}$	0.003636
OH	14	61	$^{16}\text{OH}$	0.997473
		81	$^{18}\text{OH}$	0.002000
		62	$^{16}\text{OD}$	$1.553710 \times 10^{-4}$
HF	15	19	$\text{H}^{19}\text{F}$	0.999844
		29	$\text{D}^{19}\text{F}$	$1.557410 \times 10^{-4}$
HCl	16	15	$\text{H}^{35}\text{Cl}$	0.757587
		17	$\text{H}^{37}\text{Cl}$	0.242257
		25	$\text{D}^{35}\text{Cl}$	$1.180050 \times 10^{-4}$
		27	$\text{D}^{37}\text{Cl}$	$3.773500 \times 10^{-5}$
HBr	17	19	$\text{H}^{79}\text{Br}$	0.506781
		11	$\text{H}^{81}\text{Br}$	0.493063
		29	$\text{D}^{79}\text{Br}$	$7.893840 \times 10^{-5}$
		21	$\text{D}^{81}\text{Br}$	$7.680160 \times 10^{-5}$
HI	18	17	$\text{H}^{127}\text{I}$	0.999844
		27	$\text{D}^{127}\text{I}$	$1.557410 \times 10^{-4}$
ClO	19	56	$^{35}\text{Cl}^{16}\text{O}$	0.755908
		76	$^{37}\text{Cl}^{16}\text{O}$	0.241720
OCS	20	622	$^{16}\text{O}^{12}\text{C}^{32}\text{S}$	0.937395
		624	$^{16}\text{O}^{12}\text{C}^{34}\text{S}$	0.041583
		632	$^{16}\text{O}^{13}\text{C}^{32}\text{S}$	0.010531
		623	$^{16}\text{O}^{12}\text{C}^{33}\text{S}$	0.007399
		822	$^{18}\text{O}^{12}\text{C}^{32}\text{S}$	0.001880
		634	$^{16}\text{O}^{13}\text{C}^{34}\text{S}$	$4.671757 \times 10^{-4}$
H <sub>2</sub> CO	21	126	$\text{H}_2^{12}\text{C}^{16}\text{O}$	0.986237
		136	$\text{H}_2^{13}\text{C}^{16}\text{O}$	0.011080
		128	$\text{H}_2^{12}\text{C}^{18}\text{O}$	0.001978
C <sub>2</sub> H <sub>6</sub>	22	226	$^{12}\text{C}_2\text{H}_6$	0.976990
		236	$^{12}\text{C}^{13}\text{CH}_6$	0.021953
CH <sub>3</sub> D	23	212	$^{12}\text{CH}_3\text{D}$	$6.157510 \times 10^{-4}$
		312	$^{13}\text{CH}_3\text{D}$	$6.917850 \times 10^{-6}$
C <sub>2</sub> H <sub>2</sub>	24	221	$^{12}\text{C}_2\text{H}_2$	0.977599



Molecule	Molecule Code	I Code	Formula	Abundance
		231	$^{12}\text{C}^{13}\text{CH}_2$	0.021966
$\text{C}_2\text{H}_4$	25	211	$^{12}\text{C}_2\text{H}_4$	0.977294
		311	$^{12}\text{C}^{13}\text{CH}_4$	0.021959
$\text{GeH}_4$	26	411	$^{74}\text{GeH}_4$	1.000000
		211	$^{72}\text{GeH}_4$	1.000000
		011	$^{70}\text{GeH}_4$	1.000000
		311	$^{73}\text{GeH}_4$	1.000000
		611	$^{76}\text{GeH}_4$	1.000000
$\text{HCN}$	27	124	$\text{H}^{12}\text{C}^{14}\text{N}$	0.985114
		134	$\text{H}^{13}\text{C}^{14}\text{N}$	0.011068
		125	$\text{H}^{12}\text{C}^{15}\text{N}$	0.003622
		224	$\text{D}^{12}\text{C}^{14}\text{N}$	$1.534456 \times 10^{-4}$
$\text{C}_3\text{H}_8$	28	221	$^{12}\text{C}_3\text{H}_8$	0.965835
$\text{C}_2\text{N}_2$	29	224	$^{12}\text{C}_2^{14}\text{N}_2$	0.970752
$\text{C}_4\text{H}_2$	30	211	$^{12}\text{C}_4\text{H}_2$	0.955998
$\text{HC}_3\text{N}$	31	124	$\text{H}^{12}\text{C}_3^{14}\text{N}$	0.963346
$\text{HOCl}$	32	165	$\text{H}^{16}\text{O}^{35}\text{Cl}$	0.755790
		167	$\text{H}^{16}\text{O}^{37}\text{Cl}$	0.241683
$\text{N}_2$	33	44	$^{14}\text{N}^{14}\text{N}$	0.992687
$\text{CH}_3\text{Cl}$	34	215	$^{12}\text{CH}_3^{35}\text{Cl}$	0.748937
		217	$^{12}\text{CH}_3^{37}\text{Cl}$	0.239491
$\text{H}_2\text{O}_2$	35	166	$\text{H}_2^{16}\text{O}^{16}\text{O}$	0.994952
$\text{H}_2\text{S}$	36	121	$\text{H}_2^{32}\text{S}$	0.949884
		141	$\text{H}_2^{34}\text{S}$	0.042137
		131	$\text{H}_2^{33}\text{S}$	0.007498
$\text{HCOOH}$	37	261	$\text{H}^{12}\text{C}^{16}\text{O}^{16}\text{OH}$	0.983898
$\text{COF}_2$	38	269	$^{12}\text{C}^{16}\text{O}^{19}\text{F}_2$	0.986544
$\text{SF}_6$	39	29	$^{32}\text{S}^{19}\text{F}_6$	0.950180
$\text{C}_3\text{H}_4$	40	341	$^{12}\text{C}_3\text{H}_4$	0.966587
$\text{HO}_2$	41	166	$\text{H}^{16}\text{O}_2$	0.995107
$\text{ClONO}_2$	42	564	$^{15}\text{Cl}^{16}\text{O}^{14}\text{N}^{16}\text{O}_2$	0.749570
		764	$^{17}\text{Cl}^{16}\text{O}^{14}\text{N}^{16}\text{O}_2$	0.239694
$\text{CH}_3\text{Br}$	43	79	$^{12}\text{CH}_3^{79}\text{Br}$	0.500995
		81	$^{12}\text{CH}_3^{81}\text{Br}$	0.487433
$\text{CH}_3\text{OH}$	44	216	$^{12}\text{CH}_3^{16}\text{OH}$	0.985930
$\text{NO}^+$	45	46	$^{14}\text{N}^{16}\text{O}^+$	0.993974
$\text{HNC}$	46	142	$\text{H}^{14}\text{N}^{12}\text{C}$	0.985114
$\text{C}_6\text{H}_6$	47	266	$^{12}\text{C}_6\text{H}_6$	0.934291
$\text{C}_2\text{HD}$	48	122	$^{12}\text{C}_2\text{HD}$	$3.045500 \times 10^{-4}$
$\text{CF}_4$	49	291	$^{12}\text{C}^{19}\text{F}_4$	0.988890
$\text{CH}_3\text{CN}$	50	234	$^{12}\text{CH}_3^{12}\text{C}^{14}\text{N}$	0.973866
$\text{HDO}$	51	162	$\text{H}^{16}\text{OD}$	$3.106930 \times 10^{-4}$
		182	$\text{H}^{18}\text{OD}$	$6.230030 \times 10^{-7}$

Molecule	Molecule Code	I Code	Formula	Abundance
		172	H <sup>17</sup> OD	1.158530 × 10 <sup>-7</sup>
SO <sub>3</sub>	52	26	<sup>32</sup> S <sup>16</sup> O <sub>3</sub>	0.943400
HONO	53	646	H <sup>16</sup> O <sup>14</sup> N <sup>16</sup> O	0.9937102
COFCl	54	265	<sup>12</sup> C <sup>16</sup> O <sup>F35</sup> Cl	1.000000
		267	<sup>12</sup> C <sup>16</sup> O <sup>F37</sup> Cl	1.000000
CH <sub>3</sub> I	55	217	<sup>12</sup> CH <sub>3</sub> <sup>127</sup> I	1.000000
CH <sub>3</sub> F	56	219	<sup>12</sup> CH <sub>3</sub> <sup>19</sup> F	1.000000
RuO <sub>4</sub>	57	102	<sup>102</sup> Ru <sup>16</sup> O <sub>4</sub>	1.000000
		104	<sup>104</sup> Ru <sup>16</sup> O <sub>4</sub>	1.000000
		101	<sup>101</sup> Ru <sup>16</sup> O <sub>4</sub>	1.000000
		99	<sup>99</sup> Ru <sup>16</sup> O <sub>4</sub>	1.000000
		100	<sup>100</sup> Ru <sup>16</sup> O <sub>4</sub>	1.000000
		97	<sup>97</sup> Ru <sup>16</sup> O <sub>4</sub>	1.000000
		98	<sup>98</sup> Ru <sup>16</sup> O <sub>4</sub>	1.000000
		106	<sup>106</sup> Ru <sup>16</sup> O <sub>4</sub>	1.000000
		103	<sup>103</sup> Ru <sup>16</sup> O <sub>4</sub>	1.000000
H <sub>2</sub> C <sub>3</sub> H <sub>2</sub>	58	121	H <sub>2</sub> <sup>12</sup> C <sub>3</sub> H <sub>2</sub>	1.000000

## Bibliography

- [1] N. Jacquinet-Husson, R. Armante, N.A. Scott, A. Chédin, L. Crépeau, C. Boutammine, A. Bouhdaoui, C. Crevoisier, V. Capelle, C. Boonne, N. Poulet-Crovisier, A. Barbe, D. Chris Benner, V. Boudon, L.R. Brown, J. Buldyreva, A. Campargue, L.H. Coudert, V.M. Devi, M.J. Down, B.J. Drouin, A. Fayt, C. Fittschen, J.-M. Flaud, R.R. Gamache, J.J. Harrison, C. Hill, Ø. Hodnebrog, S.-M. Hu, D. Jacquemart, A. Jolly, E. Jiménez, N.N. Lavrentieva, A.-W. Liu, L. Lodi, O.M. Lyulin, S.T. Massie, S. Mikhailenko, H.S.P. Müller, O.V. Naumenko, A. Nikitin, C.J. Nielsen, J. Orphal, V.I. Perevalov, A. Perrin, E. Polovtseva, A. Predoi-Cross, M. Rotger, A.A. Ruth, S.S. Yu, K. Sung, S.A. Tashkun, J. Tennyson, V.G. Tyuterev, J. Vander Auwera, B.A. Voronin, A. Makie, The 2015 edition of the GEISA spectroscopic database, *J. Mol. Spectrosc.* 327 (2016). <https://doi.org/10.1016/j.jms.2016.06.007>.
- [2] I.E. Gordon, L.S. Rothman, C. Hill, R. V. Kochanov, Y. Tan, P.F. Bernath, M. Birk, V. Boudon, A. Campargue, K. V. Chance, B.J. Drouin, J.M. Flaud, R.R. Gamache, J.T. Hodges, D. Jacquemart, V.I. Perevalov, A. Perrin, K.P. Shine, M.A.H. Smith, J. Tennyson, G.C. Toon, H. Tran, V.G. Tyuterev, A. Barbe, A.G. Császár, V.M. Devi, T. Furtenbacher, J.J. Harrison, J.M. Hartmann, A. Jolly, T.J. Johnson, T. Karman, I. Kleiner, A.A. Kyuberis, J. Loos, O.M. Lyulin, S.T. Massie, S.N. Mikhailenko, N. Moazzen-Ahmadi, H.S.P. Müller, O. V. Naumenko, A. V. Nikitin, O.L. Polyansky, M. Rey, M. Rotger, S.W. Sharpe, K. Sung, E. Starikova, S.A. Tashkun, J. Vander Auwera, G. Wagner, J. Wilzewski, P. Wcisło, S. Yu, E.J. Zak, The HITRAN2016 molecular spectroscopic database, *J. Quant. Spectrosc. Radiat. Transf.* 203 (2017) 3–69. <https://doi.org/10.1016/j.jqsrt.2017.06.038>.
- [3] A. Chedin, N. Husson, N. Scott, Une banque de données pour l'étude des phénomènes de transfert radiatif dans les atmosphères planétaires: la banque GEISA, *Bull. d'Information Du Cent. Données Stellaires, Fr.* 22 (1982) 21–121.
- [4] N. Husson, B. Bonnet, N.A. Scott, A. Chedin, Management and study of spectroscopic information: The GEISA program, *J. Quant. Spectrosc. Radiat. Transf.* 48 (1992) 509–518. [https://doi.org/10.1016/0022-4073\(92\)90116-L](https://doi.org/10.1016/0022-4073(92)90116-L).
- [5] N. Jacquinet-Husson, E. Arié, J. Ballard, A. Barbe, G. Bjoraker, B. Bonnet, L.R. Brown, C. Camy-Peyret, J.P. Champion, A. Chédin, A. Chursin, C. Clerbaux, G. Duxbury, J.-M. Flaud, N. Fourrié, A. Fayt, G. Graner, R. Gamache, A. Goldman, V. Golovko, G. Guelachvili, J.M. Hartmann, J.C. Hilico, J. Hillman, G. Lefèvre, E. Lellouch, S.N. Mikhailenko, O. V Naumenko, V. Nemtchinov, D.A. Newnham, A. Nikitin, J. Orphal, A. Perrin, D.C. Reuter, C.P. Rinsland, L. Rosenmann, L.S. Rothman, N.A. Scott, J. Selby, L.N. Sinitza, J.M. Sirota, A.M. Smith, K.M. Smith, V.G. Tyuterev, R.H. Tipping, S. Urban, P. Varanasi, M. Weber, The 1997 spectroscopic GEISA databank, *J. Quant. Spectrosc. Radiat. Transf.* 62 (1999) 205–254. [https://doi.org/10.1016/S0022-4073\(98\)00111-3](https://doi.org/10.1016/S0022-4073(98)00111-3).
- [6] N. Jacquinet-Husson, N.A. Scott, A. Chédin, L. Crépeau, R. Armante, V. Capelle, J. Orphal, A. Coustenis, C. Boonne, N. Poulet-Crovisier, A. Barbe, M. Birk, L.R. Brown, C. Camy-Peyret, C. Claveau, K. Chance, N. Christidis, C. Clerbaux, P.F. Coheur, V. Dana, L. Daumont, M.R. De Backer-Barilly, G. Di Lonardo, J.M. Flaud, A. Goldman, A. Hamdouni, M. Hess, M.D. Hurley, D. Jacquemart, I. Kleiner, P. Köpke, J.Y. Mandin, S. Massie, S. Mikhailenko, V. Nemtchinov, A. Nikitin, D. Newnham, A. Perrin, V.I. Perevalov, S. Pinnock, L. Régalia-Jarlot, C.P. Rinsland, A. Rublev, F. Schreier, L. Schult, K.M. Smith, S.A. Tashkun, J.L. Teffo, R.A. Toth, V.G. Tyuterev, J. Vander Auwera, P. Varanasi, G. Wagner, The GEISA spectroscopic database: Current and future archive for Earth and planetary atmosphere studies, *J. Quant. Spectrosc. Radiat. Transf.* 109 (2008) 1043–1059. <https://doi.org/10.1016/j.jqsrt.2007.12.015>.

- [7] N. Jacquinet-Husson, L. Crepeau, R. Armante, C. Boutammine, A. Chédin, N.A. Scott, C. Crevoisier, V. Capelle, C. Boone, N. Poulet-Crovisier, A. Barbe, A. Campargue, D. Chris Benner, Y. Benilan, B. Bézard, V. Boudon, L.R. Brown, L.H. Coudert, A. Coustenis, V. Dana, V.M. Devi, S. Fally, A. Fayt, J.-M. Flaud, A. Goldman, M. Herman, G.J. Harris, D. Jacquemart, A. Jolly, I. Kleiner, A. Kleinböhl, F. Kwabia-Tchana, N. Lavrentieva, N. Lacome, L.-H. Xu, O.M. Lyulin, J.-Y. Mandin, A. Maki, S. Mikhailenko, C.E. Miller, T. Mishina, N. Moazzen-Ahmadi, H.S.P. Müller, A. Nikitin, J. Orphal, V. Perevalov, A. Perrin, D.T. Petkie, A. Predoi-Cross, C.P. Rinsland, J.J. Remedios, M. Rotger, M.A.H. Smith, K. Sung, S. Tashkun, J. Tennyson, R.A. Toth, A.-C. Vandaele, J. Vander Auwera, The 2009 edition of the GEISA spectroscopic database, *J. Quant. Spectrosc. Radiat. Transf.* 112 (2011) 2395–2445. <https://doi.org/10.1016/j.jqsrt.2011.06.004>.
- [8] R. Armante, N. Scott, C. Crevoisier, V. Capelle, L. Crepeau, N. Jacquinet, A. Chédin, Evaluation of spectroscopic databases through radiative transfer simulations compared to observations. Application to the validation of GEISA 2015 with IASI and TCCON, *J. Mol. Spectrosc.* 327 (2016) 180–192. <https://doi.org/10.1016/j.jms.2016.04.004>.
- [9] D. Wunch, G.C. Toon, J.F.L. Blavier, R.A. Washenfelder, J. Notholt, B.J. Connor, D.W.T. Griffith, V. Sherlock, P.O. Wennberg, The total carbon column observing network, *Philos. Trans. R. Soc. A Math. Phys. Eng. Sci.* 369 (2011) 2087–2112. <https://doi.org/10.1098/rsta.2010.0240>.
- [10] A. Scott, N.A. and Chédin, A Fast Line-by-Line Method for Atmospheric Absorption Computations: The Automatized Atmospheric Absorption Atlas, *J. Appl. Meteorol.* 20 (1981) 802–812.
- [11] R.R. Gamache, B. Vispoel, M. Rey, A. Nikitin, V. Tyuterev, O. Egorov, I.E. Gordon, V. Boudon, Total internal partition sums for the HITRAN2020 database, *J. Quant. Spectrosc. Radiat. Transf.* 271 (2021) 107713. <https://doi.org/10.1016/j.jqsrt.2021.107713>.
- [12] S.N. Mikhailenko, S. Kassi, D. Mondelain, R.R. Gamache, A. Campargue, A spectroscopic database for water vapor between 5850 and 8340  $\text{cm}^{-1}$ , *J. Quant. Spectrosc. Radiat. Transf.* 179 (2016) 198–216. <https://doi.org/10.1016/j.jqsrt.2016.03.035>.
- [13] S.N. Mikhailenko, S. Kassi, D. Mondelain, A. Campargue, Water vapor absorption between 5690 and 8340  $\text{cm}^{-1}$ : Accurate empirical line centers and validation tests of calculated line intensities, *J. Quant. Spectrosc. Radiat. Transf.* 245 (2020) 106840. <https://doi.org/10.1016/j.jqsrt.2020.106840>.
- [14] B. Vispoel, J.H. Cavalcanti, R.R. Gamache, Modified complex Robert-Bonamy calculations of line shape parameters and their temperature dependence for water vapor in collision with  $\text{N}_2$ , *J. Quant. Spectrosc. Radiat. Transf.* 228 (2019) 79–89. <https://doi.org/10.1016/j.jqsrt.2019.02.023>.
- [15] B. Vispoel, J.H. Cavalcanti, E.T. Paige, R.R. Gamache, Vibrational dependence, temperature dependence, and prediction of line shape parameters for the  $\text{H}_2\text{O}-\text{N}_2$  collision system, *J. Quant. Spectrosc. Radiat. Transf.* 253 (2020) 107030. <https://doi.org/10.1016/j.jqsrt.2020.107030>.
- [16] A. Campargue, S. Kassi, A. Yachmenev, A.A. Kyuberis, J. Küpper, S.N. Yurchenko, Observation of electric-quadrupole infrared transitions in water vapor, *Phys. Rev. Res.* 2 (2020) 23091. <https://doi.org/10.1103/PhysRevResearch.2.023091>.
- [17] A. Campargue, A.M. Solodov, A.A. Solodov, A. Yachmenev, S.N. Yurchenko, Detection of electric-quadrupole transitions in water vapour near 5.4 and 2.5  $\mu\text{m}$ , *Phys. Chem. Chem.*

Phys. 22 (2020) 12476–12481. <https://doi.org/10.1039/D0CP01667E>.

- [18] J. Tennyson, P.F. Bernath, L.R. Brown, A. Campargue, M.R. Carleer, A.G. Császár, R.R. Gamache, J.T. Hodges, A. Jenouvrier, O. V Naumenko, O.L. Polyansky, L.S. Rothman, R.A. Toth, A.C. Vandaele, N.F. Zobov, L. Daumont, A.Z. Fazliev, T. Furtenbacher, I.E. Gordon, S.N. Mikhailenko, S. V Shirin, IUPAC critical evaluation of the rotational–vibrational spectra of water vapor. Part I—Energy levels and transition wavenumbers for H<sub>2</sub>17O and H<sub>2</sub>18O, *J. Quant. Spectrosc. Radiat. Transf.* 110 (2009) 573–596. <https://doi.org/10.1016/j.jqsrt.2009.02.014>.
- [19] A.A. Kyuberis, N.F. Zobov, O. V. Naumenko, B.A. Voronin, O.L. Polyansky, L. Lodi, A. Liu, S.M. Hu, J. Tennyson, Room temperature line lists for deuterated water, *J. Quant. Spectrosc. Radiat. Transf.* 203 (2017) 175–185. <https://doi.org/10.1016/j.jqsrt.2017.06.026>.
- [20] S. V. Shirin, N.F. Zobov, O.L. Polyansky, Theoretical line list of D<sub>2</sub>16O up to 16,000 cm<sup>-1</sup> with an accuracy close to experimental, *J. Quant. Spectrosc. Radiat. Transf.* 109 (2008) 549–558. <https://doi.org/10.1016/j.jqsrt.2007.07.010>.
- [21] R.R. Gamache, J.-M. Hartmann, An intercomparison of measured pressure-broadening and pressure-shifting parameters of water vapor, *Can. J. Chem.* 82 (2004) 1013–1027. <https://doi.org/10.1139/v04-069>.
- [22] L.H. Coudert, The bending potential energy function of HDO obtained from high-resolution data, *J. Mol. Spectrosc.* 330 (2016) 112–119. <https://doi.org/10.1016/j.jms.2016.07.008>.
- [23] P. Bièvre, M. Gallet, N.E. Holden, I.L. Barnes, Isotopic Abundances and Atomic Weights of the Elements, *J. Phys. Chem. Ref. Data.* 13 (1984) 809–891. <https://doi.org/10.1063/1.555720>.
- [24] S.N. Yurchenko, B.A. Voronin, R.N. Tolchenov, N. Doss, O. V. Naumenko, W. Thiel, J. Tennyson, Potential energy surface of HDO up to 25 000 cm<sup>-1</sup>, *J. Chem. Phys.* 128 (2008) 1–13. <https://doi.org/10.1063/1.2806165>.
- [25] M.J. Down, Assignment of Trace Atmospheric Species, University College London, 2014. <https://discovery.ucl.ac.uk/id/eprint/1419269/>.
- [26] S.A. Tashkun, V.I. Perevalov, R.R. Gamache, J. Lamouroux, CDSD-296, high-resolution carbon dioxide spectroscopic databank: An update, *J. Quant. Spectrosc. Radiat. Transf.* 228 (2019) 124–131. <https://doi.org/10.1016/J.JQSRT.2019.03.001>.
- [27] S.A. Tashkun, V.I. Perevalov, R.R. Gamache, J. Lamouroux, CDSD-296, high resolution carbon dioxide spectroscopic databank: Version for atmospheric applications, *J. Quant. Spectrosc. Radiat. Transf.* 152 (2015) 45–73. <https://doi.org/10.1016/J.JQSRT.2014.10.017>.
- [28] <ftp://ftp.iao.ru/pub/CDSD-296/>, (n.d.).
- [29] V. Wilquet, A. Mahieux, A.C. Vandaele, V.I. Perevalov, S.A. Tashkun, A. Fedorova, O. Korablev, F. Montmessin, R. Dahoo, J.-L. Bertaux, Line parameters for the 01111–00001 band of <sup>12</sup>C<sup>16</sup>O<sup>18</sup>O from SOIR measurements of the Venus atmosphere, *J. Quant. Spectrosc. Radiat. Transf.* 109 (2008) 895–905. <https://doi.org/10.1016/J.JQSRT.2007.12.021>.
- [30] G.L. Villanueva, M.J. Mumma, R.E. Novak, T. Hewagama, Identification of a new band system of isotopic CO<sub>2</sub> near 3.3 μm: Implications for remote sensing of biomarker gases on Mars, *Icarus.* 195 (2008) 34–44. <https://doi.org/10.1016/j.icarus.2007.11.014>.

- [31] V.G. Tyuterev, A. Barbe, D. Jacquemart, C. Janssen, S.N. Mikhailenko, E.N. Starikova, Ab initio predictions and laboratory validation for consistent ozone intensities in the MW, 10 and 5  $\mu\text{m}$  ranges, *J. Chem. Phys.* 150 (2019). <https://doi.org/10.1063/1.5089134>.
- [32] S. Mikhailenko, A. Barbe, High resolution infrared spectrum of  $16\text{O}_3$ : The 3600–4300  $\text{cm}^{-1}$  range reinvestigated, *J. Quant. Spectrosc. Radiat. Transf.* 244 (2020). <https://doi.org/10.1016/j.jqsrt.2019.106823>.
- [33] V. Kokoouline, D. Lapiere, A. Alijah, V. Tyuterev, Localized and delocalized bound states of the main isotopologue  $48\text{O}_3$  and of  $18\text{O}$ -enriched  $50\text{O}_3$  isotopomers of the ozone molecule near the dissociation threshold, *Phys. Chem. Chem. Phys.* 22 (2020) 15885–15899. <https://doi.org/10.1039/D0CP02177F>.
- [34] S. Vasilchenko, A. Barbe, E. Starikova, S. Kassi, D. Mondelain, A. Campargue, V. Tyuterev, Detection and assignment of ozone bands near 95% of the dissociation threshold: Ultrasensitive experiments for probing potential energy function and vibrational dynamics, *Phys. Rev. A.* 102 (2020) 52804. <https://doi.org/10.1103/PhysRevA.102.052804>.
- [35] Y.L. Babikov, S.N. Mikhailenko, A. Barbe, V.G. Tyuterev, S&MPO – An information system for ozone spectroscopy on the WEB, *J. Quant. Spectrosc. Radiat. Transf.* 145 (2014) 169–196. <https://doi.org/10.1016/j.jqsrt.2014.04.024>.
- [36] A. Barbe, S. Mikhailenko, E. Starikova, M.-R. De Backer, V.G. Tyuterev, D. Mondelain, S. Kassi, A. Campargue, C. Janssen, S. Tashkun, R. Kochanov, R. Gamache, J. Orphal, Ozone spectroscopy in the electronic ground state: High-resolution spectra analyses and update of line parameters since 2003, *J. Quant. Spectrosc. Radiat. Transf.* 130 (2013) 172–190. <https://doi.org/10.1016/j.jqsrt.2013.06.007>.
- [37] A. Barbe, S. Mikhailenko, Starikova E., V. Tyuterev, Ozone FTS spectra in the infrared range revisited, *J. Quant. Spectrosc. Radiat. Transf.* to be publ (2021).
- [38] S&MPO website, (n.d.). <https://smmpo.iao.ru>.
- [39] J.M. Flaud, A. Barbe, C. Camy-Peyret, J.J. Plateaux, High resolution analysis of the  $5\nu_3$ ,  $3\nu_1 + \nu_2 + \nu_3$ , and  $\nu_1 + 4\nu_3$  bands of  $16\text{O}_3$ : line positions and intensities, *J. Mol. Spectrosc.* 177 (1996) 34–39. <https://doi.org/10.1006/jmsp.1996.0114>.
- [40] J.-M. Flaud, C. Camy-Peyret, V.M. Devi, C.P. Rinsland, M.A.H. Smith, The  $\nu_1$  and  $\nu_3$  bands of  $16\text{O}_3$ : Line positions and intensities, *J. Mol. Spectrosc.* 124 (1987) 209–217. [https://doi.org/10.1016/0022-2852\(87\)90135-4](https://doi.org/10.1016/0022-2852(87)90135-4).
- [41] J.-M. Flaud, C. Camy-Peyret, C.P. Rinsland, M.A.H. Smith, V. Malathy Devi, Line parameters for  $16\text{O}_3$  bands in the  $7\text{-}\mu\text{m}$  region, *J. Mol. Spectrosc.* 134 (1989) 106–112. [https://doi.org/10.1016/0022-2852\(89\)90132-X](https://doi.org/10.1016/0022-2852(89)90132-X).
- [42] A. Barbe, A. Chichery, V. Tyuterev, S. Taskhun, S. Mikhailenko, The  $2\nu_2$  and  $3\nu_2 - \nu_2$  bands of ozone, *Spectrochim. Acta Part A Mol. Biomol. Spectrosc.* 54 (1998) 1935–1945. [https://doi.org/10.1016/S1386-1425\(98\)00156-5](https://doi.org/10.1016/S1386-1425(98)00156-5).
- [43] H.M. Pickett, E.A. Cohen, L.R. Brown, C.P. Rinsland, M.A.H. Smith, V.M. Devi, A. Goldman, A. Barbe, B. Carli, M. Carlotti, The vibrational and rotational spectra of ozone for the (0, 1, 0) and (0, 2, 0) states, *J. Mol. Spectrosc.* 128 (1988) 151–171. [https://doi.org/10.1016/0022-2852\(88\)90214-7](https://doi.org/10.1016/0022-2852(88)90214-7).
- [44] J.M. Flaud, G. Wagner, M. Birk, C. Camy-Peyret, C. Claveau, M.R. De Backer-Barilly, A.

- Barbe, C. Piccolo, Ozone absorption around 10  $\mu\text{m}$ , *J. Geophys. Res. Atmos.* 108 (2003). <https://doi.org/10.1029/2002JD002755>.
- [45] M. Birk, G. Wagner, J.M. Flaud, D. Hausamann, Linestrengths in the  $\nu_3$ - $\nu_2$  Hot Band of Ozone, *J. Mol. Spectrosc.* 163 (1994) 262–275. <https://doi.org/10.1006/jmsp.1994.1022>.
- [46] A. Barbe, O. Sulakshina, J.J. Plateaux, A. Hamdouni, S. Bouazza, High-Resolution Infrared Spectra of Ozone in the 2300-2600  $\text{cm}^{-1}$  Region, *J. Mol. Spectrosc.* 170 (1995) 244–250. <https://doi.org/10.1006/jmsp.1995.1068>.
- [47] S. Bouazza, S. Mikhailenko, B. A. L. Regalia, V. Tyuterev, P. J.J, The  $\nu_1+\nu_2+2\nu_3$  and  $\nu_2+3\nu_3$  Bands of  $^{16}\text{O}_3$ , *J. Mol. Spectrosc.* 174 (1995) 510–519.
- [48] V.G. Tyuterev, R. V Kochanov, S.A. Tashkun, Accurate ab initio dipole moment surfaces of ozone: First principle intensity predictions for rotationally resolved spectra in a large range of overtone and combination bands, *J. Chem. Phys.* 146 (2017) 64304. <https://doi.org/10.1063/1.4973977>.
- [49] A. Barbe, E. Starikova, M.-R. De Backer, High resolution infrared spectra of the  $^{16}\text{O}^{16}\text{O}^{17}\text{O}$  and the  $^{16}\text{O}^{17}\text{O}^{16}\text{O}$  ozone isotopic species. The 5 and 10 micron spectral ranges revisited, *J. Quant. Spectrosc. Radiat. Transf.* 203 (2017) 293–299. <https://doi.org/10.1016/j.jqsrt.2017.03.034>.
- [50] A. Barbe, E. Starikova, M.R. De Backer, V.G. Tyuterev, Analyses of infrared FT spectra of asymmetric ozone isotopologue  $^{16}\text{O}^{16}\text{O}^{18}\text{O}$  in the range 950–3850  $\text{cm}^{-1}$ , *J. Quant. Spectrosc. Radiat. Transf.* 218 (2018) 231–247. <https://doi.org/10.1016/j.jqsrt.2018.06.022>.
- [51] V.G. Tyuterev, S.A. Tashkun, H. Seghir, High-order contact transformations: general algorithm, computer implementation, and triatomic tests, in: L.N. Sinitsa, S.N. Mikhailenko (Eds.), *Proc. SPIE - Int. Soc. Opt. Eng.*, SPIE, 2004: pp. 164–175. <https://doi.org/10.1117/12.545641>.
- [52] S.A. Tashkun, V.I. Perevalov, A.W. Liu, S.M. Hu, Global modeling of the  $^{15}\text{N}^{216}\text{O}$  line positions within the framework of the polyad model of effective Hamiltonian and a room temperature  $^{15}\text{N}^{216}\text{O}$  line list, *J. Quant. Spectrosc. Radiat. Transf.* 175 (2016) 1–7. <https://doi.org/10.1016/j.jqsrt.2016.01.038>.
- [53] S.A. Tashkun, V.I. Perevalov, E. V. Karlovets, S. Kassi, A. Campargue, High sensitivity cavity ring down spectroscopy of  $\text{N}_2\text{O}$  near 1.22  $\mu\text{m}$ : (II)  $^{14}\text{N}^{216}\text{O}$  line intensity modeling and global fit of  $^{14}\text{N}^{218}\text{O}$  line positions, *J. Quant. Spectrosc. Radiat. Transf.* 176 (2016) 62–69. <https://doi.org/10.1016/j.jqsrt.2016.02.020>.
- [54] V. Werwein, J. Brunzendorf, A. Serdyukov, O. Werhahn, V. Ebert, First measurements of nitrous oxide self-broadening and self-shift coefficients in the 0002-0000 band at 2.26  $\mu\text{m}$  using high resolution Fourier transform spectroscopy, *J. Mol. Spectrosc.* 323 (2016) 28–42. <https://doi.org/10.1016/J.JMS.2016.01.010>.
- [55] V. Werwein, J. Brunzendorf, G. Li, A. Serdyukov, O. Werhahn, V. Ebert, High-resolution Fourier transform measurements of line strengths in the 0002-0000 main isotopologue band of nitrous oxide, *Appl. Opt.* 56 (2017) E99. <https://doi.org/10.1364/AO.56.000E99>.
- [56] V. Werwein, G. Li, A. Serdyukov, J. Brunzendorf, O. Werhahn, V. Ebert, High-resolution Fourier transform measurements of air-induced broadening and shift coefficients in the 0002–0000 main isotopologue band of nitrous oxide, *J. Mol. Spectrosc.* 348 (2018) 68–78. <https://doi.org/10.1016/J.JMS.2017.07.002>.

- [57] G. Li, I.E. Gordon, L.S. Rothman, Y. Tan, S.-M. Hu, S. Kassı, A. Campargue, E.S. Medvedev, Rovibrational line lists for nine isotopologues of the CO molecule in the  $X1\Sigma^+$  ground electronic state, *Astrophys. J. Suppl. Ser.* 216 (2015) 15. <https://doi.org/10.1088/0067-0049/216/1/15>.
- [58] R.J. Le Roy, LEVEL: A computer program for solving the radial Schrödinger equation for bound and quasibound levels, *J. Quant. Spectrosc. Radiat. Transf.* 186 (2017) 167–178. <https://doi.org/10.1016/j.jqsrt.2016.05.028>.
- [59] J.A. Coxon, P.G. Hajigeorgiou, Direct potential fit analysis of the  $X1\Sigma^+$  ground state of CO, *J. Chem. Phys.* 121 (2004) 2992–3008. <https://doi.org/10.1063/1.1768167>.
- [60] E.S. Medvedev, V. V Meshkov, A. V Stolyarov, V.G. Ushakov, I.E. Gordon, Impact of the dipole-moment representation on the intensity of high overtones, *J. Mol. Spectrosc.* 330 (2016) 36–42. <https://doi.org/10.1016/j.jms.2016.06.013>.
- [61] E. Medvedev, V. Meshkov, A. Stolyarov, I. Gordon, Peculiarities of high-overtone transition probabilities in carbon monoxide revealed by high-precision calculation, *J. Chem. Phys.* 143 (2015) 154301. <https://doi.org/10.1063/1.4933136>.
- [62] M. Ghysels, D. Mondelain, S. Kassı, A. V. Nikitin, M. Rey, A. Campargue, The methane absorption spectrum near 1.73  $\mu\text{m}$  (5695–5850  $\text{cm}^{-1}$ ): Empirical line lists at 80 K and 296 K and rovibrational assignments, *J. Quant. Spectrosc. Radiat. Transf.* 213 (2018) 169–177. <https://doi.org/10.1016/j.jqsrt.2018.04.007>.
- [63] A. V. Nikitin, X. Thomas, L. Daumont, M. Rey, K. Sung, G.C. Toon, M.A.H. Smith, A.W. Mantz, A.E. Protasevich, S.A. Tashkun, V.G. Tyuterev, Assignment and modelling of  $12\text{CH}_4$  spectra in the 5550–5695, 5718–5725 and 5792–5814  $\text{cm}^{-1}$  regions, *J. Quant. Spectrosc. Radiat. Transf.* 219 (2018) 323–332. <https://doi.org/10.1016/j.jqsrt.2018.08.006>.
- [64] A. V. Nikitin, X. Thomas, L. Daumont, M. Rey, K. Sung, G.C. Toon, M.A.H. Smith, A.W. Mantz, S.A. Tashkun, V.G. Tyuterev, Measurements and modeling of long-path  $12\text{CH}_4$  spectra in the 5300–5550  $\text{cm}^{-1}$  region, *J. Quant. Spectrosc. Radiat. Transf.* 202 (2017) 255–264. <https://doi.org/10.1016/j.jqsrt.2017.07.030>.
- [65] V. Tyuterev, S. Tashkun, M. Rey, R. Kochanov, A. Nikitin, T. Delahaye, Accurate spectroscopic models for methane polyads derived from a potential energy surface using high-order contact transformations, *J. Phys. Chem. A.* 117 (2013). <https://doi.org/10.1021/jp408116j>.
- [66] O.M. Lyulin, A. V. Nikitin, V.I. Perevalov, I. Morino, T. Yokota, R. Kumazawa, T. Watanabe, Measurements of N<sub>2</sub>- and O<sub>2</sub>-broadening and shifting parameters of methane spectral lines in the 5550–6236  $\text{cm}^{-1}$  region, *J. Quant. Spectrosc. Radiat. Transf.* 110 (2009) 654–668. <https://doi.org/10.1016/j.jqsrt.2009.02.012>.
- [67] A. V. Nikitin, O.M. Lyulin, S.N. Mikhailenko, V.I. Perevalov, N.N. Filippov, I.M. Grigoriev, I. Morino, Y. Yoshida, T. Matsunaga, GOSAT-2014 methane spectral line list, *J. Quant. Spectrosc. Radiat. Transf.* 154 (2015) 63–71. <https://doi.org/10.1016/j.jqsrt.2014.12.003>.
- [68] E. Starikova, A. V. Nikitin, M. Rey, S.A. Tashkun, D. Mondelain, S. Kassı, A. Campargue, V.G. Tyuterev, Assignment and modeling of the absorption spectrum of  $13\text{CH}_4$  at 80 K in the region of the  $2\nu_3$  band (5853–6201  $\text{cm}^{-1}$ ), *J. Quant. Spectrosc. Radiat. Transf.* 177 (2016) 170–180. <https://doi.org/10.1016/j.jqsrt.2015.12.023>.
- [69] D.D. Tran, V.T. Sironneau, J.T. Hodges, R. Armante, J. Cuesta, H. Tran, Prediction of high-



order line-shape parameters for air-broadened O<sub>2</sub> lines using requantized classical molecular dynamics simulations and comparison with measurements, *J. Quant. Spectrosc. Radiat. Transf.* 222–223 (2019). <https://doi.org/10.1016/j.jqsrt.2018.10.013>.

- [70] D.D. Tran, H. Tran, S. Vasilchenko, S. Kassi, A. Campargue, D. Mondelain, High sensitivity spectroscopy of the O<sub>2</sub> band at 1.27 μm: (II) air-broadened line profile parameters, *J. Quant. Spectrosc. Radiat. Transf.* 240 (2020) 106673. <https://doi.org/10.1016/j.jqsrt.2019.106673>.
- [71] R. Tóbiás, T. Furtenbacher, A.G. Császár, O. V Naumenko, J. Tennyson, J.-M. Flaud, P. Kumar, B. Poirier, Critical evaluation of measured rotational–vibrational transitions of four sulphur isotopologues of S<sup>16</sup>O<sub>2</sub>, *J. Quant. Spectrosc. Radiat. Transf.* 208 (2018) 152–163. <https://doi.org/10.1016/j.jqsrt.2018.01.006>.
- [72] D.S. Underwood, J. Tennyson, S.N. Yurchenko, X. Huang, D.W. Schwenke, T.J. Lee, S. Clausen, A. Fateev, ExoMol molecular line lists - XIV. The rotation-vibration spectrum of hot SO<sub>2</sub>, *Mon. Not. R. Astron. Soc.* 459 (2016) 3890–3899. <https://doi.org/10.1093/mnras/stw849>.
- [73] I. Kovacs, *High Resolution Molecular Spectroscopy*, 1976. <https://doi.org/10.1051/ept/19760712009>.
- [74] O.N. Ulenikov, E.S. Bekhtereva, O. V Gromova, V.-M. Horneman, C. Sydow, S. Bauerecker, High resolution FTIR spectroscopy of sulfur dioxide in the 1550–1950cm<sup>-1</sup> region: First analysis of the ν<sub>1</sub>+ν<sub>2</sub>/ν<sub>2</sub>+ν<sub>3</sub> bands of <sup>32</sup>S<sup>16</sup>O<sup>18</sup>O and experimental line intensities of ro-vibrational transitions in the ν<sub>1</sub>+ν<sub>2</sub>/ν<sub>2</sub>+ν<sub>3</sub> bands of <sup>32</sup>S<sup>16</sup>O<sub>2</sub>, <sup>34</sup>S<sup>16</sup>O<sub>2</sub>, <sup>32</sup>S<sup>18</sup>O<sub>2</sub> and, *J. Quant. Spectrosc. Radiat. Transf.* 203 (2017) 377–391. <https://doi.org/10.1016/j.jqsrt.2017.02.005>.
- [75] Y.G. Borkov, O.M. Lyulin, T.M. Petrova, A.M. Solodov, A.A. Solodov, V.M. Deichuli, V.I. Perevalov, CO<sub>2</sub>-broadening and shift coefficients of sulfur dioxide near 4 μm, *J. Quant. Spectrosc. Radiat. Transf.* 225 (2019) 119–124. <https://doi.org/10.1016/j.jqsrt.2018.12.030>.
- [76] X. Huang, D.W. Schwenke, T.J. Lee, Quantitative validation of Ames IR intensity and new line lists for <sup>32</sup>/<sup>33</sup>/<sup>34</sup>S<sup>16</sup>O<sub>2</sub>, <sup>32</sup>S<sup>18</sup>O<sub>2</sub> and <sup>16</sup>O<sup>32</sup>S<sup>18</sup>O, *J. Quant. Spectrosc. Radiat. Transf.* 225 (2019) 327–336. <https://doi.org/10.1016/j.jqsrt.2018.11.039>.
- [77] A. Perrin, L. Manceron, F. Kwabia Tchana, New line positions analysis of the 2ν<sub>1</sub> and ν<sub>1</sub>+ν<sub>3</sub> bands of NO<sub>2</sub> at 3637.848 and 2906.070 cm<sup>-1</sup>, *Mol. Phys.* 8976 (2020). <https://doi.org/10.1080/00268976.2019.1711235>.
- [78] A. Perrin, L. Manceron, J.-M. Flaud, F. Kwabia-Tchana, R. Armante, P. Roy, D. Doizi, The new nitrogen dioxide (NO<sub>2</sub>) linelist in the GEISA database and first identification of the ν<sub>1</sub>+2ν<sub>3</sub>-ν<sub>3</sub> band of <sup>14</sup>N<sup>16</sup>O<sub>2</sub>, *J. Mol. Spectrosc.* 376 (2020) 111394. <https://doi.org/10.1016/j.jms.2020.111394>.
- [79] A. Perrin, G. Toon, J. Orphal, Detection of atmospheric <sup>15</sup>N<sup>16</sup>O<sub>2</sub> in the ν<sub>3</sub> spectral region (6.3μm), *J. Quant. Spectrosc. Radiat. Transf.* 154 (2015) 91–97. <https://doi.org/10.1016/j.jqsrt.2014.12.006>.
- [80] S. Miljanic, A. Perrin, J. Orphal, New high-resolution analysis of the ν<sub>1</sub> + ν<sub>3</sub> band of the <sup>15</sup>N<sup>16</sup>O<sub>2</sub> isotopomer of nitrogen dioxide: Line positions and intensities, *J. Mol. Spectrosc.* 242 (2007) 176–181. <https://doi.org/10.1016/j.jms.2007.02.024>.
- [81] D.C. Benner, T.A. Blake, L.R. Brown, V.M. Devi, M.A.H. Smith, R.A. Toth, Air-broadening parameters in the ν<sub>3</sub> band of <sup>14</sup>N<sup>16</sup>O<sub>2</sub> using a multispectrum fitting technique, *J. Mol.*

Spectrosc. 228 (2004) 593–619. <https://doi.org/10.1016/j.jms.2004.07.006>.

- [82] R.J. Hargreaves, I.E. Gordon, L.S. Rothman, S.A. Tashkun, V.I. Perevalov, A.A. Lukashchenskaya, S.N. Yurchenko, J. Tennyson, H.S.P. Müller, Spectroscopic line parameters of NO, NO<sub>2</sub>, and N<sub>2</sub>O for the HITEMP database, *J. Quant. Spectrosc. Radiat. Transf.* 232 (2019) 35–53. <https://doi.org/10.1016/j.jqsrt.2019.04.040>.
- [83] N. Maaroufi, C. Jalleli, F.K. Tchana, X. Landsheere, H. Aroui, Absolute line intensities and first measurements of self-collisional broadening and shift coefficients in the 2v<sub>4</sub> band of NH<sub>3</sub>, *J. Mol. Spectrosc.* 354 (2018) 24–31. <https://doi.org/10.1016/j.jms.2018.09.003>.
- [84] V. Nemtchinov, K. Sung, P. Varanasi, Measurements of line intensities and half-widths in the 10- $\mu$ m bands of <sup>14</sup>NH<sub>3</sub>, *J. Quant. Spectrosc. Radiat. Transf.* 83 (2004) 243–265. [https://doi.org/10.1016/S0022-4073\(02\)00354-0](https://doi.org/10.1016/S0022-4073(02)00354-0).
- [85] A. V. Nikitin, Y.A. Ivanova, M. Rey, S.A. Tashkun, G.C. Toon, K. Sung, V.G. Tyuterev, Analysis of PH<sub>3</sub> spectra in the Octad range 2733–3660 cm<sup>-1</sup>, *J. Quant. Spectrosc. Radiat. Transf.* 203 (2017) 472–479. <https://doi.org/10.1016/j.jqsrt.2017.04.032>.
- [86] T.J. Johnson, R.L. Sams, S.W. Sharpe, The PNNL quantitative infrared database for gas-phase sensing: a spectral library for environmental, hazmat, and public safety standoff detection, *Chem. Biol. Point Sensors Homel. Def.* 5269 (2004) 159. <https://doi.org/10.1117/12.515604>.
- [87] A. Perrin, New analysis of the v<sub>3</sub> and v<sub>4</sub> bands of HNO<sub>3</sub> in the 7.6  $\mu$ m region, *J. Phys. Chem. A.* 117 (2013) 13236–13248. <https://doi.org/10.1021/jp401979v>.
- [88] A. Perrin, J.M. Flaud, M. Ridolfi, J. Vander Auwera, M. Carlotti, MIPAS database: New HNO<sub>3</sub> line parameters at 7.6  $\mu$ m validated with MIPAS satellite measurements, *Atmos. Meas. Tech.* 9 (2016) 2067–2076. <https://doi.org/10.5194/amt-9-2067-2016>.
- [89] G. Li, I.E. Gordon, R.J. Le Roy, P.G. Hajigeorgiou, J.A. Coxon, P.F. Bernath, L.S. Rothman, Reference spectroscopic data for hydrogen halides. Part I: Construction and validation of the ro-vibrational dipole moment functions, *J. Quant. Spectrosc. Radiat. Transf.* 121 (2013) 78–90. <https://doi.org/10.1016/J.JQSRT.2013.02.005>.
- [90] G. Li, I.E. Gordon, P.G. Hajigeorgiou, J.A. Coxon, L.S. Rothman, Reference spectroscopic data for hydrogen halides, Part II: The line lists, *J. Quant. Spectrosc. Radiat. Transf.* 130 (2013) 284–295. <https://doi.org/10.1016/J.JQSRT.2013.07.019>.
- [91] G. Li, A. Serdyukov, M. Gisi, O. Werhahn, V. Ebert, FTIR-based measurements of self-broadening and self-shift coefficients as well as line strength in the first overtone band of HCl at 1.76  $\mu$ m, *J. Quant. Spectrosc. Radiat. Transf.* 165 (2015) 76–87. <https://doi.org/10.1016/J.JQSRT.2015.06.021>.
- [92] R.E. Asfin, A.V. Domanskaya, C. Maul, Broadening and shifting coefficients of rotation–vibrational lines in the fundamental and first overtone bands of HCl and HBr induced by oxygen and air, *J. Quant. Spectrosc. Radiat. Transf.* 130 (2013) 296–303. <https://doi.org/10.1016/J.JQSRT.2013.07.014>.
- [93] B. Lejeune, E. Mahieu, M.K. Vollmer, S. Reimann, P.F. Bernath, C.D. Boone, K.A. Walker, C. Servais, Optimized approach to retrieve information on atmospheric carbonyl sulfide (OCS) above the Jungfraujoch station and change in its abundance since 1995, *J. Quant. Spectrosc. Radiat. Transf.* 186 (2017) 81–95. <https://doi.org/10.1016/j.jqsrt.2016.06.001>.

- [94] N.G. Phillips, R. Ackley, E.R. Crosson, A. Down, L.R. Hutyla, M. Brondfield, J.D. Karr, K. Zhao, R.B. Jackson, Mapping urban pipeline leaks: Methane leaks across Boston, *Environ. Pollut.* 173 (2013) 1–4. <https://doi.org/10.1016/j.envpol.2012.11.003>.
- [95] D. Golebiowski, X. de Ghellinck d'Elseghem Vaernewijck, M. Herman, J. Vander Auwera, A. Fayt, High sensitivity (femto-FT-CEAS) spectra of carbonyl sulphide between 6200 and 8200 $\text{cm}^{-1}$ , and new energy pattern in the global rovibrational analysis of  $^{16}\text{O}^{12}\text{C}_3\text{S}_2$ , *J. Quant. Spectrosc. Radiat. Transf.* 149 (2014) 184–203. <https://doi.org/10.1016/j.jqsrt.2014.07.005>.
- [96] S. Galalou, K. Ben Mabrouk, H. Aroui, F. Kwabia Tchana, F. Willaert, J.M. Flaud,  $\text{N}_2$  and  $\text{O}_2$  pressure broadening and pressure shift in the  $4\nu_2$  band of  $^{16}\text{O}^{12}\text{C}_3\text{S}_2$ , *J. Quant. Spectrosc. Radiat. Transf.* 112 (2011) 2750–2761. <https://doi.org/10.1016/j.jqsrt.2011.08.008>.
- [97] N. Moazzen-Ahmadi, J. Norooz Oliaee, I. Ozier, E.H. Wishnow, K. Sung, T.J. Crawford, L.R. Brown, V.M. Devi, An intensity study of the torsional bands of ethane at  $35\mu\text{m}$ , *J. Quant. Spectrosc. Radiat. Transf.* 151 (2015) 123–132. <https://doi.org/10.1016/j.jqsrt.2014.09.016>.
- [98] O.M. Lyulin, V.I. Perevalov, Global modeling of vibration-rotation spectra of the acetylene molecule, *J. Quant. Spectrosc. Radiat. Transf.* 177 (2016) 59–74. <https://doi.org/10.1016/j.jqsrt.2015.12.021>.
- [99] O.M. Lyulin, V.I. Perevalov, ASD-1000: High-resolution, high-temperature acetylene spectroscopic databank, *J. Quant. Spectrosc. Radiat. Transf.* 201 (2017) 94–103. <https://doi.org/10.1016/j.jqsrt.2017.06.032>.
- [100] D. Jacquemart, O. Lyulin, V.I. Perevalov, Recommended acetylene line list in the 20–240  $\text{cm}^{-1}$  and 400–630  $\text{cm}^{-1}$  regions: New measurements and global modeling, *J. Quant. Spectrosc. Radiat. Transf.* 203 (2017) 440–453. <https://doi.org/10.1016/j.jqsrt.2017.03.008>.
- [101] D. Jacquemart, P. Soulard, O.M. Lyulin, Recommended acetylene  $^{12}\text{C}_2\text{H}_2$  line list in 13.6  $\mu\text{m}$  spectral region: New measurements and global modeling, *J. Quant. Spectrosc. Radiat. Transf.* 256 (2020) 107200. <https://doi.org/10.1016/j.jqsrt.2020.107200>.
- [102] O.M. Lyulin, A. Campargue, An empirical spectroscopic database for acetylene in the regions of 5850–6341  $\text{cm}^{-1}$  and 7000–9415  $\text{cm}^{-1}$ , *J. Quant. Spectrosc. Radiat. Transf.* 203 (2017) 461–471. <https://doi.org/10.1016/j.jqsrt.2017.01.036>.
- [103] O.M. Lyulin, J. Vander Auwera, A. Campargue, The Fourier transform absorption spectrum of acetylene between 8280 and 8700  $\text{cm}^{-1}$ , *J. Quant. Spectrosc. Radiat. Transf.* 177 (2016) 234–240. <https://doi.org/10.1016/j.jqsrt.2015.11.026>.
- [104] O.M. Lyulin, J. Vander Auwera, A. Campargue, The Fourier transform absorption spectrum of acetylene between 7000 and 7500 $\text{cm}^{-1}$ , *J. Quant. Spectrosc. Radiat. Transf.* 160 (2015) 85–93. <https://doi.org/10.1016/j.jqsrt.2015.03.018>.
- [105] S. Béguier, O.M. Lyulin, S.M. Hu, A. Campargue, Line intensity measurements for acetylene between 8980 and 9420  $\text{cm}^{-1}$ , *J. Quant. Spectrosc. Radiat. Transf.* 189 (2017) 417–420. <https://doi.org/10.1016/j.jqsrt.2016.12.020>.
- [106] O.M. Lyulin, A. Campargue, D. Mondelain, S. Kassi, The absorption spectrum of acetylene by CRDS between 7244 and 7918 $\text{cm}^{-1}$ , *J. Quant. Spectrosc. Radiat. Transf.* 130 (2013) 327–334. <https://doi.org/10.1016/j.jqsrt.2013.04.028>.

- [107] O.M. Lyulin, D. Mondelain, S. Béguier, S. Kassi, J. Vander Auwera, A. Campargue, High-sensitivity CRDS absorption spectroscopy of acetylene between 5851 and 6341  $\text{cm}^{-1}$ , *Mol. Phys.* 112 (2014) 2433–2444. <https://doi.org/10.1080/00268976.2014.906677>.
- [108] S. Kassi, O.M. Lyulin, S. Béguier, A. Campargue, New assignments and a rare peculiarity in the high sensitivity CRDS spectrum of acetylene near 8000  $\text{cm}^{-1}$ , *J. Mol. Spectrosc.* 326 (2016) 106–114. <https://doi.org/10.1016/j.jms.2016.02.013>.
- [109] M. Šimečková, D. Jacquemart, L.S. Rothman, R.R. Gamache, A. Goldman, Einstein A-coefficients and statistical weights for molecular absorption transitions in the HITRAN database, *J. Quant. Spectrosc. Radiat. Transf.* 98 (2006) 130–155. <https://doi.org/10.1016/j.jqsrt.2005.07.003>.
- [110] R.R. Gamache, C. Roller, E. Lopes, I.E. Gordon, L.S. Rothman, O.L. Polyansky, N.F. Zobov, A.A. Kyuberis, J. Tennyson, S.N. Yurchenko, A.G. Császár, T. Furtenbacher, X. Huang, D.W. Schwenke, T.J. Lee, B.J. Drouin, S.A. Tashkun, V.I. Perevalov, R. V. Kochanov, Total internal partition sums for 166 isotopologues of 51 molecules important in planetary atmospheres: Application to HITRAN2016 and beyond, *J. Quant. Spectrosc. Radiat. Transf.* 203 (2017) 70–87. <https://doi.org/10.1016/j.jqsrt.2017.03.045>.
- [111] O.M. Lyulin, D. Jacquemart, N. Lacome, V.I. Perevalov, J.Y. Mandin, Line parameters of acetylene in the 1.9 and 1.7  $\mu\text{m}$  spectral regions, *J. Quant. Spectrosc. Radiat. Transf.* 109 (2008) 1856–1874. <https://doi.org/10.1016/j.jqsrt.2007.11.016>.
- [112] A. Alkadrou, M.-T. Bourgeois, M. Rotger, V. Boudon, J. Vander Auwera, Corrigendum to “Global frequency and intensity analysis of the  $\nu_{10}/\nu_7/\nu_4/\nu_{12}$  band system of  $^{12}\text{C}_2\text{H}_4$  at  $10\mu\text{m}$  using the D2h top data system,” *J. Quant. Spectrosc. Radiat. Transf.* 190 (2017) 88. <https://doi.org/10.1016/j.jqsrt.2017.01.007>.
- [113] A. Alkadrou, M.-T. Bourgeois, M. Rotger, V. Boudon, J. Vander Auwera, Global frequency and intensity analysis of the  $\nu_{10}/\nu_7/\nu_4/\nu_{12}$  band system of  $^{12}\text{C}_2\text{H}_4$  at  $10\mu\text{m}$  using the D2h Top Data System, *J. Quant. Spectrosc. Radiat. Transf.* 182 (2016) 158–171. <https://doi.org/10.1016/j.jqsrt.2016.05.024>.
- [114] J. Vander Auwera, A. Fayt, M. Tudorie, M. Rotger, V. Boudon, B. Franco, E. Mahieu, Self-broadening coefficients and improved line intensities for the  $\nu_7$  band of ethylene near  $10.5\mu\text{m}$ , and impact on ethylene retrievals from Jungfraujoch solar spectra, *J. Quant. Spectrosc. Radiat. Transf.* 148 (2014) 177–185. <https://doi.org/10.1016/j.jqsrt.2014.07.003>.
- [115] M. Rotger, V. Boudon, J. Vander Auwera, Line positions and intensities in the  $\nu_{12}$  band of ethylene near  $1450\text{cm}^{-1}$ : An experimental and theoretical study, *J. Quant. Spectrosc. Radiat. Transf.* 109 (2008) 952–962. <https://doi.org/10.1016/j.jqsrt.2007.12.005>.
- [116] U. Fink, H.P. Larson, R.R. Treffers, Germane in the atmosphere of Jupiter, *Icarus*. 34 (1978) 344–354. [https://doi.org/10.1016/0019-1035\(78\)90172-0](https://doi.org/10.1016/0019-1035(78)90172-0).
- [117] K.S. Noll, R.F. Knacke, T.R. Geballe, A.T. Tokunaga, Evidence for Germane in Saturn, *Icarus*. 75 (1988) 409–422. [https://doi.org/10.1016/0019-1035\(88\)90154-6](https://doi.org/10.1016/0019-1035(88)90154-6).
- [118] V. Boudon, T. Grigoryan, F. Philipot, C. Richard, F.K. Tchana, L. Manceron, A. Rizopoulos, J. Vander Auwera, T. Encrenaz, Line positions and intensities for the  $\nu_3$  band of 5 isotopologues of germane for planetary applications, *J. Quant. Spectrosc. Radiat. Transf.* 205 (2018) 174–183. <https://doi.org/10.1016/J.JQSRT.2017.10.017>.
- [119] <http://vamdc.icb.cnrs.fr/PHP/gecasda.php>, (n.d.).

- [120] C. Richard, V. Boudon, M. Rotger, Calculated spectroscopic databases for the VAMDC portal: New molecules and improvements, *J. Quant. Spectrosc. Radiat. Transf.* 251 (2020) 107096. <https://doi.org/10.1016/j.jqsrt.2020.107096>.
- [121] M. López-Puertas, J.-M. Flaud, J. Peralta-Calvillo, B. Funke, S. Gil-López, NO<sup>+</sup> fundamental and first hot ro-vibrational line frequencies from MIPAS/Envisat atmospheric spectra, *J. Mol. Spectrosc.* 237 (2006) 218–224. <https://doi.org/10.1016/j.jms.2006.03.015>.
- [122] J. Cernicharo, S. Bailleux, E. Alekseev, A. Fuente, E. Roueff, M. Gerin, B. Tercero, S.P. Treviño-Morales, N. Marcelino, R. Bachiller, B. Lefloch, Tentative detection of the nitrosylium ion in space, *Astrophys. J.* 795 (2014) 6–11. <https://doi.org/10.1088/0004-637X/795/1/40>.
- [123] C.P. Endres, S. Schlemmer, P. Schilke, J. Stutzki, H.S.P. Müller, The Cologne Database for Molecular Spectroscopy, CDMS, in the Virtual Atomic and Molecular Data Centre, VAMDC, *J. Mol. Spectrosc.* 327 (2016) 95–104. <https://doi.org/10.1016/j.jms.2016.03.005>.
- [124] W.C. Bowman, E. Herbst, F.C. De Lucia, Millimeter and submillimeter spectrum of NO<sup>+</sup>, *J. Chem. Phys.* 77 (1982) 4261–4262. <https://doi.org/10.1063/1.444307>.
- [125] W.C. Ho, I. Ozier, D.T. Cramb, M.C.L. Gerry, Diode laser spectroscopy of the vibrational fundamental of NO<sup>+</sup>, *J. Mol. Spectrosc.* 149 (1991) 559–561. [https://doi.org/10.1016/0022-2852\(91\)90311-W](https://doi.org/10.1016/0022-2852(91)90311-W).
- [126] R. Polák, J. Fišer, A comparative icMRCI study of some NO<sup>+</sup>, NO and NO<sup>-</sup> electronic ground state properties, *Chem. Phys.* 303 (2004) 73–83. <https://doi.org/10.1016/j.chemphys.2004.04.027>.
- [127] C.P. Rinsland, E. Mahieu, R. Zander, R. Nassar, P. Bernath, C. Boone, L.S. Chiou, Long-term stratospheric carbon tetrafluoride (CF<sub>4</sub>) increase inferred from 1985-2004 infrared space-based solar occultation measurements, *Geophys. Res. Lett.* 33 (2006) 2–5. <https://doi.org/10.1029/2005GL024709>.
- [128] E. Mahieu, R. Zander, G.C. Toon, M.K. Vollmer, S. Reimann, J. Mühle, W. Bader, B. Bovy, B. Lejeune, C. Servais, P. Demoulin, G. Roland, P.F. Bernath, C.D. Boone, K.A. Walker, P. Duchatelet, Spectrometric monitoring of atmospheric carbon tetrafluoride (CF<sub>4</sub>) above the Jungfraujoch station since 1989: Evidence of continued increase but at a slowing rate, *Atmos. Meas. Tech.* 7 (2014) 333–344. <https://doi.org/10.5194/amt-7-333-2014>.
- [129] M. Carlos, O. Gruson, C. Richard, V. Boudon, M. Rotger, X. Thomas, C. Maul, C. Sydow, A. Domanskaya, R. Georges, P. Soulard, O. Pirali, M. Goubet, P. Asselin, T.R. Huet, High-resolution spectroscopy and global analysis of CF<sub>4</sub> rovibrational bands to model its atmospheric absorption, *J. Quant. Spectrosc. Radiat. Transf.* 201 (2017) 75–93. <https://doi.org/10.1016/j.jqsrt.2017.06.039>.
- [130] V. Boudon, M. Carlos, C. Richard, O. Pirali, Pure rotation spectrum of CF<sub>4</sub> in the v<sub>3</sub>=1 state using THz synchrotron radiation, *J. Mol. Spectrosc.* 348 (2018) 43–46. <https://doi.org/10.1016/j.jms.2017.07.010>.
- [131] <http://vamdc.icb.cnrs.fr/PHP/tfmecasda.php>, (n.d.).
- [132] R. Armante, A. Perrin, F. Kwabia-Tchana, L. Manceron, The v<sub>4</sub> linelist at 11 μm: linelists for the Trans- and Cis- conformer forms of nitrous acid, (HONO), in the 2019 version of the GEISA database, *Mol. Phys.* (2021) e1951860. <https://doi.org/10.1080/00268976.2021.1951860>.

- [133] I. Kleiner, J.M. Guilmot, M. Carleer, M. Herman, The  $\nu_4$  fundamental bands of trans- and cis-HNO<sub>2</sub>, *J. Mol. Spectrosc.* 149 (1991) 341–347. [https://doi.org/10.1016/0022-2852\(91\)90290-Q](https://doi.org/10.1016/0022-2852(91)90290-Q).
- [134] A. Dehayem-Kamadjeu, O. Pirali, J. Orphal, I. Kleiner, P.-M. Flaud, The far-infrared rotational spectrum of nitrous acid (HONO) and its deuterated species (DONO) studied by high-resolution Fourier-transform spectroscopy, *J. Mol. Spectrosc.* 234 (2005) 182–189. <https://doi.org/10.1016/j.jms.2005.09.006>.
- [135] R.H. Kagann, A.G. Maki, Infrared absorption intensities of nitrous acid (HONO) fundamental bands, *J. Quant. Spectrosc. Radiat. Transf.* 30 (1983) 37–44. [https://doi.org/10.1016/0022-4073\(83\)90071-7](https://doi.org/10.1016/0022-4073(83)90071-7).
- [136] A. Perrin, J. Demaison, G. Toon, The  $\nu_1$ ,  $\nu_2$ , and  $\nu_3$  bands of carbonyl chlorofluoride (COFCl) at 5.3, 9.1, and 13.1  $\mu\text{m}$ : position and intensity parameters and their use for atmospheric studies, *J. Quant. Spectrosc. Radiat. Transf.* 112 (2011) 1266–1279. <https://doi.org/10.1016/j.jqsrt.2011.01.003>.
- [137] A. Perrin, J.-M. Flaud, H. Bürger, G. Pawelke, S. Sander, H. Willner, First High-Resolution Analysis of the Six Fundamental Bands  $\nu_1$ ,  $\nu_2$ ,  $\nu_3$ ,  $\nu_4$ ,  $\nu_5$ , and  $\nu_6$  of COF<sub>35</sub>Cl in the 340- to 2000-cm<sup>-1</sup> Region, *J. Mol. Spectrosc.* 209 (2001) 122–132. <https://doi.org/10.1006/jmsp.2001.8415>.
- [138] J. Demaison, A. Perrin, H. Bürger, Ab initio anharmonic force field and equilibrium structure of carbonyl chlorofluoride, *J. Mol. Spectrosc.* 221 (2003) 47–56. [https://doi.org/10.1016/S0022-2852\(03\)00169-3](https://doi.org/10.1016/S0022-2852(03)00169-3).
- [139] A. Perrin, I. Haykal, F. KwabiaTchana, L. Manceron, D. Doizi, G. Ducros, New analysis of the  $\nu_6$  and  $2\nu_3$  bands of methyl iodide (CH<sub>3</sub>I), *J. Mol. Spectrosc.* 324 (2016) 28–35. <https://doi.org/10.1016/j.jms.2016.04.014>.
- [140] F. Kwabia-Tchana, Y. Attafi, L. Manceron, D. Doizi, J. Vander Auwera, A. Perrin, Line intensities for the  $\nu_6$  and  $2\nu_3$  bands of methyl iodide (12CH<sub>3</sub>I), *J. Quant. Spectrosc. Radiat. Transf.* 222–223 (2019) 130–137. <https://doi.org/10.1016/j.jqsrt.2018.10.001>.
- [141] Y. Attafi, A. Ben Hassen, H. Aroui, F.K. Tchana, L. Manceron, D. Doizi, J. Vander Auwera, A. Perrin, Self and N<sub>2</sub> collisional broadening of rovibrational lines in the  $\nu_6$  band of methyl iodide (12CH<sub>3</sub>I) at room temperature: The J and K dependence, *J. Quant. Spectrosc. Radiat. Transf.* 231 (2019) 1–8. <https://doi.org/10.1016/j.jqsrt.2019.04.017>.
- [142] Y. Attafi, S. Galalou, F. Kwabia Tchana, J. Vander Auwera, A. Ben Hassen, H. Aroui, A. Perrin, L. Manceron, D. Doizi, Oxygen broadening and shift coefficients in the  $\nu_6$  band of methyl iodide (12CH<sub>3</sub>I) at room temperature, *J. Quant. Spectrosc. Radiat. Transf.* 239 (2019) 106679. <https://doi.org/10.1016/j.jqsrt.2019.106679>.
- [143] D. Papoušek, P. Pracna, M. Winnemisser, S. Klee, J. Demaison, Simultaneous Rovibrational Analysis of the  $\nu_2$ ,  $\nu_3$ ,  $\nu_5$ , and  $\nu_6$  Bands of H<sub>3</sub>12CF, *J. Mol. Spectrosc.* 196 (1999) 319–323. <https://doi.org/10.1006/jmsp.1999.7875>.
- [144] D. Jacquemart, M. Guinet, Line parameters measurements and modeling for the  $\nu_6$  band of CH<sub>3</sub>F: Generation of a complete line list for atmospheric databases, *J. Quant. Spectrosc. Radiat. Transf.* 185 (2016) 58–69. <https://doi.org/10.1016/j.jqsrt.2016.08.010>.
- [145] A.B. Ramchani, D. Jacquemart, P. Soulard, M. Guinet, Measurements and modeling of N<sub>2</sub>-broadening coefficients for the  $\nu_6$  band of CH<sub>3</sub>F, comparison with CH<sub>3</sub>Cl and CH<sub>3</sub>Br

- molecules, *J. Quant. Spectrosc. Radiat. Transf.* 203 (2017) 480–489. <https://doi.org/10.1016/j.jqsrt.2017.06.013>.
- [146] S. Reymond-Laruinaz, V. Boudon, L. Manceron, L. Lago, D. Doizi, Infrared spectroscopy of ruthenium tetroxide and high-resolution analysis of the  $\nu_3$  band, *J. Mol. Spectrosc.* 315 (2015) 46–54. <https://doi.org/10.1016/J.JMS.2015.02.008>.
- [147] S. Reymond-Laruinaz, M. Faye, V. Boudon, D. Doizi, L. Manceron, High-resolution infrared spectroscopy and analysis of the  $\nu_2/\nu_4$  bending dyad of ruthenium tetroxide, *J. Mol. Spectrosc.* 336 (2017) 29–35. <https://doi.org/10.1016/J.JMS.2017.04.010>.
- [148] J. Vander Auwera, S. Reymond-Laruinaz, V. Boudon, D. Doizi, L. Manceron, Line intensity measurements and analysis in the  $\nu_3$  band of ruthenium tetroxide, *J. Quant. Spectrosc. Radiat. Transf.* 204 (2018) 103–111. <https://doi.org/10.1016/J.JQSRT.2017.09.016>.
- [149] <http://vamdc.icb.cnrs.fr/PHP/rucasda.php>, (n.d.).
- [150] N.A. Lombardo, C.A. Nixon, R.K. Achterberg, A. Jolly, K. Sung, P.G.J. Irwin, F.M. Flasar, Spatial and seasonal variations in C<sub>3</sub>H<sub>x</sub> hydrocarbon abundance in Titan's stratosphere from Cassini CIRS observations, *Icarus.* 317 (2019) 454–469. <https://doi.org/10.1016/j.icarus.2018.08.027>.
- [151] N.A. Lombardo, C.A. Nixon, T.K. Greathouse, B. Bézard, A. Jolly, S. Vinatier, N.A. Teanby, M.J. Richter, P.J. G Irwin, A. Coustenis, F.M. Flasar, Detection of Propadiene on Titan, *Astrophys. J.* 881 (2019) L33. <https://doi.org/10.3847/2041-8213/ab3860>.
- [152] A. Coustenis, T. Encrenaz, B. Bézard, G. Bjoraker, G. Graner, M. Dang-Nhu, E. Arié, Modeling Titan's Thermal Infrared Spectrum for High-Resolution Space Observations, *Icarus.* 102 (1993) 240–260. <https://doi.org/10.1006/icar.1993.1047>.
- [153] J. Chazelas, J. Plíva, A. Valentin, L. Henry, Analysis of the  $\nu_9$   $\nu_{10}$  band system of allene, *J. Mol. Spectrosc.* 110 (1985) 326–338. [https://doi.org/10.1016/0022-2852\(85\)90298-X](https://doi.org/10.1016/0022-2852(85)90298-X).
- [154] J. Plíva, J. Kauppinen, High-resolution Fourier transform study of the perpendicular band  $\nu_{11}$  of allene at 353  $\text{cm}^{-1}$ , *J. Mol. Spectrosc.* 111 (1985) 93–101. [https://doi.org/10.1016/0022-2852\(85\)90072-4](https://doi.org/10.1016/0022-2852(85)90072-4).
- [155] Y. Koga, S. Kondo, T. Nakanaga, S. Saëki, Infrared absorption intensities of allene, *J. Chem. Phys.* 71 (1979) 2404–2411. <https://doi.org/10.1063/1.438645>.
- [156] A. Jolly, Y. Benilan, L. Manceron, Search for evidence of Butane on Titan with new spectroscopic data, *EPSC Abstr.* 11 (2017) 10–11.
- [157] S. Nissen, F. Hegelund, M.S. Johnson, B. Nelander, High-Resolution infrared study of the  $\nu_{11}$  band of Allene, *J. Mol. Spectrosc.* 216 (2002) 197–202. <https://doi.org/10.1006/jmsp.2002.8596>.
- [158] F. Hegelund, N. Andresen, M. Koivusaari, A High-Resolution Infrared Study of the  $\nu_9 + \nu_{11} - \nu_{11}$ ,  $\nu_{10} + \nu_{11} - \nu_{11}$  Hot Band System in Allene, *J. Mol. Spectrosc.* 159 (1993) 230–248. <https://doi.org/10.1006/jmsp.1993.1120>.
- [159] E. Es-sebbar, A. Jolly, Y. Benilan, A. Farooq, Quantitative mid-infrared spectra of allene and propyne from room to high temperatures, *J. Mol. Spectrosc.* 305 (2014) 10–16. <https://doi.org/10.1016/j.jms.2014.09.004>.
- [160] F. Cheruy, N.A. Scott, R. Armante, B. Tournier, A. Chedin, Contribution to the development

of radiative transfer models for high spectral resolution observations in the infrared, *J. Quant. Spectrosc. Radiat. Transf.* 53 (1995). [https://doi.org/10.1016/0022-4073\(95\)00026-H](https://doi.org/10.1016/0022-4073(95)00026-H).

- [161] L. Regalia, C. Oudot, S. Mikhailenko, L. Wang, X. Thomas, A. Jenouvrier, P. Von der Heyden, Water vapor line parameters from 6450 to 9400 $\text{cm}^{-1}$ , *J. Quant. Spectrosc. Radiat. Transf.* 136 (2014) 119–136. <https://doi.org/10.1016/j.jqsrt.2013.11.019>.
- [162] P. Macko, D. Romanini, S.N. Mikhailenko, O. V. Naumenko, S. Kassi, A. Jenouvrier, V.G. Tyuterev, A. Campargue, High sensitivity CW-cavity ring down spectroscopy of water in the region of the 1.5  $\mu\text{m}$  atmospheric window, *J. Mol. Spectrosc.* 227 (2004) 90–108. <https://doi.org/10.1016/j.jms.2004.05.020>.
- [163] R. a Toth, Line lists of water vapor parameters from 500 to 8000  $\text{cm}^{-1}$ , JPL Nasa. (2013).
- [164] R.R. Gamache, A.L. Laraia, N<sub>2</sub>-, O<sub>2</sub>-, and air-broadened half-widths, their temperature dependence, and line shifts for the rotation band of H<sub>2</sub>O, *J. Mol. Spectrosc.* 257 (2009) 116–127. <https://doi.org/10.1016/j.jms.2009.07.004>.
- [165] R.R. Gamache, Lineshape parameters for water vapor in the 3.2–17.76 $\mu\text{m}$  region for atmospheric applications, *J. Mol. Spectrosc.* 229 (2005) 9–18. <https://doi.org/10.1016/j.jms.2004.08.004>.
- [166] D.P. Dee, S.M. Uppala, A.J. Simmons, P. Berrisford, P. Poli, S. Kobayashi, U. Andrae, M.A. Balmaseda, G. Balsamo, P. Bauer, P. Bechtold, A.C.M. Beljaars, L. van de Berg, J. Bidlot, N. Bormann, C. Delsol, R. Dragani, M. Fuentes, A.J. Geer, L. Haimberger, S.B. Healy, H. Hersbach, E. V Hólm, L. Isaksen, P. Kállberg, M. Köhler, M. Matricardi, A.P. McNally, B.M. Monge-Sanz, J.-J. Morcrette, B.-K. Park, C. Peubey, P. de Rosnay, C. Tavolato, J.-N. Thépaut, F. Vitart, The ERA-Interim reanalysis: configuration and performance of the data assimilation system, *Q. J. R. Meteorol. Soc.* 137 (2011) 553–597. <https://doi.org/10.1002/qj.828>.
- [167] H. Hersbach, B. Bell, P. Berrisford, S. Hirahara, A. Horányi, J. Muñoz-Sabater, J. Nicolas, C. Peubey, R. Radu, D. Schepers, A. Simmons, C. Soci, S. Abdalla, X. Abellan, G. Balsamo, P. Bechtold, G. Biavati, J. Bidlot, M. Bonavita, G. De Chiara, P. Dahlgren, D. Dee, M. Diamantakis, R. Dragani, J. Flemming, R. Forbes, M. Fuentes, A. Geer, L. Haimberger, S. Healy, R.J. Hogan, E. Hólm, M. Janisková, S. Keeley, P. Laloyaux, P. Lopez, C. Lupu, G. Radnoti, P. de Rosnay, I. Rozum, F. Vamborg, S. Villaume, J.-N. Thépaut, The ERA5 global reanalysis, *Q. J. R. Meteorol. Soc.* 146 (2020) 1999–2049. <https://doi.org/10.1002/qj.3803>.
- [168] H. Ke, V. Boudon, C. Richard, V. Madhur, M. Faye, L. Manceron, Analysis and modeling of combination bands of sulfur hexafluoride 32SF<sub>6</sub> based on global fits. Update of the SHeCaSDa database, *J. Mol. Spectrosc.* 368 (2020) 1–14. <https://doi.org/10.1016/j.jms.2020.111251>.
- [169] A. V. Nikitin, M. Rey, I.S. Chizhmakova, V.G. Tyuterev, First Full-Dimensional Potential Energy and Dipole Moment Surfaces of SF<sub>6</sub>, *J. Phys. Chem. A.* 124 (2020) 7014–7023. <https://doi.org/10.1021/acs.jpca.0c02733>.
- [170] M. Rey, A. V. Nikitin, Y.L. Babikov, V.G. Tyuterev, TheoReTS – An information system for theoretical spectra based on variational predictions from molecular potential energy and dipole moment surfaces, *J. Mol. Spectrosc.* 327 (2016) 138–158. <https://doi.org/10.1016/j.jms.2016.04.006>.
- [171] P. Varanasi, Z. Li, V. Nemtchinov, A. Cherukuri, Spectral absorption-coefficient data on HCFC-22 and SF<sub>6</sub> for remote-sensing applications, *J. Quant. Spectrosc. Radiat. Transf.* 52



(1994) 323–332. [https://doi.org/10.1016/0022-4073\(94\)90162-7](https://doi.org/10.1016/0022-4073(94)90162-7).

- [172] N.H. Ngo, D. Lisak, H. Tran, J.M. Hartmann, An isolated line-shape model to go beyond the Voigt profile in spectroscopic databases and radiative transfer codes, *J. Quant. Spectrosc. Radiat. Transf.* 129 (2013) 89–100. <https://doi.org/10.1016/j.jqsrt.2013.05.034>.